Environmental Science Nano

CRITICAL REVIEW

View Article Online
View Journal | View Issue

Cite this: *Environ. Sci.: Nano*, 2021, **8**, 1133

Removal of antibiotics from aqueous solutions by electrocatalytic degradation

Vaishali Choudhary, Kowsalya Vellingiri, Mohammed Iqbal Thayyil and Ligy Philip *

Received 28th December 2020,
Accepted 14th March 2021

DOI: 10.1039/d0en01276a

rsc.li/es-nano

The development of affordable and modular water/wastewater treatment technologies is highly desirable to counter the adverse effects of antibiotics. Electrochemical treatment, especially electrocatalysis, has a vast potential to degrade antibiotics due to its higher treatment efficiency, low power consumption, and flexible design. Correspondingly, the current review broadly discusses the present status and future trends regarding the electrocatalytic degradation of antibiotics. At the beginning, antibiotic distribution and the merits and demerits of conventional treatment technologies are briefly conveyed. Later, the electrocatalytic removal of antibiotics is discussed in detail with a special focus on catalyst type (*e.g.*, metal-based and carbon-based nanomaterials), oxidative/reductive degradation pathways, and reaction mechanisms. A comprehensive assessment of removal efficiency, operational cost, environmental toxicity of nanomaterials, and residual by-product management has also been carried out. Overall, the feasibility of electrocatalysis technology for antibiotic removal and the critical strategies required for its development have been summarized to provide a roadmap for future research.

Environmental significance

Over the years, the quality and quantity of available water resources have been adversely affected due to the unregulated consumption and discharge of antibiotics. Thus, the development of a robust, effective treatment technology like electrocatalysis is obligatory. Electrocatalysis as a treatment option incorporates an extensive array of research fields, including materials science, nanomaterials, electroanalytical, and environmental engineering. The understanding of the architecture of nanomaterials and their environmental compatibility enables tailoring of electrocatalysts with superior performance in the degradation of antibiotics. The brief insight into electrocatalysis as a treatment option creates a layout for developing new functional nanomaterials and resolving environmental crises due to the accumulation of antibiotics and antibiotic-resistant genes.

1. Introduction

Detection of a multitude of antibiotics in various water sources is common in recent times. Antibiotics can be defined as biologically active natural, synthetic, or semi-synthetic compounds that kill microorganisms or inhibit their growth or metabolic activity.[1] Broadly, antibiotics can be categorized as β-lactams, fluoroquinolones (FQs), macrolides, sulphonamides, tetracyclines, aminoglycosides, carbapenems, cephalosporins, chloramphenicols, imidazoles, lincosamides, and others based on their therapeutic use and structure (Table 1). The global consumption of antibiotics has increased by 65% between 2000 and 2015 and is expected to reach 200% by 2030.[2] The primary sources responsible for the distribution of antibiotics in the different environment matrices such as surface water, soil, sludge, *etc.* include improper disposal from households, hospitals, industries, animal husbandry, aquaculture, wastewater treatment plants (WWTPs), and sewer leakage.[3,4] Globally, azithromycin (AZI) (254–529 ng L^{-1}), ciprofloxacin (CPX) (245–1149 ng L^{-1}), ofloxacin (OFX) (1998–518 ng L^{-1}), sulfamethoxazole (SMX) (1325–5053 ng L^{-1}) and tetracycline (TTC) (561–31.4 ng L^{-1}) are the most detected antibiotics in wastewater and surface water sources, as shown in (Fig. 1).[5–8]

Although the environmental concentrations of antibiotics are in the range of ng L^{-1} to mg L^{-1}, the biologically active and pseudo-persistent nature of these compounds is of concern. For instance, antibiotics are responsible for inhibiting photosynthesis *via* blocking photosystem II and generating reactive oxygen species (ROS) in photoautotrophic organisms.[9] In multicellular organisms, bioaccumulation of antibiotics is stated to cause a decline in the reproduction rate, feminization of male fish, imbalance in the intestine's microbiota, and propagation of detrimental bacteria.[10] The

---

Environmental and Water Resources Engineering Division, Department of Civil Engineering, IIT Madras, Chennai 600 036, India. E-mail: ligy@iitm.ac.in; Fax: +91 44 22574252; Tel: +91 44 22574274

impression of antibiotics on promoting the growth of antibiotic-resistant genes (ARGs) and antibiotic-resistant bacteria (ARB) has also been well established.[11] Most importantly, the presence of ARGs is not controlled by antibiotic consumption.[12,13] A recent report indicated that drug-resistant pathogens (ARBs) could contribute to an economic loss of 2–3.5% of GDP and death of 10 million people by 2050.[14,15] Moreover, with the increase in the global temperature (10 °C), the rise in antibiotic resistance of 4.2% in *E. coli*, 2.2% in *Klebsiella pneumonia*, and 2.7% in *Staphylococcus aureus* is projected.[16] Thus, it is imperative to develop strict regulations, supplementary surveillance, and treatment technologies to counter the impending ecosystem hazard.

2. Treatment technologies for the elimination of antibiotics in water/wastewater systems

To tackle the challenges and hazards mentioned above, developing appropriate WW treatment options is very important. Accordingly, physicochemical (*e.g.*, adsorption[18] and membrane technologies[19]), conventional biological processes[20,21] (like activated sludge process and membrane bioreactors), advanced oxidation processes[22] (*e.g.*, UV,[23] ozonation,[24] Fenton's,[25,26] and photocatalysis[27]), and constructed wetlands[28–32] have been considered as an alternative to eliminate antibiotics from water/WW systems

Vaishali Choudhary

Vaishali Choudhary received her B.Sc. (Chemistry Honors) in 2015 from the University of Delhi, India, and M.Sc. (Environmental Sciences) in 2017 from the School of Environmental Sciences, Jawaharlal Nehru University, India. She is currently pursuing her Ph.D. degree under the guidance of Prof. Ligy Philip at IIT Madras, India. Her research work focuses on developing adsorbents and catalysts for the removal of micropollutants from wastewater.

Kowsalya Vellingiri

Dr. Kowsalya Vellingiri obtained her M.Sc. from the PSGR Krishnammal College, Bharathiar University, Tamilnadu, India, in 2012. She received her Ph.D. from the Department of Civil and Environmental Engineering, Hanyang University, under the guidance of Professor Ki-Hyun Kim in 2017. Her research interests include the application of metal–organic frameworks for sorptive removal and/or luminescent sensing of hazardous pollutants. She did her PDF at EWRE Division, IIT Madras, under the mentorship of Prof. Ligy Philip and worked on the development of colorimetric sensors for inorganic pollutants. She has published more than 35 research papers in SCI journals with citations of more than 1150.

Mohammed Iqbal Thayyil

Mohammed Iqbal Thayyil obtained his B.Tech in Civil Engineering from the College of Engineering Trivandrum in 2015. He completed his M.Tech in Environmental Engineering from the same institute in 2019. He is currently pursuing his Ph.D. at the Environmental and Water Resources Engineering Division, IIT Madras, under the mentorship of Prof. Ligy Philip. His research interests include the application of bioremediation, hydroponics and electro-catalysis for the removal of nutrients and organic micropollutants from water.

Ligy Philip

Dr. Ligy Philip is a Professor of Environmental and Water Resources Engineering, Department of Civil Engineering, Indian Institute of Technology Madras, Chennai. Her research interests include water and wastewater treatment, rural water supply, sanitation and bioremediation. Her research focuses on sustainable technology development for recycling and reusing domestic and industrial wastewaters and resource recovery from waste.

Table 1 Physicochemical properties and therapeutic use of most used antibiotics

Class	Antibiotics/abbreviation/ molecular formula/ molecular weight (MW)	Chemical structure	Physicochemical properties					Removal in WWTP[a] (%)	Therapeutic use, mode of action[b]
			Solubility[a] (mg L^{-1})	$\log K_{ow}$[a]	pK_a[a]	Excretion rate[b] (%)	Acute toxicity[c] (mg L^{-1})		
β-Lactams	Amoxicillin (AMX) $C_{16}H_{19}N_3O_5$ MW = 365 g mol^{-1}	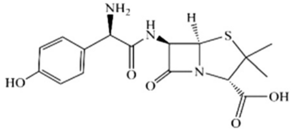	3430	0.87	2.67, 7.11, 9.55	60	GA = 157 Dap. = 28.9 Fish = 370	1.88	Semi-synthetic antibacterial agent, inactivates penicillin-binding protein in cell wall
	Ampicillin (AMP) $C_{16}H_{19}N_3O_4S$ MW = 349 g mol^{-1}	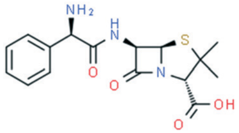	10 100	1.35	2.5, 7.3	80	GA = 71.0 Dap. = 171 Fish = 1533	1.94	Antibacterial agent, effective against Gram-positive bacteria, inactivates penicillin-binding protein in cell wall
Sulphonamide	Sulfamethoxazole (SMX) $C_{10}H_{11}N_3O_3S$ MW = 253 g mol^{-1}	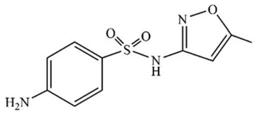	610 (37 °C)	0.89	1.85, 5.70	30	GA = 6.62 Dap. = 1.87 Fish = 410	1.88	Anti-infective agent, dihydropteroate synthase inhibitor, thus affects folic acid synthesis
	Sulfathiazole (STZ) $C_9H_8N_3NaO_2$ MW = 277 g mol^{-1}	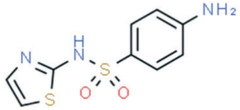	373 (25 °C)	0.05	7.1	—	GA = 5.87 Dap. = 2.87 Fish = 285	1.85	Anti-infective agent used in veterinary medicine
Sulphanilamide	Sulfisoxazole (SFX) $C_{11}H_{13}N_3O_3S$ MW = 267 g mol^{-1}	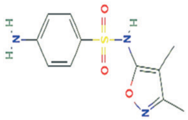	300 (37 °C)	1.01	1.5, 5.0	—	GA = 5.17 Dap. = 1.95 Fish = 180	1.98	Synthetic antibacterial agents, folic acid synthesis inactivator
Tetracycline	Oxytetracycline (OTC) $C_{22}H_{24}N_2O_9$ MW = 460 g mol^{-1}	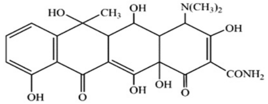	313 (25 °C)	−0.90	3.27, 7.32, 9.11	35	GA = 1426 Dap. = 21.5 Fish = 1960	1.85	Antibacterial agents inhibit the binding of RNA, thereby inhibiting protein synthesis
	Tetracycline (TTC) $C_{22}H_{24}N_2O_8$ MW = 444 g mol^{-1}	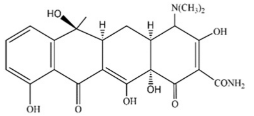	1700	−1.30	3.3, 7.7, 9.7	35	GA = 251 Dap. = 2.89 Fish = 27.3	1.85	Protein synthesis inhibitors by binding the 30S ribosomal subunit
Quinolones	Ciprofloxacin (CPX) $C_{17}H_{18}FN_3O_3$ MW = 331 g mol^{-1}	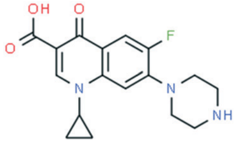	30 000	0.28	6.09, 8.74	70	GA = 1621 Dap. = 1240 Fish = 13 131	1.85	Antimicrobial agent, DNA synthesis inactivator
	Levofloxacin (LVFX) $C_{18}H_{20}FN_3O_4$ MW = 361 g mol^{-1}	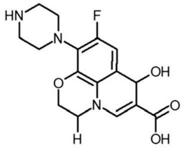	40.4 (20 °C)	2.1	6.25	85	GA = 4183 Dap. = 13 007 Fish = 28 067	1.85	Anti-infective and nucleic acid synthesis inhibitor

Table 1 *(continued)*

Class	Antibiotics/abbreviation/ molecular formula/ molecular weight (MW)	Chemical structure	Physicochemical properties: Solubility[a] (mg L^{-1})	log K_{ow}[a]	pK_a[a]	Excretion rate[b] (%)	Acute toxicity[c] (mg L^{-1})	Removal in WWTP[a] (%)	Therapeutic use, mode of action[b]
	Ofloxacin (OFX) $C_{18}H_{20}FN_3O_4$ MW = 362 g mol^{-1}	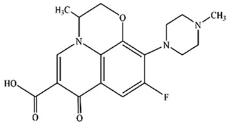	4000 (varies with pH)	−0.39	5.97, 8.28	70	GA = 2444 Dap. = 1786 Fish = 19 325	185	Anti-bacterial agent; and nucleic acid synthesis inhibitor
	Norfloxacin (NOFX) $C_{16}H_{18}FN_3O_3$ MW = 319 g mol^{-1}	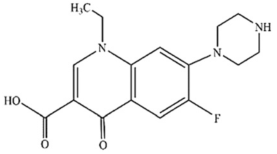	178 000 (varies with pH)	0.46	6.34, 8.75	30	GA = 2567 Dap. = 1830 Fish = 20 081	1.85	Anti-infective agent and enzyme inhibitor
	Enrofloxacin (ENF) $C_{15}H_{17}N_4O_3F$ MW = 320 g mol^{-1}	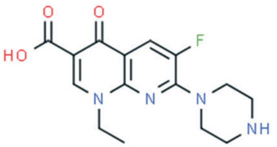	1000	−0.2	5.88, 7.7	70	GA = 2567 Dap. = 1830 Fish = 20 081	1.85	Antibacterial agent, DNA synthesis inactivation
Macrolides	Azithromycin (AZI) $C_{38}H_{72}N_2O_{12}$ MW = 749 g mol^{-1}	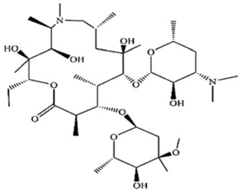	2.73 (25 °C)	4.02	8.74, 9.45	12	GA = 1.87	31	Antibacterial agent binds to the 50S ribosomal subunit of the 70S ribosome, thereby inhibiting the translocation step of protein synthesis
Imidazole	Metronidazole (MNZ) $C_6H_6N_3O_3$ M.W = 171 g mol^{-1}	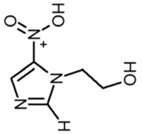	11 000 (25 °C)	−0.02	2.4	20	GA = 0.75 Dap. = 12.1 Fish = 123	1.85	Antiprotozoal agent inhibits DNA synthesis and bacterial cell growth
Chloramphenicol	Chloramphenicol (CAP) $C_{11}H_{12}Cl_2N_2O_5$ MW = 323 g mol^{-1}	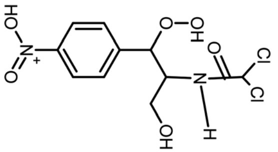	2500 (25 °C)	1.14	1.1	10	GA = 0.40 Dap. = 32.8 Fish = 72.1	1.9	Antibacterial agent and protein synthesis inhibitor
	Thiamphenicol (TAP) $C_{12}H_{15}Cl_2NO_5S$ MW = 356 g mol^{-1}	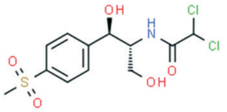	>53.4	−0.27	9.76	100	GA = 4.67 Dap. = 286 Fish = 211	1.85	Immunosuppressive and antimicrobial agent
	Florfenicol (FLO) $C_{12}H_{14}FCl_2NO_4S$ MW = 358 g mol^{-1}	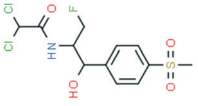	5936	−0.03	9.03	60	GA = 2.69 Dap. = 212 Fish = 145	1.85	Synthetic antimicrobial agent used in aquaculture

Table 1 *(continued)*

Class	Antibiotics/abbreviation/ molecular formula/ molecular weight (MW)	Chemical structure	Physicochemical properties					Removal in WWTP[a] (%)	Therapeutic use, mode of action[b]
			Solubility[a] (mg L^{-1})	log K_{ow}[a]	pK_a[a]	Excretion rate[b] (%)	Acute toxicity[c] (mg L^{-1})		
Nitrofuran	Furazolidone (FZD) $C_8H_7N_3O_5$ MW = 225 g mol^{-1}	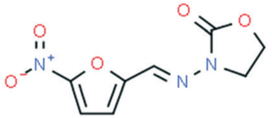	40 (25 °C)	−0.04		100	GA = 1.18 Dap. = 27.3 Fish = 4.86	1.85	Antiprotozoal activity, inhibits monoamine oxidase by binding to DNA
	Nitrofurazone (NFZ) $C_6H_6N_4O_4$ MW = 198 g mol^{-1}	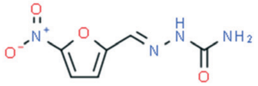	210 (25 °C)	0.23	10	100	GA = 1.85 Dap. = 57.3 Fish = 8.23	1.85	Anti-infective against Gram-negative and Gram-positive bacteria
Cephalosporin	Ceftazidime (CFD) $C_{22}H_{22}S_2N_6O_7$ MW = 546 g mol^{-1}	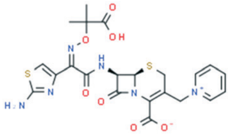	369	−1.6		90	GA = 394 Dap. = 42.3 Fish = 173 000	1.85	Anti-bacterial agent, inactivation of penicillin binding protein in the cell wall
	Ceftriaxone (CFT) $C_{18}H_{18}S_3N_8O_7$ MW = 554 g mol^{-1}	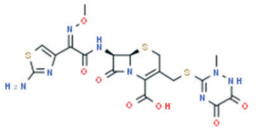	105	−1.7	~6.7	70	GA = 260 Dap. = 17 238 Fish = 1440	1.85	Antibacterial agent, inactivation of penicillin-binding protein in the cell wall, more active against Gram-negative bacteria

[a] And acute toxicity (data from ECOSAR V2.0). [b] Data from ref. 17. [c] GA = Green algae, Dap. = Daphnid.

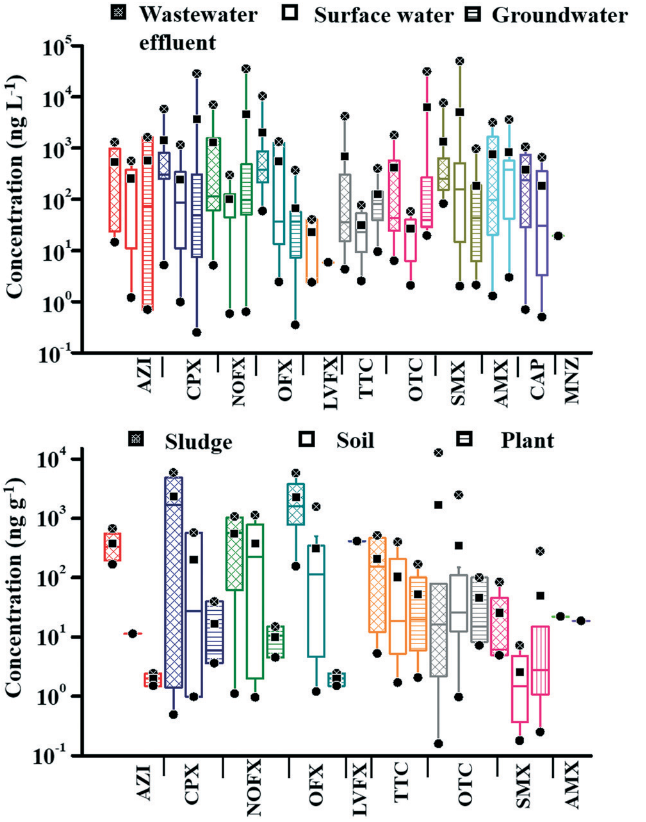

Fig. 1 Global average concentration of antibiotics in various environmental matrices.[5–8]

(Fig. 2). Among the practiced methods, adsorption and membrane filtration are widely recommended due to their ease of operation and favourable treatment efficiency.[19,33,34] Nonetheless, drawbacks such as high test concentrations (mg L^{-1}) relative to the environmental level (ng L^{-1} to μg L^{-1}), high cost of production of adsorbents like commercial resins ($15–20 per kg)[33] and carbon–metal oxide composites[34,35] and disposal of spent adsorbents and membranes limit their application. Likewise, conventional activated sludge (CAS) and membrane bioreactor (MBR) are the most prevalent biological treatments;[36] however, these systems are not explicitly designed to eliminate recalcitrant emerging contaminants (ECs). Thus, life cycle and cost–benefit analysis of novel adsorptive materials, better understanding of the removal mechanism in the presence of foulants, coexisting ions, and organic matter, fouled membrane behaviour as adsorption sites, and process optimization in the biological process need to be addressed.

Advanced oxidation processes (AOPs) are emerging technologies that provide the advantages of high treatment efficiency, robustness, ease of automation, and creation of stable end products (*e.g.*, CO_2 and H_2O). The primary reactive species in AOPs is the hydroxyl radical ($^{\bullet}$OH) (rate constant of 10^6–10^9 M^{-1} s^{-1}).[18] AOPs can be broadly classified as photochemical (photo-Fenton, UV/H_2O_2, UV/O_3, sonochemical, and photocatalysis) and non-photochemical (chlorination, ozonation, Fenton's, and electrochemical) methods (Fig. 2). Ozonation and chlorination are the most popular tertiary WW treatment technologies with the potential to degrade more than 90% of antibiotics and ARGs.[24,37–39] However, slower kinetics and toxic organohalide formation (during chlorination), and low aqueous solubility of O_3 molecule hinder the complete mineralization of

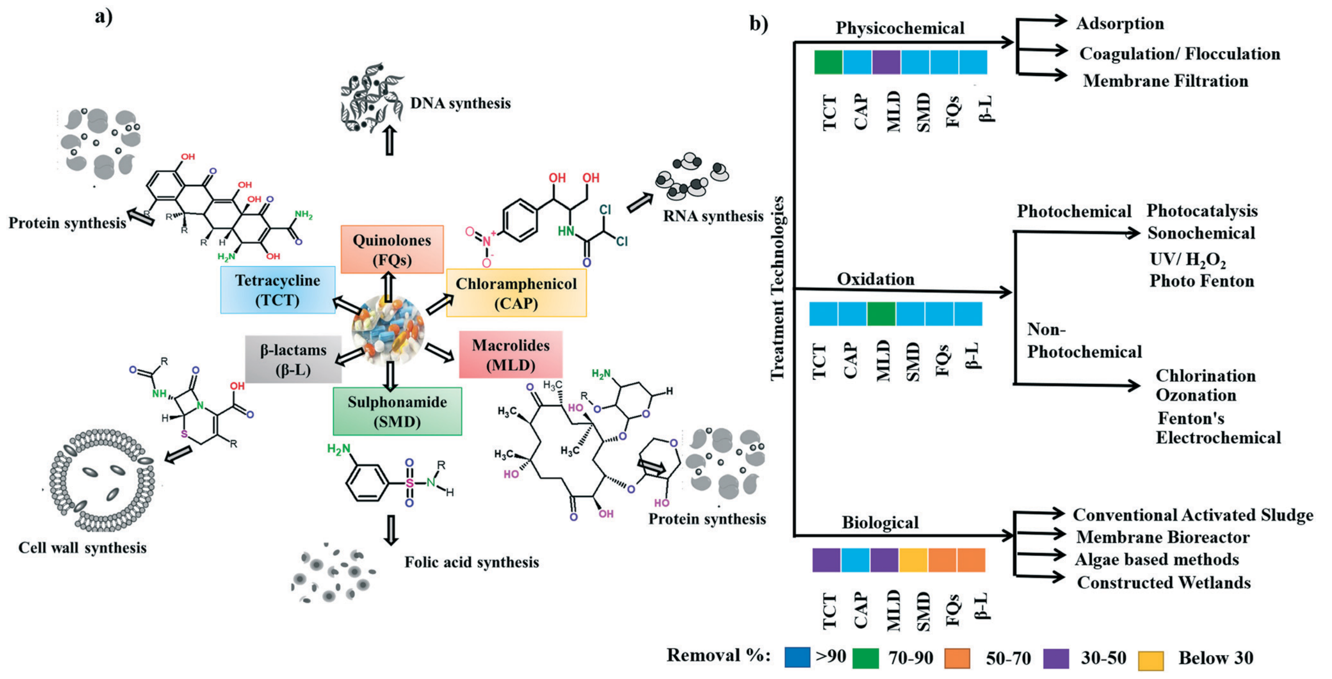

Fig. 2 Various classes of commonly used antibiotics and their mode of action (a), removal percentages of different classes of antibiotics *via* physicochemical, biological, and oxidation processes (b).

pollutants.[2,40] The Fenton's process is another well-established AOP, whereby the chain reactions in the presence of a non-toxic catalyst (Fe^{2+}), acidic medium (pH = 2.8–3.0), and oxidant (H_2O_2) produces $^{\bullet}OH$. However, slower kinetics (cause precipitation of Fe^{3+}) and organic matter presence causes unsatisfactory performance.[41] Thus, modification in terms of photo-Fenton (PF), electro-Fenton (EF), and solar photo-Fenton (SPF) has been reported.[26] Pulse power plasma (high voltage discharge) has also been utilized to degrade FQs like CPX *via* oxidizing species such as $^{\bullet}OH$, $O_2^{\bullet-}$, H_2O_2, O_3, *etc.*[42] However, high input energy, cautious handling and operation, and nitrate formation in the treated effluent are some chief constraints. In the past decade, photocatalysis has been one of the most researched AOPs whereby light photons absorbed on the catalyst surface endorse the movement of electrons (from the valence (VB) to the conduction band (CB)) and trigger the formation of reactive radicals, namely $^{\bullet}OH$ and $O_2^{\bullet}$.[27,43,44] Nonetheless, a comprehensive investigation in the development of catalysts working in the visible region of light is still inadequate.[45] In a nutshell, among the different AOPs, Fenton's process is the least effective and environmentally incompatible due to high sludge production and low mineralization rate. Even though photocatalysis is an effective treatment option, a clear-cut understanding regarding the degradation pathways, efficiency under a diverse light source, and reusability options in the perspective of a real-world scenario are not yet attained. In this context, the application of electrochemical technologies, specifically electrocatalysis, as a water/WW treatment tool is still a new frontier.

Electrochemical technologies can contribute as a stand-alone unit or in the treatment train to remove recalcitrant compounds. The modular design with the potential of automation, no chemical requirement, and multiple contaminant degradation makes the electrochemical system a preferred choice over many traditional approaches.[46] Electrochemical treatment has been identified as a proficient process for the oxidation of organic compounds,[47] reducing halogens,[48,49] electro-deionization,[50] and recovery of metals and energy.[51] However, one of the chief challenges of the process is the poor electrode efficiency and stability, which govern the capital cost, energy demand, and treatment efficacy. Subsequently, modification of the electrodes with catalysts is being considered as a possible solution. The incorporation of catalysts provides extended electrode stability, cutbacks in working potential and reduced side reactions.[52] Also, the operational factors such as applied potential, current density, pH, and electrolyte nature and cell designs play a crucial role in determining the degradation profile. Hence, an in-depth examination of electrocatalysis as a treatment technology for antibiotic removal is an important task. Accordingly, the present review article discusses the electrocatalytic degradation of antibiotics and its associated mechanisms (*e.g.*, oxidation/reduction). In addition, performance evaluation of catalysts with respect to specific antibiotics has been made, and the best-performing catalytic systems have been identified. Finally, recommendations for designing catalysts based on the properties of the targeted antibiotic are encompassed. The possibilities of scale-up with respective environmental and economic implications have also been conversed.

3. Electrochemical methods for antibiotic removal

3.1 Fundamental principle of electrochemical oxidation and reduction

Electrochemical oxidation techniques have been widely used to remove antibiotics due to their ease of operation.[53] The principal mechanism involved in the electrochemical oxidation reaction is the water splitting at the anode to form surface [S] adsorbed $^{\bullet}OH$, which leads to the oxidation of antibiotics (eqn (1) and (2)). At the same time, the oxygen (O_2) evolution reaction (OER) is an unavoidable side reaction (eqn (3)),[54]

$$[S] + H_2O \rightarrow S[^{\bullet}OH] + H^+ + e^- \tag{1}$$

$$S[^{\bullet}OH] + R \rightarrow [S] + RO + H^+ + e^- \tag{2}$$

$$S[^{\bullet}OH] + H_2O \rightarrow [S] + O_2 + 3H^+ + 3e^- \tag{3}$$

It has been well known that $^{\bullet}OH$ adsorption is mainly influenced by the anode material.[55] In this context, metal oxide anodes can strongly adsorb $^{\bullet}OH$ on their surface and convert it to a higher oxidation state, resulting in selective oxidation of target pollutants (eqn (2)). Such electrodes are named 'active electrodes' since pollutants undergo direct oxidation after adsorption on the electrode surface (Fig. 3a).[56,57] Common examples of active electrodes include graphite, Pt, IrO_2, and RuO_2. In contrast, anodes that retain a weak interaction with $^{\bullet}OH$ have been grouped as 'non-active anodes' with the characteristic of non-selective degradation *via* indirect oxidation (Fig. 3b). The application of PbO_2, SnO_2, Sb–SnO_2, and boron-doped diamond (BDD) as an oxidative non-active electrode has been widely explored. Due to mass transfer limitations, the kinetics of direct oxidation (*e.g.*, adsorption of the organic pollutant or $^{\bullet}OH$ on the anode) is relatively slower than indirect oxidation.[58] Subsequently, the efficiency of the anode for the degradation of antibiotics is adversely impacted.[56] Therefore, recognizing destruction pathways based on direct/indirect oxidation or combining both is essential for ensuring complete mineralization of antibiotics.

Concurrent to electrochemical oxidation, the reduction of the pollutant can also be exploited for the degradation. For instance, the electrochemical reduction of nitrate and organic chlorine has been well established.[49,59] Thereupon, the electrochemical reduction has also been extended to degrade antibiotics with nitro (NO_2) and halogen functionality. It has been envisioned that direct reductive dechlorination and catalytic hydrogenation (indirect) are two common pathways for the destruction of halogenated

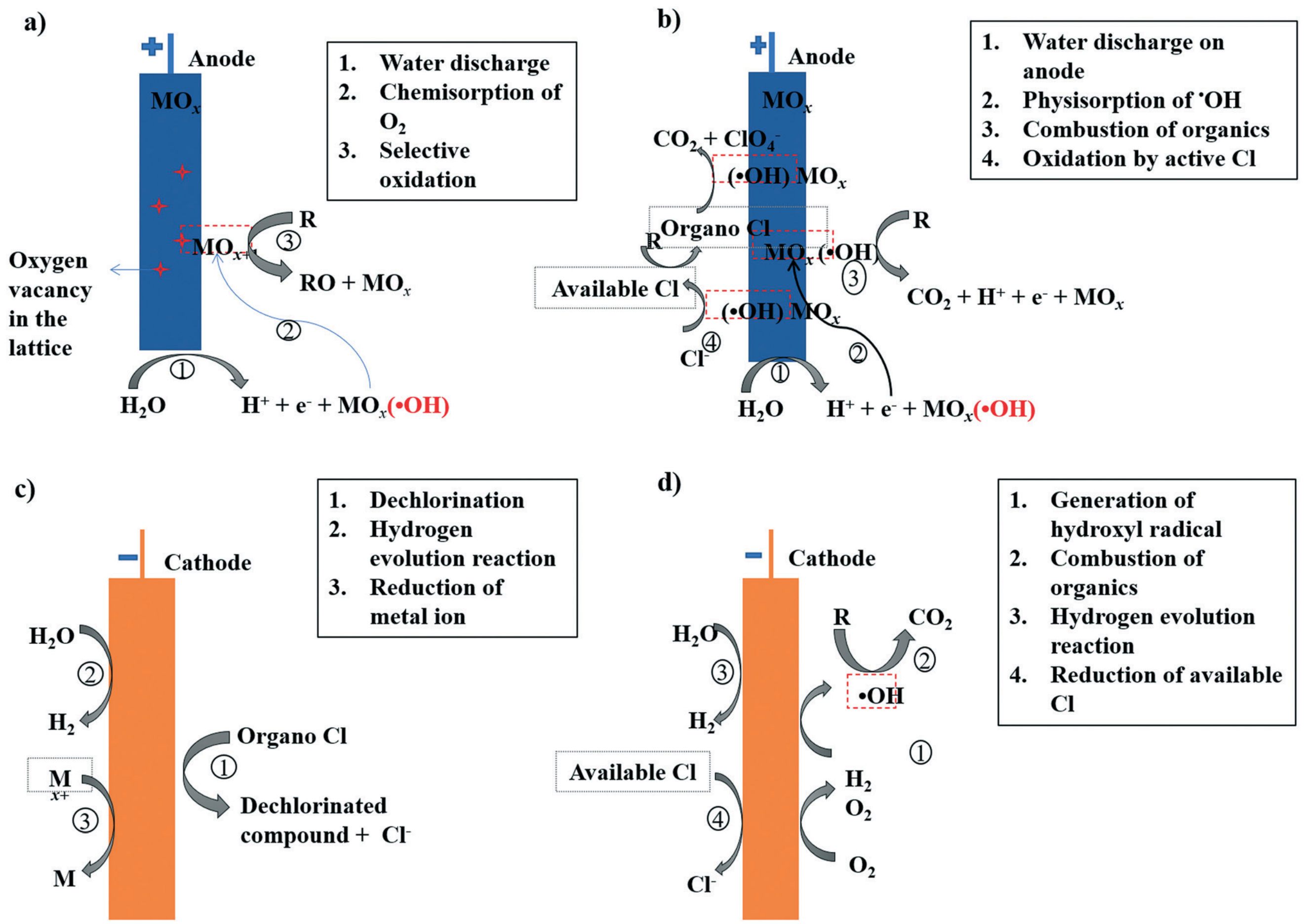

Fig. 3 General mechanisms of electrochemical degradation. Direct oxidation on active anodes (a), indirect oxidation on non-active anodes (b), direct reduction pathway at the cathode (c), and indirect reduction at the cathode (d).

compounds (Fig. 3c and d).[59] Briefly, during direct dechlorination, the C–X bond in the target pollutant cleaves to form halomethyl radical ($^•R–X_{(3-n)}$), which successively leads to the formation of electrons and negative carbon ions (eqn (4)–(6)).[60] The primary disadvantage of direct dechlorination is the higher energy requirement for cleaving the C–X bond (397–544 kJ mol^{-1}). Thus, indirect reduction known as hydrodechlorination has been benefitted. In this method, the target pollutant is absorbed on the non-active sites of the cathode and undergoes dechlorination *via* hydrogen (H_2) produced from reactive sites of the cathode (Fig. 3d).[61] For electron transfer and reductant production, an aprotic solvent like water is commonly used as it behaves as an electron acceptor, yielding H_2 for reduction of C–X (eqn (7)–(9)).

$$R–X_{(4-n)} + e^- \rightarrow {}^•R–X_{(3-n)} + X^- \tag{4}$$

$$^•R–X_{(3-n)} + e^- \rightleftarrows {}^-R–X_{(3-n)} \tag{5}$$

$$^-R–X_{(3-n)} \rightarrow :R–X_{(2-n)} + X^- \tag{6}$$

$$2H_2O + 2e^- \rightarrow H_2\uparrow + 2OH^- \tag{7}$$

$$H_2\uparrow \rightarrow [S]H^* \tag{8}$$

$$R–X_{(4-n)} + 2H^* \rightarrow {}^•R–X_{(3-n)} + H^+ + X^- \tag{9}$$

For detoxification of antibiotics with the nitro group, the primary step is the reduction of the nitro group into an amino group. During the direct electrochemical reduction *via* 2e$^-$ and 4e$^-$ transfer, the hydroxylamine is formed as the common intermediate, which finally yields azo and azoxy dimers (eqn (10)–(12)).[62] The degradation of these azo compounds is challenging and ultimately affects antibiotic mineralization efficacy.

$$RNH_2 + R'NHOH \rightarrow RN{=}NR' \tag{10}$$

$$R'NHOH + O_2 \rightarrow R'–NO \tag{11}$$

$$R'–NO + RNHOH \rightarrow R–NO{=}NR' + H_2O \tag{12}$$

To tackle such challenges, indirect electrochemical reduction has been studied.[63,64] In this process, the redox agent (electrode or catalyst) acts as an electron carrier to detach a substrate from the electrode surface (Fig. 3d).[63]

Consequently, heterogeneous catalysis *via* 6e$^-$ transfer is followed. In this way, unnecessary side reactions can be avoided, thus providing better selectivity and reduced applied potential.[64] It is noteworthy to mention that an in-depth mechanism of reducing nitro-containing antibiotics has not been well established. Studies were conducted by focusing on selective degradation; however, the response of electron mediators and solvent behavior during indirect electroreduction are still unclear. As a result, more research at the elemental level is required to fill these gaps.

3.2 Behaviour of electrolyte

The nature and concentration of supporting electrolytes play a pivotal role in electrocatalytic degradation by governing proton exchange for cathodic and anodic reactions. The presence of electrolytes provides high electrical conductivity leading to faster electron transfer and elevated degradation rate. The most typical electrolytes used for antibiotic degradation include Na_2SO_4 and NaCl, H_2CO_3, HAc–NaAc, $NH_3·H_2O–NH_4Cl$, and $Na_2HPO_4–NaH_2PO_4$.[65] In general, an increase in the concentration of electrolytes (NaCl or Na_2SO_4) enhances the removal rates. This is due to decreased ohmic resistance which leads to accelerated electron transport.[66] Nevertheless, at a very high concentration (>0.2 M Na_2SO_4), the degradation efficiency can be adversely affected due to the absorption of the reactive species on the electrode surface and the diminishing number of active sites.[66] When NaCl is used as an electrolyte, the oxidative efficiency of the system is enhanced attributed to the production of active chlorine species, *e.g.*, Cl_2, HClO, and ClO^- (eqn (13)–(15)).[67]

$$2Cl^- \rightarrow Cl_{2(aq)} + 2e^- \tag{13}$$

$$Cl_{2(aq)} + H_2O \leftrightarrow HClO + Cl^- + H^+ \tag{14}$$

$$HClO \leftrightarrow ClO^- + H^+ \tag{15}$$

Although the E^0 value of Cl_2 and HClO (1.36 V and 1.49 V *vs.* SHE) is much lower than that of $^{\bullet}OH$ (2.8 V), they can selectively target electron-rich moieties such as unsaturated C–C bonds and provide a faster degradation rate.[68] Yet, the potential threats of hazardous chlorinated by-products at high current density adversely affect the mineralization of antibiotics.[67] In this line, applying low current density and higher flow rate is recommended; however, a decrease in treatment efficiency is unavoidable.[69] Hence, K_2SO_4 was tested as a supporting electrolyte for SMX and CPX degradation.[67] The presence of SO_4^{2-} resulted in the generation of strong oxidants such as persulfate ($S_2O_8^{2-}$) (E^0 = 2.01 V) and sulfate radicals ($SO_4^{\bullet-}$) (E^0 = 2.6–3.2 V) which have the ability to selectively degrade pollutants near the electrode surface (eqn (16)–(19)). It should be noted that $S_2O_8^{2-}$ is kinetically slower and needs activation of $SO_4^{\bullet-}$ for oxidizing CPX and SMX (eqn (17)).[70] Nevertheless, at a much higher electrolyte concentration (>0.2 M), the inhibitory effects due to $^{\bullet}OH$ scavenging *via* persulfate have also been noted (eqn (18)).[66] Overall, it has been envisioned that besides $^{\bullet}OH$, $SO_4^{\bullet-}$ plays a complementary role in the selective degradation by electron transfer reactions.[67,70]

$$2SO_4^{2-} \rightarrow S_2O_8^{2-} + 2e^- \tag{16}$$

$$S_2O_8^{2-} + e^- \rightarrow {}^{\bullet}SO_4^{\bullet-} + SO_4^{2-} \tag{17}$$

$$S_2O_8^{2-} + {}^{\bullet}OH \rightarrow SO_4^{\bullet-} + HSO_4^- + 0.5O_2 \tag{18}$$

$$2SO_4^{2-} + {}^{\bullet}OH \rightarrow SO_4^{\bullet-} + OH^- \tag{19}$$

Similarly, carbonate ions are also found to enhance the catalytic property of electrochemical cells *via* the formation of percarbonate ions ($C_2O_6^-$). During the reaction, HCO_3^- undergoes reduction at the cathode to produce OH^- (eqn (20)).[71] A subsequent increase in the pH (8–9) enhances the carbonate ion concentration (CO_3^{2-}), leading to $C_2O_6^-$ production (eqn (21)–(22)).[72] The favourable effects of percarbonate ions for the degradation of norfloxacin (NOFX) were easily achieved at a high concentration (>0.05 M) of electrolyte and in the absence of Cl^- and sulfate.[71] However, on long-term use of carbonate ions as an electrolyte at high pH can cause scaling of the electrochemical cell; hindering the degradation efficiency.

$$HCO_3^- + H_2O + 2e^- \rightarrow HCO_2^- + 9OH^- \tag{20}$$

$$HCO_3^- \leftrightarrow CO_3^{2-} + H^+ \tag{21}$$

$$2CO_3^{2-} \rightarrow C_2O_6^- + 2e^- \tag{22}$$

The use of $NaNO_3$ as an electrolyte causes an inhibitory effect on the degradation of antibiotics. The NO_3^- present in the electrolyte undergoes cathodic reduction to produce NO_2^- and NH_3, which obstruct direct electron transfer and increases the pH of the solution (eqn (23) and (24)).[73] The alleviated pH favours the formation of NH_3 molecules, resulting in a continuous chain process. This phenomenon restricts the electron movement and eventually limits net degradation efficiency (eqn (25)).

$$NO_3^- + 2H^+ + 2e^- \rightarrow NO_2^- + H_2O \tag{23}$$

$$NO_2^- + 5H_2O + 6e^- \rightarrow NH_3 + 7OH^- \tag{24}$$

$$2NH_3 + \rightarrow N_2 + 6H^+ + 6e^- \tag{25}$$

Though the presence of electrolytes aids in improving the electrical conductivity and generating strong oxidant species, the compatibility of electrolytes with antibiotics and the effect of pH cannot be ignored. By using NaCl as the electrolyte, high degradation efficiency was reported for FQs like NOFX and CPX.[67,71] This can be attributable to the ability of Cl$^•$ to attack the electrophilic piperazinyl ring effectively. Additionally, the $^•$OH produced in the system contributed towards the abstraction of halogen and hydroxylation. Similar observations were also reported while using alkaline electrolyte (carbonate).[71] However, for degradation of SMX, Na_2SO_4 and NaBr were reported to provide high degradation efficiency.[68] This can be due to the ease of $SO_4^{•-}$ to participate in the electron transfer reaction with the amine functional group. In a nutshell, it can be established that the nature of the electrolyte, generation of electroactive species, and applied current play a pivotal role in the mineralization. Hence, optimization is required between operational parameters such as pH, current density, electrolyte, and reaction time for electrocatalytic degradation of antibiotics in lab-scale systems which can be further extended to practical or field scale.

3.3 Overview of the existing electrode materials

The nature of the electrode and electroactive species determines the kinetics, selectivity, and efficiency of the electrochemical process. Due to the inert nature and higher overpotential for O_2 evolution, non-active electrodes like BDD and PbO_2 have been tested to remove pharmaceuticals, endocrine disruptors, and personal care products. For instance, PbO_2 showed >90% degradation efficiency for FQs.[74] The low cost of PbO_2 electrodes provides an effective electrode option; however, secondary pollution of Pb *via* leaching has not been considered in many studies. Also, the application of PbO_2-based electrodes in the field scale may be limited due to its brittleness. As a replacement, BDD electrodes have been extensively utilized to eliminate SMX and FQs with 67–90% removal efficiency in a mixed water system.[68,75,76] The major degradation pathway for the BDD electrode includes the generation of $^•$OH and other ROS depending on the ions in the supporting electrolyte.[58] The advantages of BDD electrodes such as a wide potential window for water discharge (up to 3.5 V), stability in extremely acidic medium, and weak adsorption capacity for $^•$OH makes it suitable for electrochemical oxidation.[77] However, the high capital cost, elevated applied current (compared with Pb), slow kinetics for O_2 evolution, and non-selective degradation restrict its widespread application.[75,78] Additionally, the fabrication of BDD with optimized boron content and hybridized carbon ratio for the oxidation of antibiotics is still not well explored.[78]

Carbon (graphene)-based electrodes with diverse functional groups on the surface, higher specific surface area, amplified electrical conductivity, chemical stability, are gaining wide attention as electrocatalysts or catalysts for the removal of antibiotics.[79] The application of graphene-based electrodes seems to be a plausible option owing to its cost-effectiveness and electrochemical properties. The enriched surface properties of graphene (*e.g.*, carbonyl (C═O) and hydroxyl (–OH) groups) results in enhanced activation of H_2O to $^•$OH and H_2O_2 intermediate to $O_2^{•-}$ ($HO_2^•$).[80] Nonetheless, prior to the scale-up, the in-depth reaction mechanism and kinetics for various organic contaminants need to be assessed. Recently, dimensionally stable anodes (DSAs) like Ti–RuO_2 have also been utilized as an alternative to BDD and graphene-based systems.[74,81–83] The presence of a mixed metal oxide (MMO) coating provides inherent catalytic properties and enhanced stability to DSAs. The primary difference between the DSA and other electrodes such as BDD, Pt, and graphene is the simultaneous occurrence of both direct and indirect oxidation, *e.g.*, the DSA follows direct oxidation (electron transfer from anode to antibiotics) at the surface of the anode and/or indirect oxidation at the bulk solution (eqn (26)).[81]

$$\begin{aligned}\text{Ti–RuO}_2 + \text{Antibiotic} &\rightarrow \text{Ti–RuO}_2(\text{Antibiotic})_{\text{ad}} \\ &\rightarrow n\text{CO}_2 + \text{products} + n\text{H}^+ + n\text{e}^-\end{aligned} \tag{26}$$

Apart from this, water electrolysis is also a principal step in the DSA, which results in similar reactions to those of graphene (eqn (27)–(29)).[81] It should be noted that oxygen evolution is the main inevitable side-reaction which weakens the degradation kinetics.

$$\text{Ti–RuO}_2 + \text{H}_2\text{O} \rightarrow \text{Ti–RuO}_2(^\bullet\text{OH})_{\text{ad}} + \text{H}^+ + \text{e}^- \text{ (surface reaction/physisorption)} \tag{27}$$

$$\text{Ti–RuO}_2(^\bullet\text{OH})_{\text{ad}} \rightarrow \text{Ti–RuO}_3 + \text{H}^+ + \text{e}^- \text{ (chemical reaction/chemisorption)} \tag{28}$$

$$\text{Ti–RuO}_3 + \text{R} \rightarrow \text{Ti–RuO}_2 + \text{RO (electrochemical conversion)} \tag{29}$$

Miyata *et al.*[74] compared the competencies of active (Ti/IrO_2) and non-active (Ti/PbO_2) electrodes to oxidize antibiotics. It has been found that the active electrode showed better performance than the non-active electrode. This is because of the enhanced generation of chemisorbed $^•$OH at the anode (eqn (28) and (29)). The generated $^•$OH can further oxidize to O_2 and favours selective oxidation of target compounds. Besides, Ti is a low-cost and highly conductive stable material, thus enriching its use as the primary support material for both active and non-active electrodes.[78]

It can be summarised that the electrodes mentioned above face the limitations of higher energy requirement, the formation of toxic intermediates in particular cases, and lack of electrode stability. Even though BDD-like electrodes are the most favoured candidates for electrochemical oxidation, their high cost prohibits regular use. Furthermore, the durability, recyclability, and stability of BDD in field-scale WW treatment are unknown. Thus, viable ways to counter issues like high power input, elevated capital investment, and selective antibiotic degradation to non-toxic/less toxic end products are essential.

3.4 Performance evaluation of available electrodes

Electrochemical treatment technologies provide a desirable option for the mineralization of antibiotics. However, the diverse nature of antibiotics limits the consistent performance of the electrodes. For instance, under alkaline conditions, the degradation of N-functionalized antibiotics is highly problematic due to their protonation, whereas metal-based electrodes are unstable under highly acidic conditions (Pb leaching). Hence, understanding the behaviour of the electrode at various operational parameters for different antibiotics is necessary. Accordingly, in the current section, the performances of DSA, BDD, and carbon-based electrodes for degrading diverse classes of antibiotics were assessed in detail.

3.4.1. Dimensionally stable electrodes. DSAs are made up of a titanium (Ti) support sheltered by metal oxides (*e.g.*, Ru, Ti, Ir, Sn, and Sb).[90] Compared to BDD electrodes, DSAs have higher stability and particular electrocatalytic features (*e.g.*, production of active chlorine from chloride ions).[90,91] This unique characteristic of the DSA has attracted attention for its use in electrocatalysis, where stability and the electrode's properties are crucial parameters. In this context, iridium-based metal oxide (IrO_2) serves as a pioneering catalyst owing to oxidation *via* (i) e^- transfer from the pollutant to IrO_2 and (ii) surface reaction between the contaminant and IrO_3.[82] This ability of Ti/IrO_2 for oxidation was verified by Miyata *et al.*[74] for degrading 99.4% TTC in 360 min with 1500 mA as applied current. Though the activity of Ti/IrO_2 was found to be lower than that of Ti/PbO_2 (99.9% in 2 h), in terms of environmental sustainability (*i.e.*, to avoid secondary Pb pollution), Ti/IrO_2 was preferred. Additionally, active Cl_2 and percarbonate ions from the electrolyte (refer to section 3.2) supplemented the degradation of antibiotics. Analogously, Ti/IrO_2 was reported to possess better degradation efficiency for NOFX in real samples (*e.g.*, seawater and municipal WW) than distilled water.[71] For example, 40 mg L^{-1} NOFX was eradicated in 60 min in seawater, whereas it took 120 and 180 min for WW and distilled water, respectively (Table 2). Though the application of the DSA is successful in treating antibiotics in real samples, the toxicity or mineralization ability in a complex matrix has not been discussed in detail. Therefore, the technical gap in applying the DSA in practical environmental conditions (neutral or alkaline pH) needs to be addressed in the future.

RuO_2 is another common coating material for Ti other than IrO_2 in the DSA system because of its extended electrocatalytic activity towards diverse oxidizing species, durability, and high oxygen evolution potential (OEP) (~1.9 V). Ti/RuO_2 has been reported to degrade 79% of AZI (47.2 mg L^{-1}) in 180 min through indirect oxidation (Fig. 3b).[83] Appropriately, electrocatalysis of AZI using Ti/RuO_2 was found to be faster (180 min) than photolysis (1200 min) and photocatalysis (414 min).[92] Similarly, successful AMX abatement was also verified at low current density (5.88 mA cm^{-2}) with Ti/RuO_2 (60% in 240 min).[81] The reported observations were superior to those of a BDD electrode operated at higher current density (*e.g.*, 100% mineralization in 360 min at 41.7 mA cm^{-2},[93] 84% removal in 240 min at 40 mA cm^{-2},[84] and 94% mineralization in 480 min at 120 mA cm^{-2}) (Table 2).[87] It is worth mentioning that $^{\bullet}OH$ produced on Ti/IrO_2 or Ti/RuO_2 reacts with a covalently bound oxygen atom to form chemisorbed active oxygen species (refer to section 3.3).[94] This phenomenon increases the consumption of $^{\bullet}OH$ and ultimately reduces its availability for oxidizing antibiotics. In other words, an unhealthy competition for $^{\bullet}OH$ from antibiotics and covalent oxygen will be developed, which can adversely affect the mineralization yield of the DSA. Therefore, complete mineralization of antibiotics is not possible.[95] Consequently, BDD electrodes were found to serve as an alternative to DSAs.

3.4.2. Boron-doped diamond (BDD) electrodes. BDD anode material with a wide electrochemical window has been identified as a perfect choice to achieve the mineralization of antibiotics. For example, a BDD/carbon felt electrochemical system yielded high mineralization efficiency for TTC (98% in 360 min)[82] and AMX (94% in 480 min)[87] at an applied current of 120–500 mA, through active $^{\bullet}OH$ formation. More specifically, BDD/carbon felt outperformed other electrodes (BDD/stainless steel (SS) > $Ti/RuO_2–IrO_2$/carbon felt > $Ti/RuO_2–IrO_2$/SS).[82] This outstanding performance was accomplished due to the synergetic action of BDD and carbon felt, *i.e.*, higher H_2O_2 generation at carbon felt and utilization of generated H_2O_2 to produce superoxide radicals by BDD (eqn (30)).[96,97]

$$H_2O_2 + BDD(^{\bullet}OH) \rightarrow BDD(HO_2^{\bullet}) + H_2O \tag{30}$$

In some cases, the occurrence of parallel non-oxidative reactions, *i.e.*, consumption of $^{\bullet}OH$ by the BDD anode and production of secondary oxidants H_2O_2 and $HO_2^{\bullet}$,[87] results in poor mineralization efficiency at higher current densities (>80 mA cm^{-2}).[98] For instance, electrooxidation (EO) of low concentration of AMX (1.1 mg L^{-1} at 25 mA cm^{-2}) using BDD showed 90% removal in 30 min.[85] However, extremely poor mineralization (~1%) raises a query about the manifestation of adsorbed AMX on the catalyst surface and the ecotoxicity of the by-products. Likewise, poor removal/mineralization (72.9–67.7%) in 180 min was obtained for SMX (0.5 mg L^{-1})[58] due to slower chemical reaction near the anode surface. Controlling the kinetic parameters (*e.g.*, mass flow) is an effective way to accomplish amplified mineralization (Table 2).[99] Briefly, under mass transfer limitations every antibiotic molecule which reaches the electrode surface is predominantly oxidized. In other words, there is sufficient availability of oxidant ($^{\bullet}OH$) for degradation and subsequent mineralization.[86,96] For example, ~90% removal and mineralization of NOFX (100 mg L^{-1}) was observed by Coledam *et al.*[86] under mass transfer limitations. The authors have also observed that the achieved efficiency is independent of the boron-doping level/characteristics of BDD which adds significant merit to the BDD electrodes.[100] This specific kinetic excellence of mass transfer limitations was also used to treat various other complex antibiotics such as CPX and SMX.[67,70] It can be noted that mass transfer limitation ($i > i_{lim}$) and the use of auxiliary ions (*e.g.*, Cl^- and SO_4^{2-}) can aid

Table 2 Commonly used electrodes for electrochemical oxidation and reduction

Antibiotics	Working electrode	Features of electrode	Operational parameters	Removal % and recyclability	Reaction pathway	Remarks	Ref.
SFX	(i) Graphite (ii) Graphene	(i) Flake – smooth surface, thickness <5 μm and higher capacitance (ii) Fold morphology	Conc. = 30 mg L^{-1}, Na_2SO_4 = 10 g L^{-1}, potential = 1.5 V *vs.* SCE	(i) RE = 76% in 180 min, RC = 5 cycles	Indirect oxidation *via* generation of $OH^{\bullet}$ and $O_2^{\bullet -}$	Graphene electrode showed more electrical and thermal conductivity due to fold morphology	80
AZI	Ti–RuO_2	Ti coated with thin layer of metal oxide, high electrocatalytic activity and stability in corrosive environment	Conc. = 47.2 mg L^{-1} NaCl = 0.0007 g L^{-1} I = 300 mA	ME: 79% in 180 min	Indirect oxidation is prominent	Enhanced and selective detection in the presence of NaCl	83
TTC, OCT	(i) Ti/IrO_2 (ii) Ti/PbO_2	(i) Active electrode (ii) Non-active electrode	Conc. = 100 mg L^{-1} Na_2SO_4 and NaCl = 1 g L^{-1}, I = 1500 mA	(i) RE: 100% in 360 min (ii) RE: 100% in 120 min	Direct and indirect oxidation	(i) Ti/PbO_2 power consumption = 2.7 g OTC kW h^{-1} (ii) ↑ed electrolyte conc., ↑ed removal	74
Amoxicillin trihydrate (AMX)	Ti/RuO_2	Low cost, dimensional stability and high electroactivity, high efficiency under strong acidic conditions	Conc. = 50 mg L^{-1}, NaCl = 1–2 g L^{-1}, i = 5.88 mA cm^{-2}	RE: 70% at pH 7 in 60 min	Indirect oxidation to open β-lactam ring following pseudo first-order kinetics	(i) Maximum removal at pH 7 (ii) ↑ed removal by ↑ed current density and Cl^- conc. (iii) SEC = 3.26 to 0.66 kW h g^{-1} TOC removed	81
NOFX	Ti/IrO_2	Good electrocatalytic ability to form active chlorine species from chloride ions	Conc. = 39.8 mg L^{-1}, i = 6.53 mA cm^{-2}, urine, seawater, municipal WW (pH 8.0. Cl^- 18 mg L^{-1}, metal extract = 110 mg L^{-1}, peptone = 160 mg L^{-1}, urea = 30 mg L^{-1}, K_2HPO_4 = 28 mg L^{-1}, $MgSO_4 \cdot 7H_2O$ = 4.0 mg L^{-1}, Cl_2 = 0.90 mg L^{-1})	(i) RE (NaCl): ~70% in 20 min (ii) RE (seawater) ~100% in 60 min (iii) RE (WW) = 100% in 120 min (iv) RE (urine) = 100% in 180 min	Direct and indirect oxidation by active Cl and percarbonate to cleave piperazine ring	(i) ↑ed removal by ↑ed Cl^- and ↓ed nitrate (ii) pH effect on RE: 9 > 7.5 > 6.5 > 3	71
AMX	BDD	Non-selective, inert, large oxidation potential window	Conc. (COD) = 1–2 g L^{-1}, NaCl = 4 g L^{-1}, pH 3–9, i = 30–50 mA cm^{-2}	ME: 75% in 240 min	Indirect oxidation ($OH^{\bullet}$) *via* electrophilic attack on AMX	(i) ↑ed Cl^- ↑ed ME (ii) ↑ed treatment time ↓ed COD	84
SMX	BDD	Non-selective, inert, large oxidation potential window, and surface area = 189 cm^2	Synthetic WW ($NaHCO_3$ = 96 mg L^{-1}, NaCl = 7 mg L^{-1}, $CaSO_4 \cdot 2H_2O$ = 60 mg L^{-1}, urea = 6 mg L^{-1}, KCl = 4, $CaCl_2$ = 3 mg L^{-1}, $MgSO_4 \cdot 7H_2O$ = 125 mg L^{-1},	RE: 72.9% in 180 min	Indirect oxidation following pseudo-first-order kinetics. Oxidation is dominant than mass transfer	(i) Limited $^{\bullet}OH$ production (ii) ECs showed ↑ed removal than organic matter (iii) Limited influence of flow rate (iv) ↑temperature ↑degradation	58

Table 2 *(continued)*

Antibiotics	Working electrode	Features of electrode	Operational parameters	Removal % and recyclability	Reaction pathway	Remarks	Ref.
			NH_4 H_2PO_4 = 1.2 mg L^{-1}, meat extract = 22 mg L^{-1}, peptone = 32 mg L^{-1}), hospital WWTP effluent (COD = 78.4 mg O_2 per L), conc. = 0.5 mg L^{-1}, i = 5 mA cm^{-2}; Q = 125–500 L h^{-1}				
CPX, SMX	BDD	Non-selective, inert, large oxidation potential window	Conc. SMX = 15 mg L^{-1}, CPX = 23 mg L^{-1}, pH 7.84, K_2SO_4 = 1.74 g L^{-1}, i = 1.45–7.52 mA cm^{-2}, Q = 120–300 L h^{-1}	(i) RE (SO_4^{2-}): 100% in 250 min (ii) ME (SO_4^{2-}): 84–71% in 300 min (iii) RE (Cl^-): 100% in 240 min (iv) ME (Cl^-): 90% in 300 min	Non-selective reaction of $^{\bullet}OH$ indirect oxidation *via* addition to C–C, C–N, and C–S double bonds and H-abstraction	(i) $SO_4^{\bullet -}$ ↑ed removal (ii) Cl^- ↑ed ME under $i \approx i^0_{lim}$ (iii) ME ↓ed ($i/i^0_{lim} > 30$) (iv) No significant impact of common organics	67
AMX	BDD	Non-selective, inert, large oxidation potential window	Conc. (COD). = 1–2 g L^{-1}, NaCl = 4 g L^{-1}, pH 3–9, i = 30–50 mA cm^{-2}	ME: 75% in 240 min	Indirect oxidation ($OH^{\bullet}$) *via* electrophilic attack on AMX	(i) ↑ed Cl^- ↑ed ME (ii) ↑ed treatment time ↓ed COD	84
AMP	BDD Pt wire	Pt wire: good conductivity, inert and stable at high potentials, low oxygen evolution overpotential (1.6 V)	Conc. = 1.1 mg L^{-1}, SPS conc. = 100–500 mg L^{-1}, Na_2SO_4 = 14.2 g L^{-1}, i = 5–110 mA cm^{-2}	(i) RE (BDD): 68% in 10 min (ii) RE (Pt): 39% in 10 min	Indirect oxidation combines with non-radical electro-activation of SPS	(i) ↑ed removal with ↑ed persulfate conc. (ii) ↑ed current and ↓ed initial conc. (iii) No impact of bicarbonate (iv) 40% ↓ in humic acid (10 mg L^{-1})	85
NOFX	BDD	OER (2 V) ↑ed when boron doping ↑ed, ↑ed blockage of active sites with ↑ed boron doping (sp^2 carbon)	Conc. = 100 mg L^{-1}, Na_2SO_4 = 14.2 g L^{-1}, i = 10 mA cm^{-2}	RE: 80% in 120 min ME: 90% in 300 min	Mass transport controlled first-order reaction indirect oxidation	(i) ↑ed removal under mass transfer limitation (ii) No effect of pH and pK_a of NOFX	86
SMX	BDD	Non-selective, inert, large oxidation potential window	Conc. = 30 mg L^{-1}, Na_2SO_4 = 14.2 g L^{-1}, pH 7, i = 45 mA cm^{-2}	RE:100% in 60 min, ME: 73.8% in 360 min	Oxidation aided by $^{\bullet}OH$, resulting in the replacement and oxidation of NH_2 group and addition of OH group	(i) ↑ed removal with ↑ed current density (ii) No effect of pH (iii) ↑ed removal with Cl^- and SO_4^{2-} and ↓ed with nitrate and humic acid	75
SMX	BDD	Non-selective, inert, large oxidation potential window	Conc. = 10 mg L^{-1}, Na_2SO_4 = 1 g L^{-1}, NaCl = 0.4 g L^{-1}, NaBr = 0.71 g L^{-1}, I = 2.5 A	RE: 86.0% in 90 min with oxygen injection	Transformation and oxidation of functional moiety	(i) ↑ed oxidation in the presence of NaCl and NaBr (ii) ↑ed removal on oxygenation when Na_2SO_4 and NaBr are electrolyte (iii) No effect of pH	68

Table 2 *(continued)*

Antibiotics	Working electrode	Features of electrode	Operational parameters	Removal % and recyclability	Reaction pathway	Remarks	Ref.
TTC	(i) Pt (ii) BDD (iii) DSA ($Ti/RuO_2–IrO_2$)	$Ti/RuO_2–IrO_2$: relatively low O_2 evolution overpotential and chemisorption of radicals	Conc. = 100 mg L^{-1} Na_2SO_4 = 7.1 g L^{-1}, pH 4.3, I = 500 mA	(i) ME (Pt/carbon felt) 80% (ii) ME (BDD/carbon felt): 98% (iii) ME ($Ti/RuO_2–IrO_2$/stainless steel): 22% in 300 min	Direct and indirect oxidation assisted by $^{\bullet}OH$ and H_2O_2	(i) ME order: $Ti/RuO_2–IrO_2$/stainless steel (SS) < $Ti/RuO_2–IrO_2$/carbon-felt < BDD/carbon-felt (ii) Carbon-felt cathode ↑ed oxidation compared to SS	82
AMX	(i) Pt (ii) BDD (iii) DSA ($Ti/RuO_2–IrO_2$) (iv) Ti_4O_7	Ti_4O_7: high electrical conductivity at room temperature, good corrosion resistance and high chemical stability ($i > 5$ mA cm^{-2}), non-active electrode	Conc. = 19.6 mg L^{-1}, Na_2SO_4 = 7.1 g L^{-1}, pH ~ 5.7, I = 120 mA	(i) ME (Pt): 41% (ii) ME (BDD): 94% (iii) ME (DSA): 36% (iv) ME (Ti_4O_7): 69% in 480 min	Cleavage of the peptide bond followed by hydroxylation, dehydrogenation, and decarboxylation	(i) ME ↑ed with ↑ed current density (ii) ME order: BDD > Ti_4O_7 > DSA > Pt (iii) ME enhanced on the carbon-felt cathode (H_2O_2 production) (iv) ↑ed current (>120 mA), ↓ed ME for BDD due to recombination	87
NFZ, MNZ, CAP, FLO	Graphite fiber brush twisted with Ti wire		Conc. = 35 mg L^{-1}, phosphate buffer solution (PBS) = 20.57 g L^{-1}, potential = −0.15 to −1.25 V	(i) RE (NFZ): 94.7% (ii) RE (MNZ): 82.3% (iii) RE (CAP): 76.3% (iv) RE (FLO): 25.8% in 540 min at −0.45 V	Reduction of nitro group followed by dechlorination	(i) ↑ed cathode potential ↑ed the degradation efficiency (ii) ME order: NFZ > MNZ > CAP > FLO (iii) NaCl buffer solution and 0.002 M PBS, ↓ed ME of CAP and FLO	88
FZD	Graphite fiber brush twisted with Ti wire		Conc. 1–35 mg L^{-1} phosphate buffer solution = 20.6 g L^{-1} potential −0.15 to −1.25 V	RE: 93.9% in 540 min at −0.45 V	Reduction of the nitro group and destruction of furan and oxazole ring	(i) ↑ed cathode potential and conc. ↑ed the degradation efficiency (ii) RE in electrolyte: $Na_2CO_3–NaHCO_3$ < PBS < NaCl	89

RE: removal efficiency, ME: mineralization, RC: recyclability, ↑ – increase, ↓ – decrease, SEC: specific energy consumption.

in accomplishing higher mineralization efficiency for antibiotics. Nevertheless, the degradation of antibiotics under mass transfer limitations is non-selective.[101] In a nutshell, the mineralization efficiency of the BDD electrode is highly dependent on the physicochemical properties of the antibiotics and experimental (*e.g.*, applied current density) and kinetic (*e.g.*, mass flow between the electrodes) parameters. The non-selective degradation of antibiotics and the undetermined fate of the BDD electrode after use might raise the question of the ecotoxicity of the end products. Hence, with the high cost and described technical gaps, the application of BDD as a reliable electrochemical treatment system for antibiotics is limited.

3.4.3. Carbon-based electrodes. Carbon-based electrodes (*e.g.*, graphite and graphene) have the potential to act as a robust anode and cathode for oxidative and reductive degradation of recalcitrant pollutants. The excellent conductivity of graphite and a large number of delocalized electrons allow its direct use as an electron donor in electrochemical reactions.[102] Likewise, the symmetrical honeycomb structure of graphene provides efficient electron transfer, making it suitable for oxidation and reduction reactions.[103] The withstandability of the graphene electrode at higher current densities is superior to that of commonly used metal electrodes (six order higher than copper). Accordingly, an attempt was made to understand the reductive degradation efficiency of graphite fiber brushes as the cathode for degrading chloramphenicol (CAP), nitrofurazone (NFZ), metronidazole (MNZ), furazolidone (FZD), and florfenicol (FLO).[88,89] For efficient reductive degradation, the conversion of the nitro group to amine and dehalogenation is essential. Consequently, the degradation efficiency of >95% at −0.95 V under neutral conditions was reported for all the selected antibiotics.[88] It was demonstrated that FZD could be reduced at −0.15 V into 3-(5-hydroxylaminefurfurylideneamino)-2-oxazolidinone (HOAM), 3-(5-aminefurfurylideneamino)-2-oxazolidinone (AMF), and the N–N fraction product (5-nitro-2-furyl) methenamine

(NFM). However, alleviated negative cathode potential assisted in the faster and complete degradation of FZD with hydrogen evolution as a side reaction. For instance, at a cathode potential higher than −1.25 V, 98.8% degradation, 97.4–100% mineralization, and complete inhibition of antibacterial activity were achieved in 540 min.[89]

When the reductive degradation efficiency of NFZ, MNZ, CAP, and FLO was tested, NFZ initiated degradation at a much lower potential (−0.15 V, degradation 84.9% in 540 min) than the other three antibiotics (−0.3 V, degradation 59.3–10.2% in 540–720 min). The presence of the nitro group on the furan ring and the N–N on the side chain of NFZ allowed degradation at a much lower cathode potential. The cathode potential of ≤0.8 V was recommended to ensure the decolorization of NFZ and production of linear chain end products ([[(5-hydroxyamino-2-furyl)-methyl]-hydrazinecarboxamide (AMH), [(5-amino-2-furyl)-methylene]-hydrazinecarboxamide (AMN), 5-hydroxy-cadaverine, 5-amino-pentanamide, and NFM). For the degradation of CAP, the end products included nitroso product (NO), aromatic amine product (AMCl2), and dechlorinated AMCl2 products (AMCl and AM), while for FLO, various dehalogenated end products were obtained. When the cathode potential was higher than −0.45 and −0.75 V for CAP and FLO, respectively, degradation efficiency was significantly reduced to 44.3% and 25.8%.[88] This could be due to steric hindrance in hydro dehalogenation for the second or third halogen atom in CAP and FLO at higher cathode potential. Thus, the potential in the range of −0.95 to −1.25 V was recommended. The degradation of MNZ was followed by the formation of 2-methyl-5-amineimidazole-1-ethanol as a non-toxic amine end product at the applied potential range of −0.3 to −1.25 V.[88] The relative ease of degradation of MNZ can be attributed to the reactive N-containing group. Overall, the cathodic reducibility followed the order NFZ > FDZ > MNZ > CAP > FLO. The primary parameter for efficient cathodic reduction is the continuous supply of electrons, which is governed by the nature of the electrode and the applied potential. Though the lower reduction potential seems to be a feasible option for complete degradation of the pollutant, the increased energy consumption and the stability of the electrode are the two crucial parameters that need to be understood before practical use.

Another advantage of the carbon electrode over BDD or the DSA is its use as both a cathode and an anode. For instance, the surface properties such as surface defects and functional groups (*e.g.*, carbonyl (C═O), hydroxyl (–OH), and phenolic (–C_6H_5)) in graphene make it apt for oxidative degradation.[104] The hydrophilic functional groups enhance the charge transfer between the electrode and the adsorbed water molecules.[105] Consequently, the generated $^{\bullet}$OH is a prominent reactive species in the graphene-based oxidative electrochemical system. This efficacy of graphene and graphite for oxidative degradation has been verified for SFX with 100% and 76% removal in 180 min, respectively, *via* indirect oxidation.[80] The difference in removal between graphene and graphite is mainly due to the lower

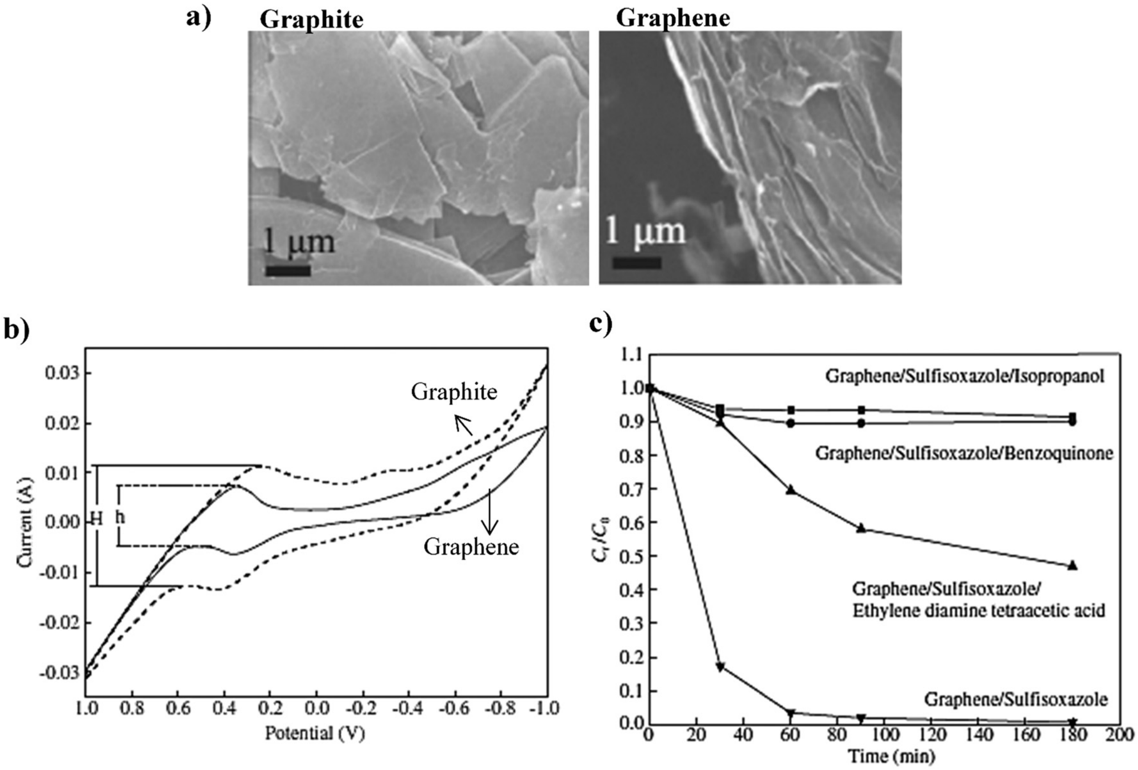

Fig. 4 Structural advantages of graphene (a) in the electrochemical oxidation of SIZ (b and c). Reprinted with permission from ref. 80. Copyright 2016, Elsevier.

competence of the graphite electrode to oxidize H_2O_2 and H_2O (eqn (31)–(33)) which restricts the production of $^{\bullet}OH$ and $O_2^{\bullet-}$ in comparison with graphene.

$$H_2O + e^- \rightarrow {}^{\bullet}OH + H^+ \tag{31}$$

$$2^{\bullet}OH \rightarrow H_2O_2 \tag{32}$$

$$H_2O_2 + e^- \rightarrow O_2^{\bullet-} + H^+ \tag{33}$$

Furthermore, graphite possesses elevated structural functionalities and capacitance (*e.g.*, fold morphology and −0.005 to 0.005 A) than graphene (*e.g.*, layered structure and −0.01 to 0.01 A). This indirectly implies that graphene is a better electrode material than graphite (Fig. 4a and b).[106] Apart from its superior activity in the degradation, graphene was also found to have excellent recycling ability (5 cycles with 100% removal efficiency). Overall, graphene can be readily used to degrade N- and S-functionalized antibiotics with greater confidence (Table 2). However, only a limited number of studies related to the electrocatalytic ability of graphene have been conducted so far. It opens up a platform for researchers in the area of graphene/graphite technology to conduct intensive research about the factors controlling the degradation of antibiotics using low-cost carbon materials (*e.g.*, graphene).

To this end, the performance abilities of BDD and DSA electrodes are almost well understood in terms of process parameters (*e.g.*, current density, electrolyte, reaction mechanism, *etc.*). The use of graphene as an electrode is not well established; thus, it requires further investigation. In terms of cost, the DSA is a better material compared to BDD; however, etching of Ti support due to corrosion needs to be encountered. Likewise, the high cost of BDD can be overwhelmed by its superior performance at low current density (mass transfer limitation), but this is not a competent way to attain complete mineralization of specific antibiotics. Incorporating a suitable catalyst or dopant for the modification of the electrode is desirable for extending the lifetime of the electrode, selectivity towards end products, and higher mineralization efficiency. The following section offers a detailed description of the so-far tested catalysts for improving conventional/traditional electrodes (*e.g.*, BDD, DSA, PbO_2, and graphene/graphite) to treat antibiotics.

4. Oxidative electrocatalysis

Electrocatalytic oxidation describes an electrolytic reaction at the anode assisted by catalysts in the solid phase (coated/impregnated on electrodes) that act as both electron donor/acceptor.[77] Thus, the anode material plays a vital role in electrochemical oxidation. In this regard, traditional anodes are often decorated with catalysts such as metal or carbon-based materials. The modification of the well-known electrodes (*e.g.*, PbO_2, Ti, graphite, and carbon nanotubes (CNTs)) with metals (Cu, Mo, Co, Ce, and Ru) enhances the surface roughness and functionalization. This heterogeneity also reduces the OEP of the reaction and improves the reaction kinetics, selectivity, and efficiency.[48] Additionally, issues such as higher energy requirements, high cost of operation, and the formation of undesirable by-products can be tackled. Various functionalization/modification strategies of the catalysts have been tested to improve the performances of previously described anodes. Also, operational factors, such as applied potential and the presence of coexisting ions, invariably affect the efficiency of the processes and the stability of the catalyst (Table 3). Hence, the following sections discuss the efficacy of incorporating the catalyst on the electrode to degrade antibiotics successfully.

4.1 Modified Ti electrodes

A durable electrode material such as the DSA (*e.g.*, Ti/RuO_2) with relatively higher oxygen evolution potential (~2 V) provides an option to tackle the common challenges of the PbO_2 electrode (*e.g.*, acidic operational conditions and brittleness). For instance, Ti/RuO_2 degraded ~80% OFX in 30 min in synthetic WW at neutral pH. The dominant reactive species involved in the indirect oxidation were $^{\bullet}OH$, $HO_2^{\bullet}$, HOCl, and ClO^- (ref. 107) (as discussed in sections 3.3 and 3.2). However, the poor mineralization efficiency (46.3%) due to restricted oxidation by H_2O_2 and $HO_2^{\bullet}$ questions the environmental compatibility of the electrode.[76,129] Thus, identifying a catalyst with high mineralization capability to obtain treated effluents with less toxicity is crucial. In this line, SnO_2 has been tested as a dopant owing to its superior catalytic activity, ease of combination with Ti, and adequate electrical conductivity.[130] It should be noted that the low conductivity of pristine SnO_2 limits its direct application in water/WW treatment.[131] Thus, multi-metal doping *via* Sb, Ce, and La increases the conductivity and OEP by forming cracks/crystal defects in the electrodes.[109] For instance, SnO_2–Sb/Ti was effectively exploited as an electrocatalyst to completely degrade (99.5% in 120 min) CPX (50 mg L^{-1}) with moderate current density of 30 mA cm^{-2}.[108] The achieved higher efficiency was due to the uniform distribution of Sb on SnO_2 which increased the mass transfer diffusion.[110] It should be noted that under higher current density (100 mA cm^{-2}), SnO_2–Sb becomes unstable, leading to inevitable leaching.[132,133] Thus, it is highly recommended to optimize the applied potential over SnO_2–Sb/Ti prior to its application as an electrocatalyst for degrading antibiotics.

Other than the structural defects created by the co-dopant (Sb) in Ti electrodes, the high oxygen evolution overpotential of metals such as Ce (3.14 V) leads to improved electrocatalytic activities.[109] Precisely, doping of Ce into SnO_2–Sb/Ti induces an additional energy band, which in turn constructs expedient channels for electron transfer.[134] This kind of electronic characteristics aided good removal (72.4%) and mineralization (41.6%) efficiency for TTC.[109] The two main demerits of Ce–SnO_2–Sb/Ti are the limited formation of active sites[109] and the complex synthesis of catalysts tagged

Table 3 Summary of oxidative electrocatalysts for antibiotic removal

Antibiotics	Working electrode		Structural properties of electrocatalyst	Features of electrodes	Operational parameters	Removal % and recyclability	Degradation mechanism	Remarks	Ref.
	Support	Catalyst							
(a) Electrocatalysts for Ti electrodes									
OFX	Ti	RuO_2	Porous and uniform coating	Increase OEP (~2 V)	Conc. = 50 mg L^{-1}, NaCl = 1 g L^{-1}, pH = 6.8, I = 1 A	RE: ~80% in 30 min, MET: 46.3% in 240 min	Defluorination, breaking of piperazinyl ring, dealkylation	(i) ↑ in current ↓ ME (ii) ↑ in current ↑ in k_f (iii) ↑ in NaCl ↑ RE	107
CPX	Ti	SnO_2–Sb	SnO_2 laminated the Ti surface	Uniform distribution of Sb increased mass transfer diffusion	Conc. = 50 mg L^{-1}, H_2SO_4 = 49 g L^{-1}, pH 5.4, i = 30 mA cm^{-2}	RE: 99.5% in 120 min, MET: 70% in 120 min	Oxidation of piperazine ring, hydroxylation of quinolone moiety, defluorination	(i) ↑ in conc. ↓ RE (ii) ↑ in current ↓ in k_f (iii) pH had no effect	108
TTC	Ti	SnO_2–Sb–Ce	Nano-hollow sphere morphology	Increase in OEP (3.14 V) and conductivity	Conc. = 5 mg L^{-1}, Na_2SO_4: 14.2 g L^{-1}, i = 20 mA cm^{-2}	RE: 72.4% in 120 min, MET: 41.6% in 120 min	Hydroxylation, deamination followed by ring-opening	(i) ↑ in conc. ↓ RE (ii) Limited formation of active sites at higher electrodeposition	109
CFD	Ti	SnO_2–Cu	Uniformly distributed porous matrix	Cu enhanced physisorption of $^{\bullet}OH$ on SnO_2; Cu increased OEP to 2.1 V	Conc. = 1 mg L^{-1}, Na_2SO_4: 1 g L^{-1}, pH 3.4, i = 20 mA cm^{-2}	RE: 97.5% in 60 min, MET: 41.6% in 60 min	7-Aminocephalosporanic acid, breaking of the beta-amide ring, mineralization	(i) p-type semiconductor (ii) Cu overcomes the recombination of electron–hole of Ti	110
(b) Electrocatalysts for PbO_2 electrodes									
CAP	PbO_2	Al	Uniform distribution of Al decreased leaching of Pb	Improves stability; minimizes leaching of Pb	Conc = 500 mg L^{-1}, Na_2SO_4 = 28.4 g L^{-1}, pH 3, i = 30 mA cm^{-2}	RE: 87.3% in 150 min, MET: 52.1% in 150 min RC: 8 cycles 4.1% reduction	Radical reaction, ring-opening, and mineralization	Optimum electrodeposition ratio for Al/Pb is 1%	66
AMX	PbO_2	Cu	Smaller crystal size results in more active sites; more $^{\bullet}OH$ generation	Low cost; higher OEP	Conc. = 100 mg L^{-1}, Na_2SO_4 = 14.2 g L^{-1}, pH 3.5, i = 30 mA cm^{-2}	RE: 99.4% in 150 min, MET: 46.3% in 150 min RC: 8 cycles 4.1% reduction	Ring-opening and mineralization	Higher current density of 100 mA cm^{-2} limits the application	111
LVFX	PbO_2	La–Y	Lanthanide contractions enhanced the reaction rate	↑ed production of $^{\bullet}OH$	Conc. = 800 mg L^{-1}, Na_2SO_4 = 14.2 g L^{-1}, pH 3, i = 30 mA cm^{-2}	RE: 97.2% in 150 min, MET: 38.4% in 150 min	Piperazinyl hydroxylation, decarboxylation, and defluorination	Contribution of Y was better than La	112

Table 3 *(continued)*

	Working electrode								
Antibiotics	Support	Catalyst	Structural properties of electrocatalyst	Features of electrodes	Operational parameters	Removal % and recyclability	Degradation mechanism	Remarks	Ref.
ENF	Ti/PbO_2	SnO_2–Sb–La	La increased the electron mobility	Synergy from multiple ions increased TOC removal	Conc. = 10 mg L^{-1}, Na_2SO_4 = 2.84 g L^{-1}, i = 8 mA cm^{-2}	MET: 95.1% in 30 min	Decarboxylation, the substitution of –COOH by –OH, cleavage of quinolone and piperazine rings	Energy cost (2.1 W h L^{-1})	73
SMX	Ti/PbO_2	Sb_2O_3–SnO_2/Er	Er substitutes Pb in lattice point defects	Increase OEP 1.78 V; point defects promote $^{\bullet}$OH and sulfate radicals	Conc. = 10 mg L^{-1}, Na_2SO_4 = 2.84 g L^{-1}, i = 10 mA cm^{-2}	RE: 100% in 20 min, MET: 63.2% in 180 min	Hydroxylation, cleavage of S–N bond, isoxazole ring-cleavage	90% SMX degradation, 0.58–8.97 W h L^{-1} energy consumption	113
IMD	Ti/PbO_2	Terbium (Tb)	Doping of Tb ↑ed the mechanical stability by suppressing e^-–h^+ recombination	Increase OEP, stability and conductivity	Conc. = 1 mg L^{-1}, NaCl = 7 g L^{-1}, pH 9, i = 8 mA cm^{-2}	RE: 76.1% in 150 min, MET: 70.1% in 180 min, RC: 10 cycles 8.6% reduction	Cleavage of imidazoline ring, chlorination, dechlorination, and ring-opening	Energy cost: 0.27kW h kg COD^{-1}	114
MNZ	PbO_2	Carbon black	Carbon ↑ed interaction of water molecules	Higher conductivity led to ↑ed $^{\bullet}$OH	Conc. = 200 mg L^{-1}, Na_2SO_4 = 14.2 g L^{-1}, pH 8.2, i = 20 mA cm^{-2}	RE: 91.8% in 120 min, MET: 70.1% in 180 min RC: 8 cycles 8.6% reduction	Hydroxylation followed by ring-opening	No leaching after 180 min	115
(c) Electrocatalysts for carbon electrodes									
CFT	Nanographite	SnO_2–TiO_2	Particles in the range of 5–15 nm was uniformly dispersed, ↓ed resistance	TiO_2 and SiO_2 laminated the surface of NG	Conc. = 10 mg L^{-1}, Na_2SO_4 = 14.2 g L^{-1}, pH 7.7, potential = 2 V	RE: 98.7% in 120 min	Hydroxylation and ring opening	SnO_2–TiO_2–NG > TiO_2/NG (97.7%) > NG (81.8%)	116
CFT	Nanographite	RuO_2–TiO_2	Mesoporous and has large surface area, low charge transfer resistance	TiO_2 gives stability and anti-fouling; RuO_2 increases conductivity	Conc. = 10 mg L^{-1}, Na_2SO_4 = 14.2 g L^{-1}, potential = 2 V	RE: 97.5% in 60 min, MET: 44.7% in 120 min RC: 15 cycles and 3.2% reduction	Hydroxylation and ring-opening	(i) RuO_2 decreases charge transfer resistance (ii) Cost of Ru needs to be encountered	117
TCH	CNT	Agarose–In_2O_5Sn	Coating of agarose yielded uniform morphology and helped in $O_2^{\bullet-}$ production	(i) Large surface area and pi–pi interactions increase catalytic action (ii) CNT acts as a good adsorbent	Conc. = 10 mg L^{-1}, potential = 4 V	RE: 96% in 30 min, MET: 82.1% in 180 min RC: 4 cycles 12% reduction	Ketone formation from –N$(CH_3)_2$, demethylation	Toxic intermediates were produced	118

Table 3 *(continued)*

Antibiotics	Working electrode		Structural properties of electrocatalyst	Features of electrodes	Operational parameters	Removal % and recyclability	Degradation mechanism	Remarks	Ref.
	Support	Catalyst							
CFD	Nanographite	MoO_3	Sesame cake-like structure ↑es ROS production; octahedral structure enhanced charge transfer	Improved conductivity; prevents agglomeration	Conc. = 10 mg L^{-1}, Na_2SO_4 = 14.2 g L^{-1}, pH 3.4, potential = 2 V	RE: 99.9% in 60 min, MET: 82.1% in 180 min RC: 10 cycles	7-Aminocephalosporanic acid, breaking of the beta-amide ring, mineralization	>10 cycles electrocatalytic activity ↓es	119
CFD	CNT	La_2O_3–CuO_2	La improves mesostructure; Cu increase (OEP)	Anti-corrosion; acts as electron acceptor; CNT acts as electron donor	Conc. = 1 mg L^{-1}, Na_2SO_4 = 1 g L^{-1}, pH 6.8, i = 0.8 mA cm^{-2}	RE: 90% in 30 min, RC: 10 cycles (∼90%)	7-Aminocephalosporanic acid, breaking of the beta-amide ring, mineralization	Close observation recommended in the mineralization stage of the β-lactam ring	120
CFD	Multiwalled CNT	Ce	Large surface area, lightweight; compact morphology	↑ed corrosion resistance	Conc. = 1 mg L^{-1}, Na_2SO_4 = 1 g L^{-1}, pH 6, i = 3 mA cm^{-2}	RE: 100% in 60 min	Decarboxylation and hydrolysis	(i) Degradation was irreversible (ii) Highest current efficiency	121
CFD	Graphite/CNT	PbO_2–Ce	Enhanced life span *via* morphological modification	Increase OEP (2.4 V); increase in $^{\bullet}$OH radical	Conc. = 50 mg L^{-1}, Na_2SO_4: 7.1 g L^{-1}, i = 3 mA cm^{-2}	RE: 100% in 120 min, MET: 54.2% in 120 min RC: 10 cycles 2% reduction	Carboxylation, decarboxylation, radical reaction, ring opening, and mineralization	Cl^- ions accelerated catalytic behaviour	122
CFD	CNT	CeO_2–ZrO_2–TiO_2	Regular distribution of ZrO_2 and CeO_2 increased $^{\bullet}$OH formation	TiO_2 increased strength; CeO_2–ZrO_2 increase in $^{\bullet}$OH	Conc. = 1 mg L^{-1}, Na_2SO_4 = 1 g L^{-1}, pH 10, i = 3 mA cm^{-2}	RE: 83.5% in 120 min, RC: 10 cycles 17% reduction	Carboxylation, decarboxylation, radical reaction, ring-opening, and mineralization	(i) Complete removal at 4 mA cm^{-2} (ii) Best result	123
(d) Electrocatalysts for other electrodes									
STZ	Ni foam	N doped C	Introduction of CN decreased resistance 4.8 times	Improved cathode performance results in 13.8 times higher current efficiency and H_2O_2 accumulation	Conc. = 50 mg L^{-1}, Na_2SO_4 = 50 mM, pH 3, i = 10 mA cm^{-2}, Q (air) = 500 mL min^{-1}	RE: 100% in 180 min, MET: 90% in 180 min RC: 5 cycles 0% reduction	Hydroxylation of a benzene ring and substitution of the amino group, cleavage of S–C and S–N bonds, ring--opening, mineralization	5.2 times ↓ed energy consumption	124
CFD	Partly graphitized carbon (PGC)	Co_9S_8	Existence of Co^{2+}/Co^{3+} in PGC skeleton ↑ed hydrophilicity	ORR catalyst; fast electron transfer	Conc. = 50 mg L^{-1}, Na_2SO_4 = 14.2 g L^{-1}, pH 5, i = 30 mA cm^{-2}	RE: 99.9% in 240 min, MET: 84.3% in 480 min	Carboxylation, decarboxylation, radical reaction, ring opening, and mineralization	Particle size in the range of 10–20 nm results in better production of $^{\bullet}$OH	125

Table 3 *(continued)*

Antibiotics	Working electrode		Structural properties of electrocatalyst	Features of electrodes	Operational parameters	Removal % and recyclability	Degradation mechanism	Remarks	Ref.
	Support	Catalyst							
CAP	Al_2O_3 (particle electrodes)	Ti–Sn–Sb	Synergy between Ti, Sn, and Sb developed strong $^{\bullet}OH$ generation	SnO_2 has high catalytic action; Sb enhances this by defects	Conc. = 100 mg L^{-1}, pH 6, $i = 0.5$ mA cm^{-2}, $Q = 1$ L min^{-1}	RE: 92% in 180 min, ME: 41% in 180 min	Hydroxylation, dehydroxylation, breaking of the amide group, ring opening, and mineralization	Ring opening was found to be an evident step	126
TTC	Al_2O_3 (particle electrodes)	Bi–Sn–Sb	Formed triclinic Bi_2O_3 (3D) particles pose greater catalytic activity	SnO_2 has high catalytic action; Sb enhances this by defects	Conc. = 100 mg L^{-1}, pH 5.9, $I = 0.1$ A	RE: 86% in 180 min	Hydroxylation, deamination followed by ring opening	Increase in the initial concentration limits the active sites in the electrode	127
CPX	SnO_2	Sb	Compact arrangement of nanoparticles (50–200 nm)	Larger electrochemical area (3.74 cm^2) offered OEP 2.2 V	Conc. = 1 mg L^{-1}, $Na_2SO_4 = 1$ g L^{-1}, pH 3, $i = 8$ mA cm^{-2}	RE: 100% in 60 min, MET: 93% in 90 min	Defluorination, destruction of piperazine ring of quinolones	Higher number of coatings (minimum 16 coatings) required	128

TCH: tetracycline hydrochloride, RE: removal efficiency, RC: recyclability, ME: mineralization efficiency, MET: mineralization TOC efficiency, ↑ – increase, ↓ – decrease, ORR: oxygen reduction reaction, OEP: oxygen evolution potential.

with the higher chemical cost. Accordingly, Ti/SnO_2–Cu with the OEP of 2.1 V was fabricated.[110] The addition of Cu instead of Sb in the Ti/SnO_2 electrode yielded a highly coarse, porous, and 3D structure with uniform distribution of active layers.[110] Subsequently, interparticle charge transfer was imminent due to the local distortion in the Ti crystals.[135,136] Ultimately, oxygen adsorption of Ti/SnO_2–Cu (38.7%) was far better than that of Ti/SnO_2–Sb (13.7%), with 90% removal of CFD in 60 min. This distinguishing value of Ti/SnO_2–Cu clearly indicates that during the electrooxidation, $^{\bullet}OH$ has a more significant impact than electro-incineration (absorption of the electron by antibiotics on the surface of the electrode).

Overall, it could be established that the non-active electrodes play an imperative role in the degradation of antibiotics. The prerequisite structural investigation based on the nature of the target is vital for achieving higher mineralization efficiency. The p-block and f-block elements offer a broad paradigm to create permanent defects/cracks and oxygen storage spaces in the Ti support. Accordingly, the external surface area of the electrode directly assists a rise in OEP. Nonetheless, prolonged synthesis procedures with diverse methodologies in the multiple doping electrode systems (*e.g.*, Ce–SnO_2–Sb/Ti (ref. 109)) lead to complexity in practical applications. In addition, the main purpose of using a dopant/catalyst on the surface of Ti is to avoid the electron–hole recombination phenomenon by properly shielding the exposed area of Ti. This is because the electrons present in the electron–hole pairs help create new oxidation centers on the TiO_2 surface, which increases the catalytic property of the composites.[137] Therefore, proper coating methods are necessary to cover the Ti surface effectively; otherwise, leaching of the catalyst (Ce/Cu/Si/SnO_2) may quickly affect the inherent property of the Ti support (increased rate of corrosion or decreased life span). Commonly, deactivation of electrodes is accompanied by catalyst detachment, metal substrate passivation, catalyst consumption, and structural damage under prolonged usage.[114,138] Thus, identifying the capability/durability of the catalyst is essential prior to upscaling.

4.2 Modified PbO_2 electrodes

The simplicity and excellent oxidation ability of PbO_2 have attracted attention for its use to degrade antibiotics in water and WW systems. However, inhibition of the catalytic activity of PbO_2 under acidic conditions is found to be the major constraint. Thus, applying modifiers (*e.g.*, Ti and Al) as an active layer on the surface to avoid leaching has been investigated.[111] However, the latter modifications are not satisfactory for removing larger complex molecules (*e.g.*, antibiotic).[83] Thus, doping with materials of superior electronic characteristics (*e.g.*, transition metals and lanthanides) and low cost (*e.g.*, carbon black) is being preferred. Likewise, depending on the nature of antibiotics, different combinations of dopant (bi, tri, or tetra) are hosted on the surface of PbO_2. For instance, the utilization of Al^{3+} as a dopant contributed a considerable increment in $^{\bullet}OH$ production.[66] Subsequently, 87.3% removal in 150 min at a high concentration of CAP (500 mg L^{-1}) was obtained. Though the efficiency of Al–PbO_2 is satisfactory, the presence of insufficient active sites in an anodic region resulted in low mineralization efficiency (52.1% in 150 min). Thus, doping of Cu has been verified owing to its superior conductivity (Cu is $5.9 \times 10^5\ \Omega^{-1}\ cm^{-1}$) than Al ($3.8 \times 10^5\ \Omega^{-1}\ cm^{-1}$), smaller crystal size (33 nm), and effective surface areas (PbO_2 and Cu–PbO_2 were 2.81 and 2.91 cm^2).[111] Cu–PbO_2 demonstrated higher removal of AMX (99.4% in 150 min at i = 30 mA cm^{-2}) with excellent recyclability (8th cycle – 4.1% reduction). The major limitation of Cu–PbO_2 was the conversion of $^{\bullet}OH$ into H_2O_2 at higher current density (up to 100 mA cm^{-2}), which adversely affected the mineralization efficiency (46.3% in 150 min).[139,140] In order to increase the mineralization efficiency of Cu–PbO_2, two methods can be employed: (i) using an appropriate current density to prevent the conversion of $^{\bullet}OH$ into H_2O_2 and (ii) addition of a catalyst (*e.g.*, TiO_2 nanosheets) to convert H_2O_2 into $O_2^{\bullet-}$. The TiO_2 nanosheets are known to develop $O_2^{\bullet-}$ from H_2O_2 by external energy (*e.g.*, current density, heat, light).[141] Therefore, co-doping of TiO_2 nanostructures with Cu–PbO_2 may help solve the issues related to the lower mineralization and conversion of $^{\bullet}OH$ into H_2O_2.

The unique outer electronic configuration of rare earth elements such as La, Y, and Tb has also been used to stimulate the electrochemical properties of the PbO_2 electrode. For example, PbO_2 modified with La and Y resulted in outstanding performance for LVFX degradation (PbO_2 (83.3%), Y–PbO_2 (90.9%), La–PbO_2 (85.6%), and La–Y–PbO_2 (95.4%)).[112] To achieve better degradation efficiency, the pH of the system was maintained at 3 (97.2%). This is positively related to the ionic characteristics of LVFX at different pH (*e.g.*, pH <5.7: cationic, $5.7 < 7.9$: zwitterionic, >7.9: anionic). This excellent performance of lanthanide catalysts was mainly due to lanthanide contractions and the spin–orbit coupling phenomenon.[142] Moreover, the combination of Y and La created synergy in the electronic levels of composite (La–Y–PbO_2) and enhanced overall electrical conductivity, ultimately increasing the degradation efficiency. Careful observation on the degradation performances between Y and La indicates that the contribution of Y (90.9%) was higher than that of La (85.6%) in La–Y–PbO_2 for the degradation of LVFX.[112] This might be due to the relatively lower electrical conductivity of La ($1.6 \times 10^4\ \Omega^{-1}\ cm^{-1}$) than Y ($1.8 \times 10^4\ \Omega^{-1}\ cm^{-1}$).[143] In addition, the uniform distribution of lanthanides enhances the roughness of PbO_2 and eventually decreases the chance of instant brittleness.[144]

Composite electrodes made up of Ti/SnO_2–Sb/La–PbO_2 have also been reported to achieve higher TOC (95.1% in 30 min) and defluorination rates (95.3% in 8 min) for FQs.[73] The obtained higher mineralization and formation of less toxic end products (*e.g.*, CO_2, H_2O, NO_3^-, and F^-) were better than selective $^{\bullet}OH$ oxidation of FQs using permanganate(VII)[145] and ferrate(VI).[146] In continuation, Ti/SnO_2–Sb/Er–PbO_2 was also employed to degrade complex (N- and S-functionalized) antibiotics (*e.g.*, SMX).[113] The well-known electrocatalytic ability of Er helped to achieve 62.3% removal of TOC and 22.4% and 98.8% removal of N and S in

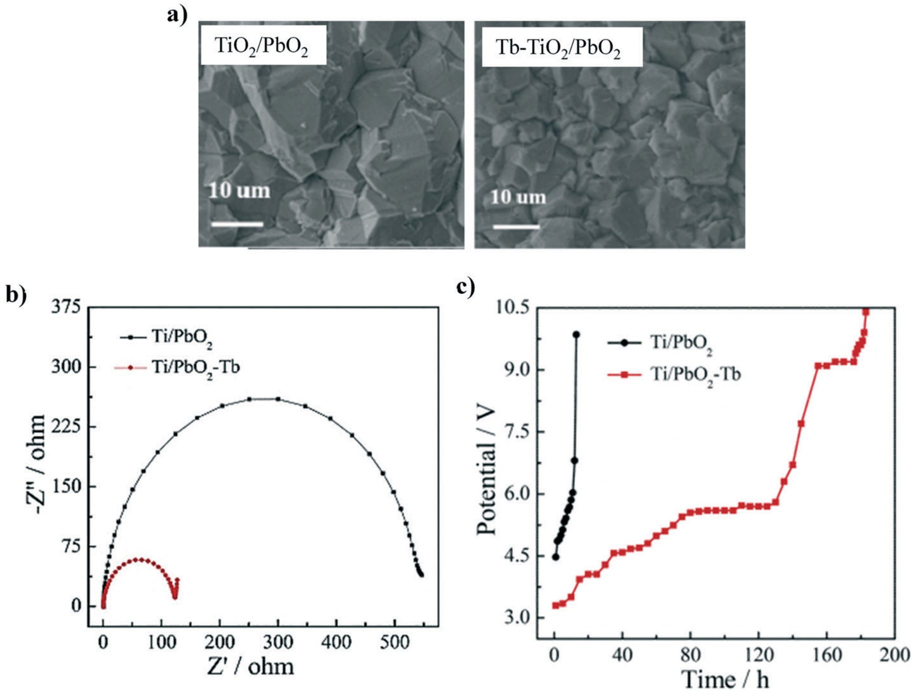

Fig. 5 Morphological (a) and electrochemical (b and c) properties of Tb–Ti/PbO_2. Reprinted with permission from ref. 114. Copyright 2020, Elsevier.

the form of NO_3^- and SO_4^{2-}, respectively.[113] The distinctive behaviour of the electrode over other La-based dopants is due to its ability to simultaneously degrade the metabolite of SMX (acetyl-sulfamethoxazole (Ac-SMX)). It is worth saying that the obtained rate constant (0.268 min^{-1}) and electric energy consumption (0.58–8.97 W h L^{-1}) to degrade SMX were approximately four times lower than that of Ac-SMX (6.88–44.2 W h L^{-1}). This clearly emphasizes the obscurity involved in the complete degradation of recalcitrant pollutants like SMX. Also, it defines the need for tracking the destructive behaviour of the metabolite and the mineralization of the parent compound. Apart from enhancing electron mobility, lanthanides have also been utilized to increase the mechanical stability of PbO_2. The composite electrode Tb–Ti/PbO_2 was able to degrade (76.1%) imidacloprid (IMD) because of higher OEP (2.82 V). The doping of Tb into PbO_2 suppressed the electron–hole recombination of Ti by shielding the exposed area of Ti with pyramid-like microparticles (Fig. 5a).[114] This uniform coating of Tb also favourably altered the crystalline orientation of PbO_2 (*e.g.*, diffraction peak changed from the (211) to the (110) plane). Consequently, enhanced electrochemical properties,[147,148] reusability (67.5% after 10th cycle), and extended service lifetime (Tb–Ti/PbO_2: 183 h and Ti/PbO_2: 13 h) were obtained (Fig. 5b and c).[114] Thus, Tb served as the best co-dopant among other lanthanides for PbO_2 modification.

Though the electrocatalytic performance of metal- and lanthanide-doped PbO_2 is significant, the ecotoxicity effect of spent catalysts is a major problem.[149] In this regard, eco-friendly materials as a dopant have been verified. Wang *et al.*[115] studied the degradation of MNZ on PbO_2 using conductive carbon black as a modifier. The low electrical resistance, nontoxic nature, strong interface performance, and stable structure of conductive carbon black made it a preferable choice compared to metal oxides and rare earth metals.[150] The improved direct electron transfer rate *via* carbon black resulted in 91.8% MNZ removal in 120 min with excellent recyclability (87.5% after the 8th cycle).[115] Along with the high electrical conductivity, elevated $^{\bullet}OH$ generation at the surface due to the exclusive interaction of the water molecules with active sites (carbon) resulted in the outstanding behaviour of the electrode.[115] After electrolysis of C–PbO_2 over 180 min, the leaching test indicated the absence of toxic heavy metal (*e.g.*, Ti, Sb, and Sn) in the spent solution. Also, the detected dissolved concentration of Pb^{2+} was 0.008 mg L^{-1}, which is within the World Health Organization (WHO) permissible value (0.01 mg L^{-1}). This indicates the possible application of environmentally friendly materials to augment the stability and efficiency of the parent electrode and counter toxic end product formation.

Overall, the modification in the traditional PbO_2 electrode with metal oxide and rare earth metal opens up the opportunity to tackle poor stability, low oxidation evolution potential, poor mineralization efficiency, and reusability. However, the requirement of highly acidic conditions (pH ~3) raises the question about electrode compatibility in real applications. The correlation between the properties of antibiotics and catalysts at different pH conditions has not been thoroughly studied yet. Such progress is vital from the perspective of fabrication of the material and the application of the designed electrode in actual WW treatment.

4.3 Modified carbon electrodes

The surface functionality of the electrode plays a key role in the anodic electrocatalysis reaction. Considering this, extensive work has been carried out on various carbon materials such as graphite, graphene, or CNT in the field of electrochemistry. However, the lower OEP (1.7 V) of graphite/graphene limits their pristine application in the electrocatalysis process.[151] Hence, several metal oxide dopants such as RuO_2, SnO_2, and TiO_2 have been investigated to increase the electrode's potential window, *e.g.*, the oxygen evolution overpotential of SnO_2–TiO_2 and TiO_2–RuO_2 is 1.9 V and 2 V, respectively.[107,152] The doping of metal oxides enhances the $^{\bullet}OH$ production *via* activation of H_2O molecules. Hence, embedding these metal oxides into nanographite enriches its electrocatalytic activity towards antibiotics. As proof of this, Guo *et al.*[116] reported 98.7% degradation efficiency (120 min) for CFT using SnO_2–TiO_2/nanographite as the anode. Similarly, the RuO_2–TiO_2/nanographite-based electrode showed 97.3% (k_{app}: 0.03477 min^{-1}) degradation efficiency for CFT in 120 min and this efficiency was superior to that of the pristine nanographite (76.6% and k_{app} = 0.02278 min^{-1}) and TiO_2/nanographite (90.3% and k_{app} = 0.01473 min^{-1}).[117] The enhanced performance of SnO_2–TiO_2 and RuO_2–TiO_2 was based on their physicochemical properties (*e.g.*, electrical conductivity (1 S cm^{-1}), chemical stability, isoelectric point (5.5), and high surface reactivity).[153] For instance, doping of TiO_2 and RuO_2 on nanographite increases the electron transfer resistance (decrease in electronic conductivity). This also ensures appropriate electron mobility in the electrochemical cell (Fig. 6a), which in turn elevates the production of reactive $^{\bullet}OH$ species.[117,154] This increased generation of $^{\bullet}OH$ on the surface of RuO_2–TiO_2/nanographite ultimately helps to degrade antibiotics through indirect oxidation (Fig. 6b). Meanwhile, TiO_2 also develops electrons and holes in the CB and VB, respectively, thus offering extra synergy for direct oxidation of CFT by anodic holes.[155,156] Overall, the collaborative advantages of RuO_2 and TiO_2 are responsible for the enhanced efficacy of RuO_2–TiO_2/nanographite. Moreover, this kind of multiple doping of metal oxides on nanographite eventually contributes to excellent recycling capacity. For instance, the performance efficacy of RuO_2–TiO_2/nanographite decreased by only 3.2% after 15 cycles (cycle 1: 97.3% and cycle 15: 94.2%).[117]

Along similar lines, MoO_3/nanographite composite also acts as a promising choice.[119] Specifically, the coating of Mo over nanographite developed lattice distortion (the original peak of nanographite at 26.5° was shifted to the left) in graphite by

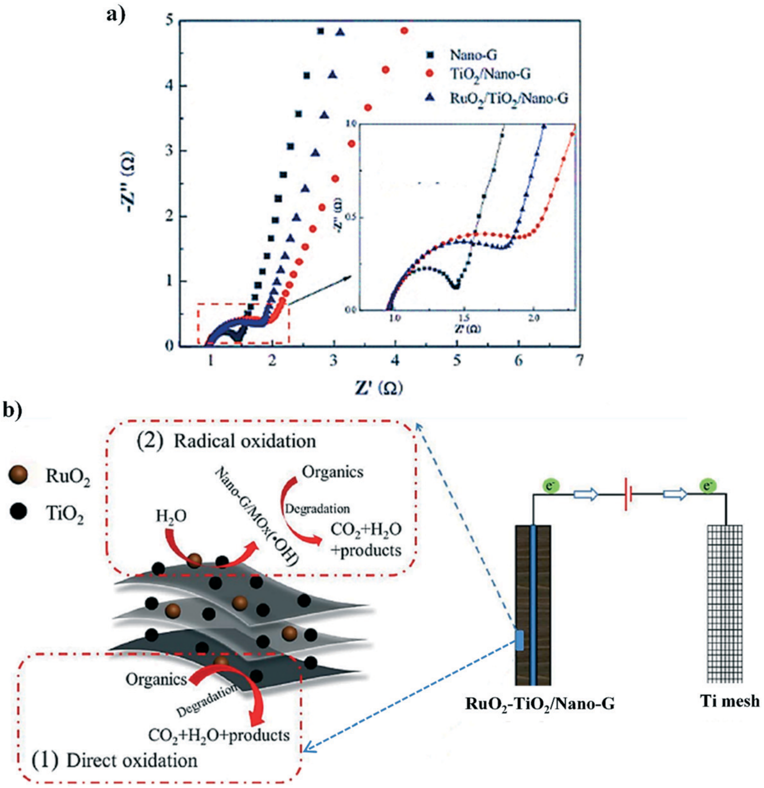

Fig. 6 Electrochemical properties (a) and mechanism (b) involved in the electrocatalytic degradation of antibiotics using RuO_2–TiO_2/nanographite. Reprinted with permission from ref. 117. Copyright 2018, Elsevier.

decreasing the layer spacing of graphite (Fig. 7c). The unique sesame cake-like structure of MoO_3/nanographite (Fig. 7a) composite considerably supported the exposure of CFD to •OH and facilitated 99.9% degradation efficiency (60 min and 2 V).[119]

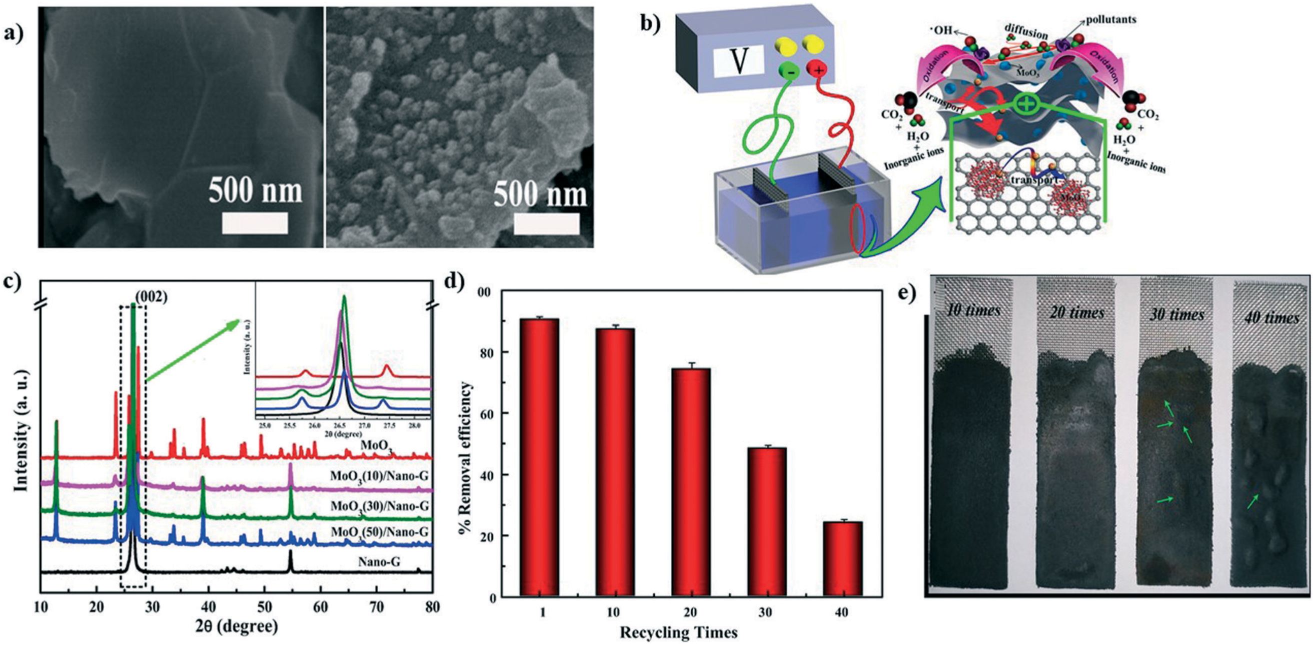

Fig. 7 Electrochemical behaviours of MoO_3/nanographite composite for the degradation of CFD. SEM images of nanographite and MoO_3/nanographite (a), concurrent production and transport of •OH (b), change in crystallinity of graphite after inclusion of Mo (c), and feature of MoO_3/nanographite at different reusability cycles (d and e). Reprinted with permission from ref. 119. Copyright 2018, Elsevier.

The behaviour of MoO_3 and nanographite as an electron acceptor and donor, respectively, decreased the electrode resistance.[157] More importantly, the uniform distribution of MoO_3 nanoparticles on the nanographite increased the contact at the interface and developed a potential drop which boosted $^{\bullet}OH$ production (Fig. 7b). The structural advantage of the sesame-like structure of MoO_3/nanographite was further proven by the low degradation efficiency for pristine nanographite (46.7%) and DSA (69.2%).[119] Additionally, the reuse capacity of MoO_3/nanographite was studied for more than 40 cycles, with a gradual decrease in the degradation efficiency after 10 cycles and a significant decline at 40 cycles (Fig. 7d).[119] It is noteworthy to point out that the reuse potential of MoO_3/nanographite is very high compared to transition metal-based catalyst (Ti/SnO_2–Cu).[110] Whilst the extreme environmental conditions involved in the electrochemical process (baking, applied voltage, and intense oxidizing environment) results in the detachment of binder (polyvinylpyrrolidone) from the matrix of an electrode (Fig. 7e).[119] Overall, the MoO_3/nanographite electrode is a feasible option for electrocatalytic degradation of antibiotics due to its connected nanostructure.

Analogous to graphite support, CNTs are also an attractive option due to their large surface area, improved corrosion resistance, and superior pi–pi interactions.[118,121] For instance, La_2O_3–CuO_2/CNT shows comparable performance with MoO_3/nanographite with 90% degradation of CFD (1 mg L^{-1}) in 30 min at a much lower current density (0.8 mA cm^{-2}).[120] This superior activity of La_2O_3–CuO_2 was mainly accompanied by the developed synergy between the doping elements and the native electrode surface (Fig. 8a). Specifically, CNTs served as an excellent electron donor, La improved the crystalline nature of the active surface, and Cu increased the corrosion resistance and oxygen evolution potential. Likewise, CNT/agarose (AG)/indium tin oxide (ITO)

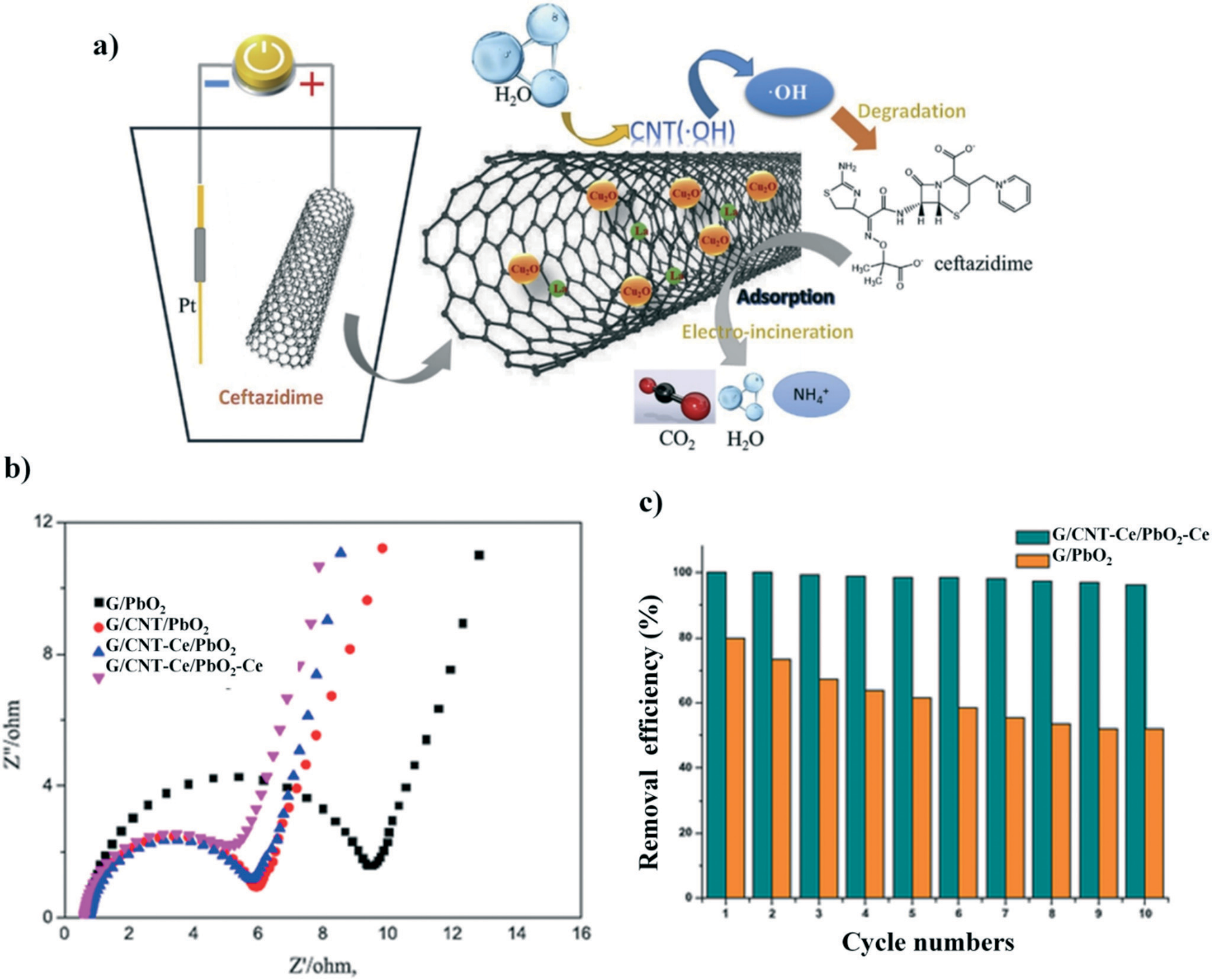

Fig. 8 Removal mechanism of La_2O_3–CuO_2 (a). Reprinted with permission from ref. 120. Copyright 2019, Elsevier. Electrochemical properties of graphite/CNT–Ce/PbO_2 (b). Recycling capability of graphite/CNT–Ce/PbO_2 towards ceftazidime (c). Reprinted with permission from ref. 122. Copyright 2020, Elsevier.

was assessed for the degradation of TCH (10–100 mg L^{-1}) at neutral pH.[118] More than 90% degradation was observed due to the non-selective oxidation *via* the superoxide anion. However, the mineralization efficiency was not satisfactory. More importantly, the intermediates generated registered maximal chronic toxicity for green algae and *Escherichia coli* ACTCC25922.[118] Thus, to reduce the toxicity of the intermediates, rare earth metals such as Ce and Zr were utilized as a dopant.

Doping of Ce improved the morphological properties of multiwalled carbon nanotubes (MWCNTs) by forming proper crystal orientation and enriching the movement of outer shell electrons. This free movement of electrons assisted active oxygen accumulation on the surface of the electrode.[158] Subsequently, MWCNT–Ce yielded a maximum CFD removal (100% in 60 min) at 3 mA cm^{-2}.[121] Similarly, the addition of CeO_2 to the graphite/CNT–Ce/PbO_2 electrode assisted the rise in the OEP (2.4 V), production of $^{\bullet}OH$, and faster electron transfer rate (R_{ct}: 5.12 Ω cm^{-2}).[122] Apart from the morphological improvement, the addition of CeO_2 also refined the electronic structure of the electrode and favourably affected the reusability of the electrode (Fig. 8b and c). Correspondingly, the graphite/CNT–Ce/PbO_2–Ce anode successfully degraded 50 mg L^{-1} of CFD with an extended life span (graphite/CNT–Ce/PbO_2–Ce – 1500 min, graphite/CNT–Ce/PbO_2 – 1260 min, and graphite/PbO_2 – 720 min).[122] Compared to pristine graphite, multi-doping of Ce on graphite (graphite/CNT–Ce/PbO_2–Ce) improved the efficiency of the catalyst for CFD degradation. However, the chemical cost for utilizing rare-earth elements is critical with respect to the environmental and economic front. Consequently, using low-cost and abundant metal oxides such as TiO_2 is explored as a co-catalyst for CNTs to offer better surface coverage and improved resistance to corrosion.[159] For instance, CeO_2–ZrO_2 eutectic doped on TiO_2/CNT enabled new oxygen vacancies, enriching electron mobility and controlling the release of $^{\bullet}OH$.[160] The superconducting point of Ti (0.4) and Zr (0.61) ensured desirable improvements (72.9–83.4%) in the electrical property of CeO_2–ZrO_2/TiO_2/CNT.[123] This proves that TiO_2, along with oxides of lanthanides, protects electrode deactivation and guarantees a continuous controlled supply of $^{\bullet}OH$ in the system.

Generally, the application of metal oxides on a carbon-based support enhances the recyclability of the electrode with constant degradation efficiency. However, it has been reported that MWCNTs and graphene possess higher toxicity than carbon black and graphite.[161] Specifically, the health impact (*e.g.*, lung irritation) of exposure to 2.5 mg m^{-3} MWCNTs is higher than exposure to 10 mg m^{-3} graphene. It is noteworthy to mention that apart from graphite, the most used anode material is CNT (Table 3). Thus, it is crucial to understand the toxicity-related issues during the use of CNTs. Moreover, dopants like Co also demonstrate potential toxicity.[66] The use of less toxic metals such as Al should be developed. In a nutshell, carbon-based electrodes are low-cost, long-life materials, stable, and highly conductive. Nonetheless, the modification of this pristine material *via* various rare earth elements as dopants is expensive. Thus, the fabrication of electrocatalysts using economically viable precursors (*e.g.*, Ti, Al, and so on) resolves the sustainability and cost-related issues.

4.4 Miscellaneous electrodes

Conventional electrodes (*e.g.*, Ti, carbon-based, and PbO_2) have shown remarkable performance for electrochemical oxidation but have significant limitations such as low stability, mass transfer limitations, *etc.* Hence, electrodes like nickel foam (Ni-F) or particle electrodes have been explored. Ni-F electrode is efficient for generating $O_2^{\bullet -}$ *via* oxygen reduction reactions (ORRs). Additionally, particle electrodes made up of Cu, Al, or Sb have also been tested to degrade antibiotics. In this section, examples of electrodes other than Ti, Pb, and carbon-based electrodes are discussed.

4.4.1. Cathode assisted anodic oxidation. Degradation of antibiotics is primarily acquired by the anodic oxidation reaction where $^{\bullet}OH$ generated at the anode helps to mineralize the antibiotic. Additionally, the cathode can also produce $^{\bullet}OH$ *via* H_2O_2 and offers additional synergy during the electro-oxidation of organics.[162] It should be noted that in AOPs, the contribution of $^{\bullet}OH$ produced from the cathodic reaction was only about 20%.[163] However, an efficient cathode can support the electronic transmission rate *via* controlling the production of $^{\bullet}OH$ from H_2O_2. In this line, Co_9S_8/partly graphitized carbon (PGC) and Ti/IrO_2/RuO_2 were used as cathode and anode, respectively.[125] This system achieved 84.3% mineralization in 480 min *via* (i) generation of H_2O_2 (eqn (34) and (35)) and (ii) dissociation of H_2O_2 to $^{\bullet}OH$ (eqn (36)).

$$Co_9S_8 + 9OH^- \leftrightarrow Co_9S_8(OH)_9 + 9e^- \quad (34)$$

$$O_2^{\bullet -} + e^- + 2H^+ \rightarrow H_2O_2 \quad (35)$$

$$H_2O_2 + e^- \rightarrow OH^- + {}^{\bullet}OH \quad (36)$$

The smooth 3D porous structure and high electrical conductivity of the Ni-F substrate also favour its application in the ORR/electro-Fenton (EF) type of electrochemical reactions.[164] Though Ni-F has a spongy, porous, and large surface area, the need for additional active sites for O_2 production (eqn (37) and (38)) limits its direct application in antibiotic treatment.[165]

$$Ni^0 + 2O_2 \rightarrow Ni^{2+} + 2O_2^{\bullet -} \quad (37)$$

$$O_2^{\bullet -} + e^- + 2H^+ \rightarrow H_2O_2 \quad (38)$$

To overcome these inherent disadvantages, carbonaceous materials have been broadly preferred as robust catalysts.[150,166] The carbon catalysts on Ni-F provide enhanced surface area and charge transfer properties. Various types of carbon-based catalysts such as glucose-derived coatings,[167] activated carbon fiber,[168] and functional group doped carbon[115] have been prepared, and their ability to enhance the oxidation has been tested. The $2e^-$ reduction capability of carbon enables its use in EF processes.[124] Thus, the coating/electrodeposition of carbonaceous material on commercial electrodes such as PbO_2 or Ni-F is recognized as a growing research area. For instance, nitrogen-doped porous carbon CN/Ni-F increased the effective surface area ($3.01\ m^2\ g^{-1}$ for Ni-F and $257\ m^2\ g^{-1}$ for CN/Ni-F), minimized charge transfer resistance ($95.7\ \Omega$ to $19.7\ \Omega$), and increased the production of H_2O_2 (Ni-F: 95 μM and CN/Ni-F: 1519 μM) along with elevated current efficiency (13.8 times higher).[124] Also, the sharing of a nitrogen lone pair of electrons to the π electrons of carbon increased the oxygen reduction potential of the electrode.[169] Subsequently, 100% removal and 90% mineralization efficacy of STZ was attained. It has also been envisioned that $^{\bullet}OH$ generated from EF has a higher impact than $^{\bullet}OH$ formed *via* direct oxidation of H_2O in the degradation of STZ.

It is worth mentioning that secondary pollution/toxicity from the chemical compounds (*e.g.*, Co) leached in the preparation stage is inevitable. Hence, effort needs to be taken to control the leachability of toxic metals by co-doping an element such as Ti, Sn, and Sb or fabricating the interlayer structure. In similar lines, the use of carbon sources derived from low-cost/waste material (*e.g.*, biochar) is advised. Nevertheless, nitrogen functionalization also involves using toxic chemicals (*e.g.*, *p*-phenylenediamine),[170] which further raises ecotoxicity-related issues. Similarly, the use of urea as an inexpensive, non-toxic nitrogen dopant (nitrogen content >46%) serves as a suitable alternative to *p*-phenylenediamine.[171] Thus, efforts are needed to test the efficacy of urea-derived nitrogen functionalized carbon as a catalyst for cathodes (*e.g.*, Ni-F).

4.4.2. Particle electrodes. Recently, particle electrodes such as activated carbon, alumina (γ-Al_2O_3), zeolite, and ion exchange resins are also being explored as a support material for electrochemical degradation.[172] The advantage of the particle electrode is the highly porous nature and behaviour of each particle as an independent 3D electrolytic cell.[173] Thus, the conventional challenges of mass transfer and limited degradation potential of the electrode can be resolved. Accordingly, Ti–Sn/γ-Al_2O_3-based particle anode was used to treat $100\ mg\ L^{-1}$ CAP.[126] The uniform particle distribution of Ti and Sn–Sb over γ-Al_2O_3 supported gradual enhancement in the removal rate (92% in 180 min). Similarly, Bi–Sn–Sb/γ-Al_2O_3-based particle anode was prepared and tested to remove TTC (Table 3).[127] The SnO_2 particles loaded onto the porous Al_2O_3 were responsible for the high electrocatalytic activity. Simultaneously, the presence of Sb induced defects onto the intercalated layer of SnO_2 and supported the oxidation of SnO_2 in the metal oxide lattice.[174] The removal efficiency of 86% (pH ∼5.9) was attained *via* non-selective oxidation by $^{\bullet}OH$.[127] The addition of Ti or Bi over Sn/γ-Al_2O_3 supported the formation of rigid morphology. This kind of surface compactness regulated the charge distribution and acted as a protection shield of the electrode. Despite this, justifying the exact role of elements in a multi-doped system like Ti–Sn–Sb/γ-Al_2O_3 or Bi–Sn/γ-Al_2O_3 is challenging because each element's behaviour in the presence of others is different from their individual properties. Thus, detailed characterization analysis is recommended for identifying the roles of each component in a cumulative system.

The facilitation of Sb over SnO_2 was further confirmed from its higher removal characteristics (100% removal and 93% mineralization) towards CPX.[128] This superior performance of Sb-doped SnO_2 was mainly due to the effective electrode surface area and the compact arrangement of nanoparticles (50–200 nm). This appropriate morphology possessed excellent OEP (2.2 V), which assisted $^{\bullet}OH$ production. Though the electrode's efficacy was superior, the multiple electrocatalyst coatings (16 times) on the substrate is a major hurdle in practical fabrication. Thus, reducing the time consumption in the coating process or modifying the electrode with other suitable materials is needed. Overall, the application of particle electrodes to increase the degradation efficiency of the pollutant is highly desirable. However, the morphology, size, and synergy of the co-dopant play a pivotal role in ROS production. Moreover, in practical use, the durability of the particle electrode, leaching and agglomeration of nanoparticle from the electrode, and stability under various flow rates are challenging. Hence, different electrochemical cell configurations such as flowing electrode or flow by electrode should also be assessed before establishing the particle electrode at the pilot scale.

5. Reductive electrocatalysis

Similar to electrochemical oxidation, electrochemical reduction is also a clean and robust approach to remove antibiotics. Mostly, the process has been used for the mineralization of halogenated or nitro-containing antibiotics. The prime factors determining the feasibility of cathodic reduction technology in WW treatment are the efficiency, selectivity, and continuous supply of electrons from the cathode. Accordingly, both biotic and abiotic cathodes have been verified as a tool for reducing antibiotics like CAP, nitrofuran, and MNZ.[169] However, complete dehalogenation and reduction of nitro groups is not highly viable. For instance, a potential of ≥ -1.25 V is required for the complete dehalogenation of CAP or FLO.[88] Due to the drawback of considerably high applied potential, various modifications in the bare cathode with noble metals and transition metals have been practiced (Table 4). In this line, the current section debriefs the reader towards the various dopants used in electrode modifications and limitations of the developed electrode in real-time application.

Table 4 Summary of reductive electrocatalysts for antibiotic removal

	Working electrode								
Antibiotics	Support	Catalyst	Structural properties of electrocatalysts	Features of electrode	Operational parameters	Removal % and recyclability	Degradation mechanism	Remarks	Ref.
CAP, FLO, TAP	Ti	C–Co–P/O	Amorphous, nanocluster array with size 300–400 nm	Porous, stable	Conc. = 20 mg L^{-1}, Na_2SO_4 = 14.2 g L^{-1}, applied voltage = −1.2 V *vs.* SCE	DCE (CAP): 98.7% DCE (TAP): 74.2% DCE (FLO): 91% in 60 min, RC: 19 cycles	Reduction *via* H* and formation of Co–Cl bond	(i) DCE and RC better than Pd/C (ii) ↓ed removal of TAP than CAP and FLO was due to its molecular structure	175
FLO	Ti	C–Co–P	Crystalline vertical nanoarray on both sides of Ti with an effective surface area of 21.3 $m^2\ g^{-1}$	Porous, stable	Conc. = 20 mg L^{-1}, Na_2SO_4 = 14.2 g L^{-1}, applied voltage = −1.2 V *vs.* Ag/AgCl	DCE: 97.4% in 60 min, RC: 4 cycles	Reduction *via* direct electron transfer and H*	(i) Vertical nanostructure enhanced electron and mass transfer (ii) Crystal structure aided H* production (iii) ↑ed removal at alkaline pH	176
FLO, TAP	Glassy carbon electrode	MWCNT	(i) Surface area = 7.05 mm^2, high electrical conductivity	(i) No graphitized polymer carbon (ii) Low electrical resistance, high thermal and chemical stability	Conc. = 2 mg L^{-1}, $NH_3{\cdot}H_2O$–NH_4Cl = 8.9 g L^{-1}, applied voltage = −1.2 V *vs.* Ag/AgCl	RE (FLO): 78%, RE (TAP): 76% in 720 min at −1.3 V, RC: 6 cycles	Dehalogenation *via* H* and carbonyl reduction	(i) RE of electrode dependent on the ratio of MWCNT and dihexadecyl phosphate (ii) ↑ed conc. ↓ed removal	65
FLO	Ni-Foam	Ultrafine Pd	(i) Ultrafine (8 μm size) (ii) No agglomeration. 8.89% Pd (iii) Surface area 4.26 $m^2\ g^{-1}$	3D, porous, electrically conductive, synergies with Pd	Conc. = 20 mg L^{-1}, Na_2SO_4 = 14.2 g L^{-1}, applied voltage −1.2 V *vs.* Ag/AgCl	RE: 99.5% in 120 min, RC: 20 cycles	Production of H* from water molecule or proton at Pd–Ni micro interface	(i) Ni-foam and Pd worked in synergy to produce H* (ii) Instability of electrode at pH below 4	177
MNZ	Graphite felt	Nafion/titanocene	Selective reduction of nitro to amino groups	High surface area, porous, and superior stability	Conc. = 100 mg L^{-1}, applied voltage = −0.5 V *vs.* SCE	RE: 99% in 60 min; RC: 3 cycles	Indirect reduction *via* $6e^-$ transfer	Leaching of titanocene affects the ME	178

DCE: dechlorination efficiency, RE: removal efficiency, RC: recyclability, ME: mineralization, ↑ – increase, ↓ – decrease.

5.1 Modified Ti electrodes

Cobalt-based catalysts have opened new fronts in the development of non-noble metal electrocatalysts. The oxidation potential of Co-doped materials has been well discussed in the previous section. Likewise, the dehalogenation activity of some cobalt compounds such as cobalt(I) salen and cobalt–phosphorus-derived compounds has been previously reported.[179,180] The cobalt–phosphorus-derived compounds have been identified for their potential to generate reactive hydrogen (H*) by activating water molecules or protons at particular applied cathode potentials, thus providing the basis for exploitation of Co-based material as an effective candidate for reductive catalysts.[176] Cobalt–phosphorus/oxide (Co–P/O) has been reported with a dehalogenation efficiency of 91%, 98.7%, and 74.2% for FLO, CAP, and TAP, respectively, at −1.2 V *vs.* saturated calomel electrode (SCE). The relatively low dechlorination efficiency for TAP was due to inadequate separation of electronic densities in the lowest unoccupied molecular orbital (LUMO) and the highest occupied molecular orbital (HOMO). Consequently, a cutback in the polarity and redox reactivity of TAP is observed.[181] The durability of the Co–P/O electrode system was confirmed by extended removal (86%) of FLO in the 19th cycle lasting 2280 min.[175] Overall, Co–P/O showed excellent dechlorination efficiency (91%) and stability. However, the major demerit of Co–P/O was its non-crystalline structure which restricts the production of H* and considerably increased applied potential (−1.2 V *vs.* SCE).[176] Thus, crystalline cobalt phosphide nanosheet arrays (C–Co–P) were developed on a Ti plate (C–Co–P/Ti) to augment the production of H*, electron transfer, and mass transfer (Fig. 9a). The vertical (height = 2.5 μm) nanosheet array provided a large number of active sites and faster mass transfer by nanoscale convection and enhanced exposure between the catalyst and FLO.[182] The interconnected structure of the CoP sheet reduced the electrode resistance.[183] The high crystallization in C–CoP with the dominant (200) plane of CoP and lattice spacing of 0.25 nm facilitated effective adsorption of H_2.[184] Consequently, 95.7% removal of FLO in 30 min at −1.2 V (*vs.* Ag/AgCl) was achieved using C–CoP/Ti. The obtained dehalogenation efficiency was much higher than those of amorphous CoP/Ti (22.8%), Pd/Ti (35.9%), and bare Ti (18.9%). The dehalogenation of FLO resulted in four main products, *i.e.*, FLO-Cl (one chlorine atom was removed from FLO), FLO-2Cl (two chlorine atoms were removed from FLO), FLO-F (one fluorine atom was removed from FLO), and FLO-2ClF (two chlorine atoms and one fluorine atom were removed from FLO), when C–CoP/Ti was used as an electrode. Accordingly, both indirect (H*) and direct (electron transfer) reduction supported the degradation of FLO (Fig. 9b).[175,176] C–CoP/Ti showed feasibility in degradation at a pH range of 3–9 for 5 cycles without leaching, thus demonstrating the robust and cost-effective nature of C–CoP/Ti for electrochemical applications. It is imperative to mention that increasing the potential to −1.5 V results in a side reaction (hydrogen evolution reaction) that could affect the system. Also, the highly alkaline (pH 12) nature of the treated effluent restricts its direct use for consumption. Hence, monitoring the power fluctuation and variation in pH is necessary for electrochemical reduction systems. Additionally, the optimization of the proton availability in the reaction medium is also highly desirable to maintain neutral pH. Overall, the application of non-noble metals like Co is an efficient way to reduce cost. However, prior to field application the behaviour of the catalyst in the

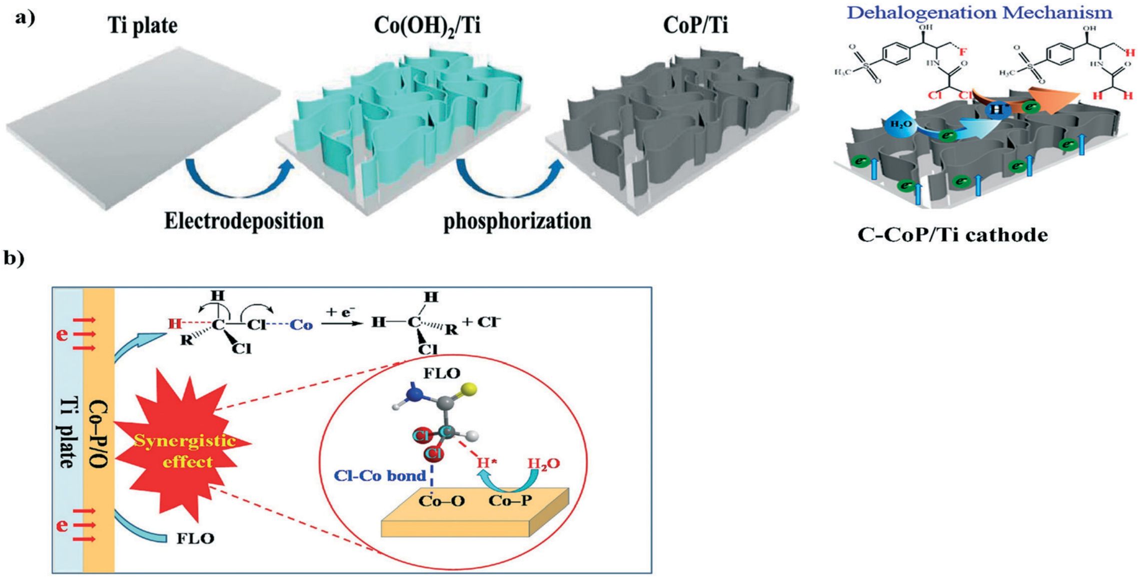

Fig. 9 Fabrication and dehalogenation process of CoP nanosheet arrays on a Ti plate (a). Reprinted with permission from ref. 176. Copyright 2019, American Chemical Society. Electrocatalytic reductive dehalogenation of FLO on Co–P/O (b). Reprinted with permission from ref. 175. Copyright 2018, Elsevier.

presence of foulant and deactivating agent should be thoroughly understood. Since the nature of the cathode material plays a crucial role in reducing the high overpotential associated with breaking of the C–X bond, the application of metal precursors such as Fe, Cu, and Ni should also be explored owing to their remarkable electrocatalytic activities. The high reductive degradation potential of Fe (nZVI) and CuO has been well established for nitrate and halogenated volatile organic compound degradation.[48,49] However, their use as reductive electrocatalysts for antibiotics has not been verified so far.

5.2 Modified carbon electrodes

Carbon-based electrodes such as graphite felt, carbon paper, carbon fibers, *etc.* have been employed for electrochemical systems due to their high conduction, porous nature, relatively large surface area, and mechanical/thermal stability.[185] Moreover, graphite felt as a substrate has a much lower cost than metal-based electrodes like Ni-F or Ti. Accordingly, electrocatalytic treatment was used as a pretreatment unit with titanocene dichloride ($(C_5H_5)_2TiCl_2$) as catalysts and graphite felt as the stable substrate for MNZ defunctionalization.[178] Titanocene has been investigated for selective reduction of nitro groups into amino compounds. However, its non-selectivity to degrade nitro groups obstructs direct application (without support).[64] Hence, immobilization of the catalyst using Nafion® on graphite felt resulted in enhanced electron transfer reactions and recovery. The modified electrode (titanocene 2 g L^{-1}, initial concentration of Nafion®: 0.8%, and sonication time: 30 min) was able to reduce 99.9% of MNZ (100 mg L^{-1}) to the amino group *via* $6e^-$ transfer reactions (eqn (39)).[178] This is in contrast with the reduction on direct graphite felt, where direct electrochemical reduction *via* $4e^-$ transfer and subsequent $2e^-$ was the major mechanism (eqn (40) and (41)).

$$(C_5H_5)_2Ti(OH_2)_2{}^+ + RNO_2 + 7H^+ \rightarrow 6(C_5H_5)_2Ti(OH_2)_2{}^{2+} + RNH_3{}^+ + 2H_2O \quad (39)$$

$$RNO_2 + 4H^+ + 4e^- \rightarrow RNHOH \quad (40)$$

$$RNHOH + 2H^+ + 2e^- \rightarrow RNH_2 \quad (41)$$

The improved turnover number (139) (compared to bare graphite felt) and the excellent performance of titanocene-modified carbon electrode for 3 cycles (~80%) made the electrode highly desirable for heterogeneous catalytic reduction. However, the slow leaching of the metal complex catalyst (titanocene) and deactivation renders a 65% decrease in the electrochemical signal of the catalyst, hindering long-time application of the electrode.[186] In a nutshell, the study lays an outstanding foundation for applying organometallic complex-modified carbon electrodes for the reduction reaction. Nonetheless, modifications in terms of extended durability are essential.

Alternatively, the glassy carbon electrode (GCE) is another often utilized electrode for electrochemical sensing and degradation. The polymeric and non-graphitizing carbon developed from thermal degradation shows high thermal and chemical stability and low resistivity ($(\sim 3\text{–}8) \times 10^{-4}\ \Omega$ cm), making it suitable for electrocatalysis.[187] However, compared to previously described carbon materials, the accessible surface area is relatively low (0.071 cm^2) due to closed pores (30 v/v).[188] Hence, doping of GCE with various metal and non-metal nanoparticles has been reported. Accordingly, a homogenous 3D network of densely coated MWCNTs on glassy carbon electrode (MWCNT-GCE) was fabricated using dihexadecyl phosphate (DHP) in a 1 : 1 ratio for cathodic reduction of FLO.[65] In terms of performance, MWCNT-GCE has demonstrated 87% and 89% removal of TAP and FLO (2 mg L^{-1}) at −1.2 V in 1440 min owing to the large surface area, enhanced active site, and electron transfer.[65] Moreover, the reduction of FLO was more favourable at neutral pH due to the low dispersion of MWCNT/DHP in acidic medium and inhibition of dehalogenation in alkaline medium.[189] Since the increased amount of DHP can reduce electrical conductivity, concentration optimization for MWCNTs and DHP is mandatory for proper dispersion and homogenous coating. Furthermore, above the bias voltage of −1.2 V, the hydrogen evolution reaction was reported,[65] thus giving rise to unwanted side reactions. Moreover, the dehalogenation efficiency was reduced to ~50% in six regeneration cycles. Typically, the modification of MWCNTs is feasible and straightforward; however, the durability of the modified electrode is unfavourable. Furthermore, the slow kinetics and highly selective pH make the process challenging for real WW treatment.

To conclude, it has been established that carbon-based material works as an excellent support for carrying out heterogeneous and homogenous reductive catalysis. However, with a minimal number of studies, the durability of electrodes and catalysts in real WW cannot be described. Organometallic complexes of Ti have demonstrated excellent performance due to the concurrent occurrence of direct and indirect reduction reactions. In similar lines, the utilization of phthalocyanine-based metals (Co, Ni, Mn, Pt) may be explored due to their high faradic efficiency and turnover number.[190] It is also essential to identify efficient anchoring groups that are more stable in acidic or basic solutions[191] to bind molecular catalysts to the electrode surface and avoid leaching.

5.3 Miscellaneous electrodes

Noble metals such as Pd, Pt, and Ag have been well established for their dehalogenation potential *via* the involvement of atomic hydrogen (H*) as a reducing agent.[192] However, deactivation, pH-sensitive nature, and agglomeration limit their direct use. For instance, Pd is known to have a high affinity for hydrogen adsorption (H_{ads}), but using a stand-alone Pd electrode is expensive. Apart from the cost, the agglomeration of Pd in the solution results in reduced reactivity.[193] Therefore, Pd nanoparticles dispersed on stable electrode substrates like Ti/TiO_2 nanotubes,[193] reduced graphene oxide,[194] and Ni-F,[177] have been verified for electroreduction. Ni-F is highly desirable as an electrode material due to its 3D porous structure, high electrical conductivity, and stronger metal–hydrogen (M–H*) binding capacity, favouring more hydrogen evolution for hydro dechlorination.[177] Also, Ti and carbon-based substrates often interact with Pd *via* weak interaction (oxygen functional group), resulting in reduced efficiency and leaching of catalyst (Pd) during the reaction. Given that, Yang *et al.*[177] utilized ultrafine Pd nanoparticles immobilized on a 3D self-supported Ni-F surface (Pd/Ni-F) for electrocatalytic reduction of FLO. At the applied potential of −1.2 V *vs.* Ag/AgCl, 99.5% FLO (20 mg L^{-1}) degradation was reported in 120 min using Pd/Ni-F as an electrode. The obtained degradation efficiency was much higher than that of pure Ni-F (15.6%) and Pd/carbon (67.9%) electrodes.[177] The porous structure (100 to 400 μm) of Ni-F enabled improved mass transfers. Simultaneously, the displacement of Ni atoms by Pd atoms enhanced the specific surface area (1.90 to 4.26 m^2 g^{-1}), electrochemically active surface area (Pd@Ni-F electrode (13.7 mA V), Ni-F (0.87 mA V)), electron transfer (ohmic resistance was decreased from 45 Ω to 7 Ω) and atomic H* production. The Pd/Ni-F electrode showed high durability for 20 cycles (2440 min) with only a 5% drop in degradation efficiency.[177] Overall, it can be established that Pd–Ni-F is stable, durable, and efficient for FLO degradation at neutral pH. It is noteworthy to mention that at a potential higher than −1.4 V, electrolysis of H_2O diminished degradation efficiency since produced H_2 cannot split into H*. Simultaneously, at a pH of less than 4, leaching of Ni is prominent. Thus, the use of substrates such as stainless steel can also be tested. Furthermore, the application of Ag-based nanostructures such as nanowires and nanorods as a catalyst can be tested to minimize the operational cost and achieve higher degradation efficiency.

6. Design criteria of electrocatalysts

The performance evaluation of electrocatalyst towards specific antibiotics under optimal experimental conditions is vital while stepping up the lab-scale technology into field scale. This assessment may also help to determine the pros and cons of the existing electrodes; subsequently, it offers a platform to develop a novel material. In this regard, the best performing electrocatalysts for each antibiotic are identified. Recommendations for further improvement of electrocatalysts are also included. It should be noted that only limited (fewer than two) studies have been reported for electrocatalytic degradation of antibiotics such as OFX, STZ, LVF, ENF, SMX, MNZ, IMD, and CAP. For these antibiotics, a suggestion regarding the best performing electrocatalyst is not provided. Additionally, from the materials science and engineering point of view, the recommendations of designing electrocatalysts are communicated.

6.1 Tetracycline and oxytetracycline

Tetracyclines are among the most frequently used antibiotics in aquaculture and veterinary medicine due to their activity against both Gram-negative and Gram-positive microrganisms.[195] TTC and OCT are commonly used to treat respiratory and systemic infections by inhibiting protein synthesis in bacteria. The relatively low Henry's constant (from 3.45×10^{-24} to 3.91×10^{-26} atm m^3 mol^{-1}) and the octanol–water partition coefficient suggest weak volatilization and the hydrophilic nature of the compounds. Also, three pK_a values indicate their stability in acidic conditions (Table 1). The presence of high electron density functional groups such as a double bond, phenolic, and amine groups favours the attack of ROS during electrocatalytic degradation and subsequent mineralization of the molecule.[196] (Fig. 10b) The most suitable electrocatalyst to degrade TTC and OCT was SnO_2–Sb because of its excellent removal and mineralization efficiency at near-neutral pH (6) (Table 3). This provides an advantage in terms of no buffer requirement to maintain pH. However, at a high concentration of TTC (100 mg L^{-1}), degradation was slightly tricky due to the limited concentration of ROS. Correspondingly, the supply of aeration in the electrocatalytic system is known to increase ROS formation, which consequently amplifies the degradation efficiency.[127] In terms of mechanistic purpose, SnO_2 is prominently involved in the electrocatalytic process, and the presence of Sb at the backbone of Sn ensures the presence of abundant defects/active sites. These cumulative features of Sn–Sb elevated the conductivity of the electrode.[174] Apart from Sn–Sb, the Ag–ITO combination also demonstrated excellent removal efficiency for TTC (96% in 30 min) degradation.[118] Like the morphological advantages of Sn–Sb, the Ag–ITO combination also possessed diverse chemical interactions (*e.g.*, van der Waals, π–π, and cation–π interactions) on the surface of the electrode. Ultimately, it warrants continuous electron mobility in the solution, resulting in higher production of active species.[197] It is noteworthy to mention that chemical interactions developed by Ag–ITO were found to be stronger than the morphological defects created by Sn–Sb in the generation of active species/sites. For instance, irrespective of the operational parameters, CNT–Ag–ITO (82% in 180 min) exhibited higher mineralization efficiency than Ti/Sn–Sb–Ce (41.6% in 120 min) and Al_2O_3/Bi–Sn–Sb (41% in 180 min) (Table 3), thus implying that the selection of catalysts based on their chemical bonding with the electrode surface is more vital than altering the morphology of the electrode. Surface changes in the electrode (*e.g.*, defects, cracks, and lumps) play a lesser role in enhancing the mineralization efficiency. For instance, the presence of cracks/defects on the surface of the electrode restricts the free flow of electrolyte. Though defects/cracks are beneficial owing to their increase in the

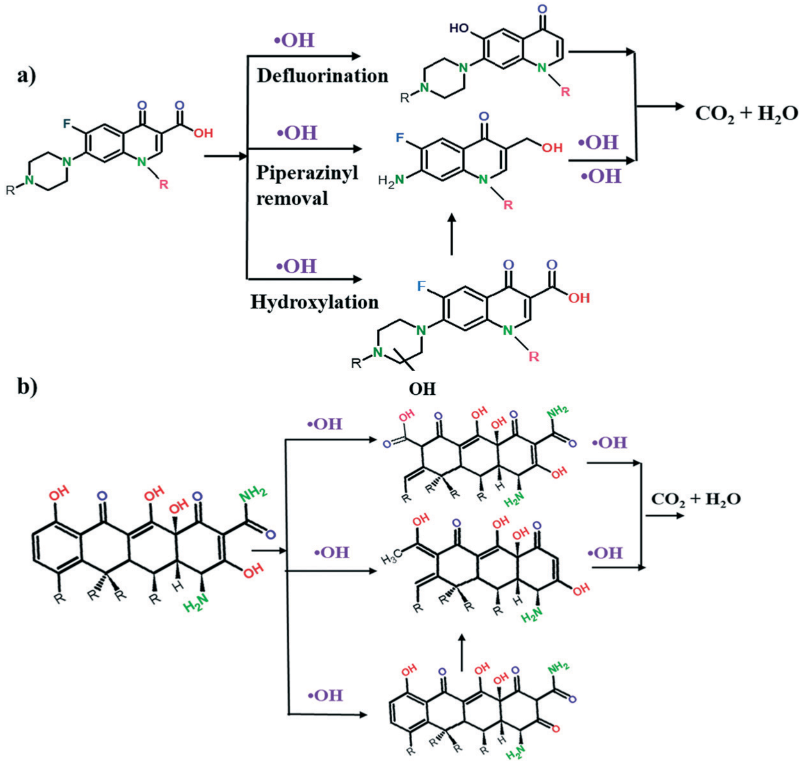

Fig. 10 General mechanisms for the degradation of (a) fluoroquinolones and (b) tetracyclines.

diffusion of reactive radicals over the electrode, a relatively large number of defects/cracks lead to surface detachment of the catalyst coating.[198] This type of deterioration causes lower production of reactive species and ends up with lower degradation/mineralization efficiency. Hence, designing a catalyst with more chemical bonds on the surface helps in achieving higher degradation and mineralization efficiency of TTC and OCT.

6.2 Ceftazidime and ceftriaxone

Ceftazidime (CFD) and ceftriaxone (CFT) are semi-synthetic third-generation cephalosporins used against Gram-negative microorganisms to treat respiratory, intestinal, and abdominal infections.[199] CFD and CFT are responsible for the inactivation of penicillin-binding proteins in organisms, restricting cell wall assembly during cell division. The presence of β-lactam groups allows resistance among Gram-negative bacteria and affects the biodegradability of the compound.[199] Accordingly, a combination of transition and rare earth metals has been tested as a catalyst for the opening of the β-lactam ring *via* the formation of a strongly polarized structure. For example, excellent degradation at near-neutral pH was obtained even for a low concentration of CFD (1 mg L^{-1}) at lower current density (0.8 mA cm^{-2}) using CNT–La_2O_3–CuO_2 (90% in 30 min)[120] and Ti–SnO_2–Cu (97.5% in 60 min at pH 3.4 and 20 mA cm^{-2}).[110] Similarly, the combination of Ce with graphite–CNT augmented CFD degradation (100% in 120 min at 3 mA cm^{-2})[122] than PGC–Co_9S_8 (99.9% in 240 min at pH 5 and 30 mA cm^{-2}).[125] This efficacy of rare earth elements can be explained by their unique 4f electronic arrangement. On the other hand, compared to a multi-dopant (*e.g.*, CeO_2–ZrO_2–TiO_2) on CNT,[123] the performance of a single dopant (*e.g.*, Ce) on MWCNT was found to be superior to treat low concentrations of CFD (1 mg L^{-1} at 3 mA cm^{-2}).[121] This explains that compared to CNT, MWCNT offers more sites for Ce occupation through partial enlargement in the surface, *i.e.*, effective sharing of Ce by the C–O and C═O bonds of MWCNT during electrodeposition. The mutual sharing of chemical bonds (especially oxygen cores) resulted in an increase in oxygen content (O_2) on the electrode's surface, ultimately resulting in higher degradation efficiency.[200] On the other hand, multi-doping of CeO_2–ZrO_2–TiO_2 onto the CNT results in surface saturation due to agglomeration of nanoparticles.[121] As a consequence, the active sites in the electrode were reduced. Therefore, it is essential to understand the surface saturation point and the fundamental chemical/mechanical properties of the original electrode before modification. Overall, it has been envisioned that the performance of the carbon electrode (either CNT or graphite) is better than that of the Ti-based electrode to treat all concentration ranges (1 mg L^{-1} to 50 mg L^{-1}) of CFD at different operating conditions. This is due to the use of CNT/graphite as nanostructured interlayers, which possibly diminishes the particle size of the catalyst (~2%) and enhances the physical–chemical stability of the material.[201] Also, the layer formation and aromatic rings in the CNT/graphite attract CFD near the electrode surface *via* π–π interactions and increase the degradation efficiency.

CFT can also be effectively treated by carbon electrodes coated with either SnO_2–TiO_2 or RuO_2–TiO_2. Though the efficiencies of these modified electrodes were similar at identical operational conditions, nanographite–RuO_2–TiO_2 yielded commendable mineralization than nanographite–SnO_2–TiO_2 (Table 3). It is worth mentioning that the ionic radii of Ru^{4+} (0.062 nm) and Sn^{4+} (0.069 nm) are similar to that of Ti^{4+} (0.068 nm). This enables the formation of a rutile-type crystal structure which results in improved redox reversibility and specific capacitance.[202,203] Moreover, the use of nanographite as a modifier provides interlayers between RuO_2/SnO_2 with TiO_2. The coexistence of RuO_2 along with nanographite and TiO_2 decreases the agglomeration and stabilizes the oxygen evolution potential and lifetime of the material.[202] This regularizing particle size (prevents agglomeration) is not present in SnO_2, which results in the lower performance of nanographite–SnO_2–TiO_2 than nanographite–RuO_2–TiO_2. The major hindrance to large-scale application of RuO_2 is the high cost (twice) compared to SnO_2. Hence, based on the treatment requirement (*e.g.*, degradation or mineralization, volume of treated water, cost), one can select anyone of the catalysts mentioned above to abate CFT.

6.3 Ciprofloxacin

Ciprofloxacin (CPX) is a second-generation broad-spectrum, synthetic FQ used for human and veterinary therapeutic use. CPX inactivates microorganisms through inhibition of DNA.[21] To inhibit the activity of hydrophilic CPX, the degradation of the quinolone moiety followed by defluorination is necessary. Moreover, the existence of CPX in the zwitterionic form (pK_a 6.1 and 8.7) (Table 1), *i.e.*, cationic < pH: 6.1 zwitterions < pH: 8.1 anionic, facilitates interactions with $^{\bullet}OH$ under acidic conditions and creates a shield against the OER. Accordingly, Sn–Sb-based electrocatalyst was identified to be apt due to its dominant efficacy for breaking the quinolone moiety and the C–F bond. The Sb–SnO_2-doped Ti electrode showed satisfactory performance (mineralization ($\geq$70% in 120 min)), indicating generation of an ample amount of active species to break the quinolone moiety, followed by CPX defluorination (C–F) (Fig. 10a).[108] The requirement of acidic pH limits its application in real water and wastewater. Conversely, OFX also belongs to quinolones and possesses a similar pK_a value (Table 1) and showed good removal at pH 6.8 using Ti/RuO_2.[107] Thus, future studies need to focus on the degradation pattern of CPX at neutral pH.

6.4 Florfenicol

Florfenicol (FLO) is a broad-spectrum, semisynthetic antibiotic belonging to the class of chloramphenicols. The mechanism of interaction includes the inhibition of protein synthesis by binding with the 50S ribosomal unit. The high lipophilicity of the compound due to the presence of a phenicol group depicts an increased risk of FLO in the environment.[204] In terms of electrocatalytic degradation, the requirement of higher energy to break halogen and sulfonyl methyl groups hindered its complete degradation. Accordingly, Co–P-based catalysts, Pd nanoparticles, and MWCNTs have been verified for 80–99.5% degradation of FLO in the applied potential range of −0.9 to −1.2 V. The extended stability (2400 min), no leaching, and >95% in 20 cycles makes ultrafine Pd doped on Ni-F the best reductive electrocatalyst. Moreover, the catalyst (Pd) and substrate (Ni-F) offered synergism to capture H*, making the electrode highly efficient. Compared with other reductive catalysts, the ease of synthesis of Pd–Ni aids in the scale-up. However, the high cost of the precursor can hinder practical use.

6.5 Engineering electrocatalysts for antibiotic removal

RuO_2 and SnO_2 are the most widely used catalyst materials which possess similar electronic properties. However, aggregation of RuO_2 in the absence of the co-catalyst and high resistivity of SnO_2 at room temperature limits their direct use.[205] Nonetheless, the relatively low cost of SnO_2 makes doping with other elements such as Ce to increase the electrical conductivity feasible.[206] Likewise, graphite and CNTs serve as an excellent catalyst by forming interlayers, which enhances the electron transition, penetration of electrolyte, and shelf-life of the electrode material. Nevertheless, their toxicity is not known so far. Accordingly, the application of the rare earth elements La, Ce, and Eu have been tested to boost the electrochemical performance of DSA, BDD, and carbon electrodes. A rare earth elements holds superior electrocatalytic property owing to their free electrons. The coupling of these ions with the SnO_2–Sb/Ti system results in a gradual increase in electron mobility and OEP. The oxygen evolution potential of rare earth metal-doped Ti/SnO_2–Sb composite is in the order Ti/SnO_2–Sb–Eu > Ti/SnO_2–La > Ti/SnO_2–Sb–Ce.[207] It is evident that Ti/SnO_2–Sb–Eu has more electrocatalytic activity than Ti/SnO_2–Sb–Ce. This is because the addition of La or Eu helps to develop a smooth and compact structure, whereas the morphology created by Ce is loose, uneven, and with coarse cracks.[207] This allows easy penetration of electrolyte and decreases the conductivity of the material. Therefore, considering the structural and electrical properties, La and Eu are better catalysts than Ce.[208]

The electrocatalysts summarized in this work for degradation of antibiotics have their own merits and demerits. Therefore, a few recommendations for improving the antibiotic degradation performance using a new type of electrode material have been provided. Porous carbons derived from metal–organic frameworks are a new class of advanced carbon materials possessing excellent surface features (surface area, porous nature, and functional moieties), unique internal cavities, shorter transport paths, and superior electrocatalytic ability to degrade/mineralize antibiotics.[209,210] Accordingly, N-doped carbon derived from MOFs can be an effective cathode material for oxygen reduction reactions and degradation of antibiotics like CAP and STZ. It is noteworthy to mention that heteroatom doping is the most recommended method to enhance the electrochemical performance of carbon materials.[211] Other options such as layered double hydroxides and monoliths are low-cost and stable materials for electrochemical oxidation and reduction applications. These materials possess higher tensile strength, corrosion resistance, and lesser agglomeration than electrode materials used so far. Additionally, the application of polyoxometalate (Mo, V, *etc.*)-based electrode materials can be investigated due to their fast mediated electron, proton, and oxygen atom transfer abilities.[212] However, the research in these areas is still at the toddler level, and significant exploration is needed in the future.

7. Toxicity implication

The feasibility of implementing electrocatalytic degradation for the removal of antibiotics is well verified. However, the practical applicability of the process is often limited by residual toxicity. Hence, for sustainable management of antibiotics *via* electrocatalytic degradation, toxicity induced by precursors or the end products should thoroughly be understood. For toxicity assessment, acute and chronic tests are often carried out using bioassays. The bioluminescence inhibition test (*Vibrio fischeri*), invertebrate toxicity test (*Daphnia magna*), and algae growth inhibition test are the most commonly used toxicity assessment tools.[213] Battery toxicity tests involving representatives from different trophic levels are also advised, as they provide better insights into permissible limits of contaminants in both terrestrial and aquatic environments.[214] Among the previously discussed electrocatalysts, the toxicity of Pb, Co, and CNTs has already been well understood. Accordingly, here the efforts are laid to understand residual toxicity in the treated effluent.

The incomplete mineralization of antibiotics is claimed to produce toxic end products. For example, 84% removal of NOFX was reported in 120 min *via* BDD electrode. However, the growth of *E. coli* was inhibited due to incomplete decomposition of the quinolone structure. The hydroxylation and ring cleavage of the piperazine moiety in NOFX was confirmed only after 300 min with 90% mineralization.[86] Consequently, the *E. coli* growth inhibition was ceased. Similar observations have been noted during the degradation of ENF using Ti/SnO_2–Sb/La–PbO_2 anode, whereby *V. fischeri* bioluminescence inhibition ratio was initially alleviated and later dropped significantly.[73] This pattern is commonly reported due to the formation of toxic intermediates such as pyridine, phenols, and aminothiazole during the course of oxidation. Hence, it is essential to optimize the reaction time for the mineralization of antibiotics to counter end product toxicity. Primary producers such as algae are crucial for the aquatic food chain. Hence, they have been utilized for ecotoxicity interpretation. Accordingly, a growth inhibition test (*D. subspicatus*) was used to evaluate the toxicity of the CPX, NOFX, and their oxidation mixtures. The reported EC_{50} values of CPX (8.8 mg L^{-1}), NOFX (6.8 mg L^{-1}), and mixture (6.7–8.7 mg L^{-1}) were either equivalent or increased.[76] Thus, the residual toxicity after electrochemical oxidation makes BDD electrodes undesirable for FQs oxidation.

Similarly, during TCH degradation by CNT/Ag/ITO, intermediates formed by oxidation of the hydroxyl group and tertiary amine groups were found to be 1400 times more toxic than the parent compound for green algae.[118] Simultaneously, when antimicrobial toxicity was assessed for *E. coli* ATCC25922, the growth was inhibited due to the formation of toxic intermediates after 120 min of reaction. Consequently, the reaction time was increased to 300 min, which decreased the hybrid toxicity of TCH and intermediates.[118] Since the toxicity interpretations were different for green algae and *E. coli*, the battery test is recommended prior to real-time application of the electrocatalysts. Overall, it is worth mentioning that rather than removal rate, mineralization efficiency should be considered as the chief criterion to compare the treatment efficiency of various AOPs. Furthermore, functional groups in antibiotics responsible for antibacterial/toxic effects should be identified, and specific attention is necessitated to convert them into less toxic/non-toxic end products. In this way, the environmental toxicity of intermediates/end products should be taken as one of the primary parameters while selecting the electrocatalyst and operation parameters.

Frontistis *et al.*[85] reported 17% inhibition to *V. fischeri* even after complete AMP removal in a real WW matrix. The residual inhibition was due to the presence of the inherent refractory compound in the WW matrix. The antibacterial activity of FLO was determined after catalytic reduction using the Co–P electrode. A significant decrease in the inhibition was noted; however, delay (480 min) in the inhibition of *E. coli* DH5α asserted the presence of antibacterial activity in the treated effluent.[176] Such residual antibacterial inhibition is a concern since long-term discharge of such treated effluent can result in the development of ARGs in the environment. Consequently, complete mineralization and inhibition of antibiotic activity are recommended. As electrolytes are an indispensable part of electrochemical degradation, the effect of the electrolyte's nature on the toxicity of the treated effluent was also considered. The use of NaCl as an electrolyte increased the effluent toxicity by 2.5 times due to the production of toxic chlorinated products such as perchlorate and organohalides.[68] To reduce the toxicity, lower current density was recommended; however, the mineralization efficiency can be adversely affected. Consequently, the application of Na_2SO_4 as an electrolyte for efficient degradation (discussed in section 3.2) and nontoxic effluent is suggested. To this end, it can be well established that the formation of toxic intermediates and end products can be highly expected if electrocatalytic degradation is incomplete. Hence, regular monitoring of the treated water serves as an effective solution. In terms of process kinetics, the nature of the electrode and the applied potential positively affect the end product formation. For instance, a non-selective electrode like BDD and reduced current density often produce more toxic end products than the modified electrode. The use of NaCl also impairs the quality of treated water due to the formation of chlorinated species. Overall, careful interventions are needed during the electrode modification to obtain a stable and selective electrode. At the same time, the optimization of reaction time, current density, and nature of electrolyte are equally essential to obtain complete mineralization and antibacterial activity inhibition.

8. Economic assessment

Cost estimation of any process is highly desirable to ensure its sustainability and direction for future developments. Generally, life cycle cost estimation is the sum of capital, infrastructure, operation, transport, and waste management costs.[215] To assess the economics of any treatment process, the most common method described is the calculation of the capital expenditures (CAPEX), operating expenses (OPEX), and the total cost (TC). The TC per volume of treated effluent is calculated as the sum of the OPEX and the remuneration over the CAPEX (RCAPEX).[216] Often, the application of electrocatalysis is limited due to the uncertainty of the cost involved. It has been verified that among the various AOPs (discussed in section 2) used for the degradation of refractory contaminants, electrochemical technologies have the lowest energy consumption in the range of 150–500 kW h m^{-3}.[46] Additionally, features like faster kinetics, less chemical requirement, and smaller sludge production significantly reduce the life cycle cost of the process. During the electrocatalytic processes, electrodes are the most significant contributor to the operation cost. The precursors involved in the fabrication of electrodes, electrode stability, and power consumption are vital criteria defining the chemical cost and operational cost. To better understand the affordability of the process, the OPEX (sum of chemical and energy consumed) for various electrodes discussed previously was calculated. For the calculation of chemical cost, individual precursor cost was obtained from the dealer. The operational energy cost was calculated using eqn (42).[33]

$$\text{Energy Cost}\left(\frac{\$}{\text{g}}\right)=\frac{E\times\text{Electrical cost}\left(\frac{\$}{\text{kW h}}\right)}{Q\times(C_\text{o}-C_\text{e})\times 10^{-3}} \tag{42}$$

where, E is the hourly energy consumed (kW h h^{-1}), Q is flow rate (m^3 h^{-1}), C_o and C_e are the inital and effluent concentration (mg L^{-1}), respectively. On comparing the cost of the modified electrode (*e.g.*, CeO_2–ZrO_2–TiO_2/CNT, La–Y/PbO_2) with that of the commercially available electrode (*e.g.*, BDD (\$7125 per m^2)), a significant reduction was noted. Among the selected electrodes, La–Y/PbO_2 showed the lowest cost of operation (\$34.2 per m^2) followed by SnO_2–Sb/Ti (\$61.2 per m^2), SnO_2–Sb–LaPbO_2/Ti (\$62.1 per m^2) and CeO_2–ZrO_2–TiO_2/CNT (\$888 per m^2). Additionally, the doping of electrode with La-based metal provided enhanced and selective degradation of the antibiotics. For assessing the energy cost during the operation, specific energy (E_sp) consumption was used as a criterion. Cu/PbO_2 and Ni/carbon electrode significantly boosted the removal of AMX[111] and STZ,[124] respectively, with E_sp of 82.2 kW h kg COD^{-1} and 95.3 kW h kg COD^{-1}, respectively. The introduction of LaPbO_2 in SnO_2–Sb/Ti decreased E_sp from 210 to 132 kW h kg COD^{-1}. However, when the energy consumption of modified electrodes is compared with that of commercial BDD (72 kW h kg COD^{-1}) electrode, the energy consumption was still at the higher end.[75] Thus, the electrical energy cost (\$ per m^2) of different modified electrodes can be arranged in the order SnO_2–Sb/Ti (\$166 per m^2) > SnO_2–Sb–LaPbO_2/Ti (\$14.7 per m^2) > CeO_2–ZrO_2–TiO_2/CNT (\$9.24 per m^2) > Ni/carbon electrode (\$6.68 per m^2) > Cu/PbO_2 (\$5.76 per m^2) > BDD (\$5.25 per m^2) > La–Y/PbO_2. Overall, La–Y/PbO_2 showed the least OPEX of ~\$38 per m^2 with an energy consumption of 40 kW h kg COD^{-1}.

The lifetime of the electrode is yet another parameter that governs the operational cost associated with electrocatalytic treatment. For instance, SnO_2-doped electrodes have shown remarkable performance and similar cost when compared with BDD. However, short service time reduces its applicability.[46] DSAs are interesting options for commercial electrodes whereby a mixed metal coating induces catalytic properties and provides extended stability for long-term applications. Other electrodes that rendered aptness from the technical and economic standpoint for antibiotic degradation were MoO_3/nanographite, Pd/Ni-F, and CeO_2–ZrO_2–TiO_2/CNT. These electrodes were reported with higher stability, *e.g.*, more than 15 cycles and less than 5% reduction in degradation efficiency. However, the complete life cycle assessment inclusive of the cost benefit is recommended prior to commercial adoption. Overall, the chemical cost involved in the lab-scale production of the electrode for electrocatalysis is considerably low compared to commercial electrodes. Nonetheless, the prolonged stability of many fabricated electrodes tested on a bench scale is unknown. Future studies in terms of techno-economic analysis, life cycle assessment, and risk prediction are essential before commercialization.

9. Conclusion and prospects

So far, electrochemical oxidation/reduction of antibiotics has proved to have numerous benefits over other treatment options in terms of efficiency, cost, adaptability, and quality of treated effluent. With the advent of cheap and renewable electricity, electrocatalysis has immense potential as a water/wastewater treatment technology. For this purpose, DSA, BDD, PbO_2, and graphene-based electrodes have been extensively used for the electrochemical degradation of antibiotics. Yet, fundamental gaps from the perspective of synthesis, durability, residual toxicity, corrosion resistance, high working potential, low mineralization efficiency, and cost still exist. Thus, the modification of conventional electrodes (Ti, PbO$_2$, carbon, *etc.*) with a catalyst (metal, non-metal, and carbon materials) is highly appreciated. The use of an appropriate catalyst–electrode combination can enhance reaction kinetics, product selectivity, and combat undesirable side reactions. Accordingly, some successful attempts have been made to mineralize antibiotics *via* electrocatalytic oxidation and reduction. It was interesting to note that the inherent properties of precursors such as high electrical conductivity, spin–orbit coupling (lanthanides), electron donor phenomenon (carbon and Co–P), atomic H* production (noble metals), and H* capture (Ni-F) have been proficiently explored. However, the critical parameters hindering most of the electrocatalytic processes were the high cost, low reusability, limited mass transfer, and residual toxicity. Thus, understanding electrode and electrolyte interaction and corrosion/fouling of electrodes in real WW are required. Simultaneously, investigating the architecture of electrocatalysts in terms of nano-structuring can provide strong synergism of bulk and interfacial properties, leading to enhanced reaction rates and degradation efficiency. The doping of electrocatalysts with single or multiple mixed metal oxides is also a reasonable approach to improve oxidative and reductive degradation. However, the leaching and dissolution of the catalyst is a major drawback. The introduction of an interlayer allows the enhancement in the stability and durability of the doped electrode. Nonetheless, the insight into the electrochemical mechanism and the transport phenomenon is not fully understood. Future research on experimental and theoretical approaches such as *in situ* electrochemical and surface characterization, density functional theory (DFT), and development of models to understand separate concentration profiles (reactant, substrate, and intermediate) are some promising ways to address this challenge.

From the environmental researchers' perspective, electrocatalysis is still at an infant stage, and it requires immense development for scaling up to the field. Two critical challenges in the scaling up of electrocatalysis are the high cost and mass transfer limitation. Thus, the utilization of reactors with 3D electrodes or photo-electrocatalysts is one of many possible solutions. Additionally, it is imperative to have a detailed life cycle assessment and techno-economic assessment for categorizing electrocatalysis as an economically feasible and environmentally sustainable water treatment option. Moreover, with recent developments in electroactive membrane technology and bio-electrochemical systems, integrating these technologies with electrocatalysis is a profitable way to improve the quality of WW. Concurrently, the combination of the photovoltaic system and desalination unit (for conductive electrolyte) with electrocatalysis can help cut back the operational cost. To make electrocatalysis a 'fit to purpose' water treatment solution, developing a high-performance electrocatalyst is essential. This opens up a new frontier for collaborations between the scientists working in the area of materials science, electrochemistry, and environmental sciences to fabricate novel advanced materials and combat emerging contaminants like antibiotics and antibiotic-resistant genes.

Abbreviations

Ac-SMX	Acetyl-sulfamethoxazole
AG	Agarose
AMCl2	Aromatic amine product
AMF	3-(5-Aminefurfurylideneamino)-2-oxazolidinone
AMH	[(5-Hydroxyamino-2-furyl)-methyl]-hydrazinecarboxamide
AMN	[(5-Amino-2-furyl)-methylene]-hydrazinecarboxamide
AMP	Ampicillin
AMX	Amoxicillin
AOPs	Advanced oxidation processes
ARB	Antibiotic-resistant bacteria
ARGs	Antibiotic-resistant genes
AZI	Azithromycin
BDD	Boron-doped diamond
$C{=}O$	Carbonyl
$C_2O_6^-$	Percarbonate ions
$-C_6H_5$	Phenolic
CAP	Chloramphenicol
CAPEX	Capital expenditure
CAS	Conventional activated sludge
CB	Conduction band
CFD	Ceftazidime
CFT	Ceftriaxone
CNT	Carbon nanotube
CO_3^{2-}	Carbonate ion
Co–P/O	Cobalt–phosphorus/oxide
CPX	Ciprofloxacin
DCE	Dechlorination efficiency
DHP	Dihexadecyl phosphate
DSA	Dimensionally stable anode
ECs	Emerging contaminants
EF	Electro-Fenton
ENF	Enrofloxacin
FLO	Florfenicol
FQs	Fluoroquinolones
FZD	Furazolidone
GCE	Glassy carbon electrode
H*	Reactive hydrogen
H_2	Hydrogen
H_{ads}	Hydrogen adsorption
HOAM	3-(5-Hydroxylaminefurfurylideneamino)-2-oxazolidinone
HOMO	Highest occupied molecular orbital
$i > i_{lim}$	Mass transfer limitation

IMD	Imidacloprid
ITO	Indium tin oxide
LUMO	Lowest unoccupied molecular orbital
LVFX	Levofloxacin
MBR	Membrane bioreactor
ME	Mineralization
MET	Mineralization TOC efficiency
M–H*	Metal–hydrogen
MMO	Mixed metal oxide
MNZ	Metronidazole
MWCNTs	Multiwalled carbon nanotubes
NFM	N–N fraction product (5-nitro-2-furyl) methenamine
NFZ	Nitrofurazone
Ni-F	Nickel foam
NO	Nitroso product
NO_2	Nitro
NOFX	Norfloxacin
nZVI	Zero valent iron
O_2	Oxygen
OEP	Oxygen evolution potential
OER	Oxygen evolution reaction
OFX	Ofloxacin
–OH	Hydroxyl
OPEX	Operating expenses
ORR	Oxygen reduction reaction
OTC	Oxytetracycline
PF	Photo-Fenton
PGC	Partly graphitized carbon
RC	Recyclability
RCAPEX	Remuneration over the CAPEX
RE	Removal efficiency
ROS	Reactive oxygen species
S	Surface
SCE	Saturated calomel electrode
SEC	Specific energy consumption
SFX	Sulfisoxazole
SMX	Sulfamethoxazole
SPF	Solar photo-Fenton
SS	Stainless steel
STZ	Sulfathiazole
TAP	Thiamphenicol
TC	Total cost
TCH	Tetracycline hydrochloride
Ti	Titanium
TOC	Total organic carbon
TTC	Tetracycline
VB	Valence band
WHO	World Health Organization
WWTP	Wastewater treatment plant
γ-Al_2O_3	Alumina
$(C_5H_5)_2TiCl_2$	Titanocene dichloride
↑	Increase
↓	Decrease
$^{\bullet}OH$	Hydroxyl radical
$^{\bullet}R{-}X_{(3-n)}$	Halomethyl radical

Author contributions

V. Choudhary and K. Vellingiri: conceived the original draft, review and editing; M. I. Thayyil: visualization; and L. Philip: supervised, review and editing and acquired funding.

Conflicts of interest

The authors declare no conflict of interest.

Acknowledgements

The first author wants to acknowledge the Department of Science and Technology (DST) for providing an Innovation in Science Pursuit for Inspired Research (INSPIRE) fellowship (DST/INSPIRE Fellowship/2017/IF170814). The fourth author wants to thank the Department of Science and Technology (DST) Government of India (Grant No. C1E/1819/268/DSTX/LIGY), for financial support.

References

1 P. Kovalakova, L. Cizmas, T. J. McDonald, B. Marsalek, M. Feng and V. K. Sharma, Occurrence and toxicity of antibiotics in the aquatic environment: A review, *Chemosphere*, 2020, 126351.

2 K. D. Burch, B. Han, J. Pichtel and T. Zubkov, Removal efficiency of commonly prescribed antibiotics via tertiary wastewater treatment, *Environ. Sci. Pollut. Res.*, 2019, **26**, 6301–6310.

3 A. Kumar and D. Pal, Antibiotic resistance and wastewater: Correlation, impact and critical human health challenges, *J. Environ. Chem. Eng.*, 2018, **6**, 52–58.

4 N. H. Tran, M. Reinhard and K. Y.-H. Gin, Occurrence and fate of emerging contaminants in municipal wastewater treatment plants from different geographical regions-A review, *Water Res.*, 2018, **133**, 182–207.

5 K. Balakrishna, A. Rath, Y. Praveenkumarreddy, K. S. Guruge and B. Subedi, A review of the occurrence of pharmaceuticals and personal cue products in Indian water bodies, *Ecotoxicol. Environ. Saf.*, 2017, **137**, 113–120.

6 I. T. Carvalho and L. Santos, Antibiotics in the aquatic environments: A review of the European scenario, *Environ. Int.*, 2016, **94**, 736–757.

7 S. Fekadu, E. Alemayehu, R. Dewil and B. Van der Bruggen, Pharmaceuticals in freshwater aquatic environments: A comparison of the African and European challenge, *Sci. Total Environ.*, 2019, **654**, 324–337.

8 J. Lyu, L. Yang, L. Zhang, B. Ye and L. Wang, Antibiotics in soil and water in China–A systematic review and source analysis, *Environ. Pollut.*, 2020, 115147.

9 X.-P. Nie, B.-Y. Liu, H.-J. Yu, W.-Q. Liu and Y.-F. Yang, Toxic effects of erythromycin, ciprofloxacin and sulfamethoxazole exposure to the antioxidant system in Pseudokirchneriella subcapitata, *Environ. Pollut.*, 2013, **172**, 23–32.

10 E. C. Lima, Removal of emerging contaminants from the environment by adsorption, *Ecotoxicol. Environ. Saf.*, 2018, **150**, 1–17.

11 W.H.O., *WHO report on surveillance of antibiotic consumption: 2016–2018 early implementation*, 2018.

12 L. Huang, Y.-B. Xu, J.-X. Xu, J.-Y. Ling, J.-L. Chen, J.-L. Zhou, L. Zheng and Q.-P. Du, Antibiotic resistance genes (ARGs) in duck and fish production ponds with integrated or non-integrated mode, *Chemosphere*, 2017, **168**, 1107–1114.

13 Y.-H. Kim and C. E. Cerniglia, Influence of erythromycin A on the microbial populations in aquaculture sediment microcosms, *Aquat. Toxicol.*, 2005, **73**, 230–241.

14 J. O'Neill, Tackling drug-resistant infections globally: Final report and recommendations: The review on antimicrobial resistance; 2016 available from: https://amr-review.org, Publications.html, 2017.

15 J. O'Neill, *Antimicrobial resistance: Tackling a crisis for the health and wealth of nations. Review on antimicrobial resistance, Review on Antimicrobial Resistance*, London, United Kingdom, https://amr-review.org/sites/default/files/AMR%20Review%20Paper, 2014.

16 D. R. MacFadden, S. F. McGough, D. Fisman, M. Santillana and J. S. Brownstein, Antibiotic resistance increases with local temperature, *Nat. Clim. Change*, 2018, **8**, 510–514.

17 Q. Bu, Y. Cao, G. Yu, X. He, H. Zhang, J. Sun, M. Yun and Z. Cao, Identifying targets of potential concern by a screening level ecological risk assessment of human use pharmaceuticals in China, *Chemosphere*, 2020, **246**, 125818.

18 M. B. Ahmed, J. L. Zhou, H. H. Ngo, W. Guo, N. S. Thomaidis and J. Xu, Progress in the biological and chemical treatment technologies for emerging contaminant removal from wastewater: A critical review, *J. Hazard. Mater.*, 2017, **323**, 274–298.

19 S. Kim, K. H. Chu, Y. A. Al-Hamadani, C. M. Park, M. Jang, D.-H. Kim, M. Yu, J. Heo and Y. Yoon, Removal of contaminants of emerging concern by membranes in water and wastewater: A review, *Chem. Eng. J.*, 2018, **335**, 896–914.

20 C. Grandclément, I. Seyssiecq, A. Piram, P. Wong-Wah-Chung, G. Vanot, N. Tiliacos, N. Roche and P. Doumenq, From the conventional biological wastewater treatment to hybrid processes, the evaluation of organic micropollutant removal: A review, *Water Res.*, 2017, **111**, 297–317.

21 A. S. Oberoi, Y. Jia, H. Zhang, S. K. Khanal and H. Lu, Insights into the fate and removal of antibiotics in engineered biological treatment systems: A critical review, *Environ. Sci. Technol.*, 2019, **53**, 7234–7264.

22 G. Lofrano, R. Pedrazzani, G. Libralato and M. Carotenuto, Advanced oxidation processes for antibiotics removal: A review, *Curr. Org. Chem.*, 2017, **21**, 1054–1067.

23 M. Pirsaheb, H. Hossaini and H. Janjani, An overview on ultraviolet persulfate based advances oxidation process for removal of antibiotics from aqueous solutions: A systematic review, *Desalin. Water Treat.*, 2019, **165**, 382–395.

24 J. Gomes, R. Costa, R. M. Quinta-Ferreira and R. C. Martins, Application of ozonation for pharmaceuticals and personal care products removal from water, *Sci. Total Environ.*, 2017, **586**, 265–283.

25 L. V. de Souza Santos, A. M. Meireles and L. C. Lange, Degradation of antibiotics norfloxacin by Fenton, UV and UV/H_2O_2, *J. Environ. Manage.*, 2015, **154**, 8–12.

26 X. Liu, Y. Zhou, J. Zhang, L. Luo, Y. Yang, H. Huang, H. Peng, L. Tang and Y. Mu, Insight into electro-Fenton and photo-Fenton for the degradation of antibiotics: Mechanism study and research gaps, *Chem. Eng. J.*, 2018, **347**, 379–397.

27 J. J. Rueda-Marquez, I. Levchuk, P. F. Ibañez and M. Sillanpää, A critical review on application of photocatalysis for toxicity reduction of real wastewaters, *J. Cleaner Prod.*, 2020, 120694.

28 Y.-J. Choi, L.-H. Kim and K.-D. Zoh, Removal characteristics and mechanism of antibiotics using constructed wetlands, *Ecol. Eng.*, 2016, **91**, 85–92.

29 G. Yidong, W. Bo, G. Yongxia, L. Wen, Z. Xiaoli, X. Huang and Y. Jianghua, Occurrence and fate of antibiotics in the aqueous environment and their removal by constructed wetlands in China: A review, *Pedosphere*, 2017, **27**, 42–51.

30 V. K. Sharma, N. Johnson, L. Cizmas, T. J. McDonald and H. Kim, A review of the influence of treatment strategies on antibiotic resistant bacteria and antibiotic resistance genes, *Chemosphere*, 2016, **150**, 702–714.

31 C. Ramprasad and L. Philip, Surfactants and personal care products removal in pilot scale horizontal and vertical flow constructed wetlands while treating greywater, *Chem. Eng. J.*, 2016, **284**, 458–468.

32 X. Liu, X. Guo, Y. Liu, S. Lu, B. Xi, J. Zhang, Z. Wang and B. Bi, A review on removing antibiotics and antibiotic resistance genes from wastewater by constructed wetlands: Performance and microbial response, *Environ. Pollut.*, 2019, **254**(Part A), 112996.

33 P. S. Kumar, L. Korving, M. C. van Loosdrecht and G.-J. Witkamp, Adsorption as a technology to achieve ultra-low concentrations of phosphate: Research gaps and economic analysis, *Water Res.: X*, 2019, **4**, 100029.

34 M. Malakootian, A. Nasiri and H. Mahdizadeh, Preparation of $CoFe_2O_4$/activated carbon@ chitosan as a new magnetic nanobiocomposite for adsorption of ciprofloxacin in aqueous solutions, *Water Sci. Technol.*, 2018, **78**, 2158–2170.

35 H. Sharifpour, N. Javid and M. Malakootian, Investigation of single-walled carbon nanotubes in removal of Penicillin G (Benzyl penicillin sodium) from aqueous environments, *Desalin. Water Treat.*, 2018, **124**, 248–255.

36 A. T. Besha, A. Y. Gebreyohannes, R. A. Tufa, D. N. Bekele, E. Curcio and L. Giorno, Removal of emerging micropollutants by activated sludge process and membrane bioreactors and the effects of micropollutants on membrane fouling: A review, *J. Environ. Chem. Eng.*, 2017, **5**, 2395–2414.

37 B. Li and T. Zhang, Different removal behaviours of multiple trace antibiotics in municipal wastewater chlorination, *Water Res.*, 2013, **47**, 2970–2982.

38 Q.-B. Yuan, M.-T. Guo and J. Yang, Fate of antibiotic resistant bacteria and genes during wastewater chlorination: Implication for antibiotic resistance control, *PLoS One*, 2015, **10**, e0119403.

39 I. Iakovides, I. Michael-Kordatou, N. Moreira, A. Ribeiro, T. Fernandes, M. F. R. Pereira, O. C. Nunes, C. M. Manaia, A. M. Silva and D. Fatta-Kassinos, Continuous ozonation of urban wastewater: Removal of antibiotics, antibiotic-resistant Escherichia coli and antibiotic resistance genes and phytotoxicity, *Water Res.*, 2019, **159**, 333–347.

40 N. Javid, Z. Honarmandrad and M. Malakootian, Ciprofloxacin removal from aqueous solutions by ozonation with calcium peroxide, *Desalin. Water Treat.*, 2020, **174**, 178–185.

41 J. Wang and S. Wang, Removal of pharmaceuticals and personal care products (PPCPs) from wastewater: A review, *J. Environ. Manage.*, 2016, **182**, 620–640.

42 R. K. Singh, L. Philip and S. Ramanujam, Continuous flow pulse corona discharge reactor for the tertiary treatment of drinking water: Insights on disinfection and emerging contaminants removal, *Chem. Eng. J.*, 2019, **355**, 269–278.

43 Z. Wei, J. Liu and W. Shangguan, A review on photocatalysis in antibiotic wastewater: Pollutant degradation and hydrogen production, *Chin. J. Catal.*, 2020, **41**, 1440–1450.

44 M. Malakootian, A. Nasiri, A. Asadipour and E. Kargar, Facile and green synthesis of $ZnFe_2O_4$@ CMC as a new magnetic nanophotocatalyst for ciprofloxacin degradation from aqueous media, *Process Saf. Environ. Prot.*, 2019, **129**, 138–151.

45 A. Surenjan, T. Pradeep and L. Philip, Application and performance evaluation of a cost-effective vis-LED based fluidized bed reactor for the treatment of emerging contaminants, *Chemosphere*, 2019, **228**, 629–639.

46 B. P. Chaplin, The prospect of electrochemical technologies advancing worldwide water treatment, *Acc. Chem. Res.*, 2019, **52**, 596–604.

47 R. Andreozzi, V. Caprio, C. Ciniglia, M. De Champdoré, R. Lo Giudice, R. Marotta and E. Zuccato, Antibiotics in the environment: Occurrence in Italian STPs, fate, and preliminary assessment on algal toxicity of amoxicillin, *Environ. Sci. Technol.*, 2004, **38**, 6832–6838.

48 Z. Chen, Y. Liu, W. Wei and B.-J. Ni, Recent advances in electrocatalysts for halogenated organic pollutant degradation, *Environ. Sci.: Nano*, 2019, **6**, 2332–2366.

49 W. Duan, G. Li, Z. Lei, T. Zhu, Y. Xue, C. Wei and C. Feng, Highly active and durable carbon electrocatalyst for nitrate reduction reaction, *Water Res.*, 2019, **161**, 126–135.

50 B. S. Rathi and P. S. Kumar, Electrodeionization theory, mechanism and environmental applications. A review, *Environ. Chem. Lett.*, 2020, 1–19.

51 C. Liu, T. Wu, P.-C. Hsu, J. Xie, J. Zhao, K. Liu, J. Sun, J. Xu, J. Tang and Z. Ye, Direct/alternating current electrochemical method for removing and recovering heavy metal from water using graphene oxide electrode, *ACS Nano*, 2019, **13**, 6431–6437.

52 N. Singh and B. R. Goldsmith, Role of electrocatalysis in the remediation of water pollutants, *ACS Catal.*, 2020, **10**, 3365–3371.

53 R. Wang, X. Ma, T. Liu, Y. Li, L. Song, S. C. Tjong, L. Cao, W. Wang, Y. Qing and Z. Wang, Degradation aspects of endocrine disrupting chemicals: A review on photocatalytic processes and photocatalysts, *Appl. Catal., A*, 2020, 117547.

54 J. Feng and D. C. Johnson, Electrocatalysis of anodic oxygen-transfer reactions: Fe-doped beta-lead dioxide electrodeposited on noble metals, *J. Electrochem. Soc.*, 1990, **137**, 507.

55 C. Comninellis, *Electrochemical oxidation of organic pollutants for wastewater treatment, Studies in environmental science*, Elsevier, 1994, vol. 59, pp. 77–102.

56 A. De Battisti and C. A. Martínez-Huitle, *Electrocatalysis in Wastewater Treatment, Electrochemical Water and Wastewater Treatment*, Elsevier, 2018, pp. 119–131.

57 S. Hussain, S. U. Khan and S. Gul, *Antibiotics and Antimicrobial Resistance Genes, Electrochemical Treatment of Antibiotics in Wastewater*, Springer, 2020, pp. 355–394.

58 G. Loos, T. Scheers, K. Van Eyck, A. Van Schepdael, E. Adams, B. Van der Bruggen, D. Cabooter and R. Dewil, Electrochemical oxidation of key pharmaceuticals using a boron doped diamond electrode, *Sep. Purif. Technol.*, 2018, **195**, 184–191.

59 C. Lei, F. Liang, J. Li, W. Chen and B. Huang, Electrochemical reductive dechlorination of chlorinated volatile organic compounds (Cl-VOCs): Effects of molecular structure on the dehalogenation reactivity and mechanisms, *Chem. Eng. J.*, 2019, **358**, 1054–1064.

60 A. A. Isse, B. Huang, C. Durante and A. Gennaro, Electrocatalytic dechlorination of volatile organic compounds at a copper cathode. Part I: Polychloromethanes, *Appl. Catal., B*, 2012, **126**, 347–354.

61 L. J. Matheson and P. G. Tratnyek, Reductive dehalogenation of chlorinated methanes by iron metal, *Environ. Sci. Technol.*, 1994, **28**, 2045–2053.

62 M. Zaghdoudi, F. Fourcade, I. Soutrel, D. Floner, A. Amrane, H. Maghraoui-Meherzi and F. Geneste, Direct and indirect electrochemical reduction prior to a biological treatment for dimetridazole removal, *J. Hazard. Mater.*, 2017, **335**, 10–17.

63 D. Floner, L. Laglaine and C. Moinet, Indirect electrolysis involving an ex-cell two-phase process. Reduction of nitrobenzenes with a titanium complex as mediator, *Electrochim. Acta*, 1997, **42**, 525–529.

64 I. Saidi, I. Soutrel, D. Floner, F. Fourcade, N. Bellakhal, A. Amrane and F. Geneste, Indirect electroreduction as pretreatment to enhance biodegradability of metronidazole, *J. Hazard. Mater.*, 2014, **278**, 172–179.

65 D. Deng, F. Deng, B. Tang, J. Zhang and J. Liu, Electrocatalytic reduction of low-concentration thiamphenicol and florfenicol in wastewater with multi-walled carbon nanotubes modified electrode, *J. Hazard. Mater.*, 2017, **332**, 168–175.

66 J. Chen, Y. Xia and Q. Dai, Electrochemical degradation of chloramphenicol with a novel Al doped PbO_2 electrode: Performance, kinetics and degradation mechanism, *Electrochim. Acta*, 2015, **165**, 277–287.

67 Y. Lan, C. Coetsier, C. Causserand and K. G. Serrano, On the role of salts for the treatment of wastewaters containing pharmaceuticals by electrochemical oxidation using a boron doped diamond anode, *Electrochim. Acta*, 2017, **231**, 309–318.

68 J. D. García-Espinoza and P. M. Nacheva, Degradation of pharmaceutical compounds in water by oxygenated electrochemical oxidation: Parametric optimization, kinetic studies and toxicity assessment, *Sci. Total Environ.*, 2019, **691**, 417–429.

69 M. H. Bergmann, J. Rollin and T. Iourtchouk, The occurrence of perchlorate during drinking water electrolysis using BDD anodes, *Electrochim. Acta*, 2009, **54**, 2102–2107.

70 P. Neta, V. Madhavan, H. Zemel and R. W. Fessenden, Rate constants and mechanism of reaction of sulfate radical anion with aromatic compounds, *J. Am. Chem. Soc.*, 1977, **99**, 163–164.

71 S. D. Jojoa-Sierra, J. Silva-Agredo, E. Herrera-Calderon and R. A. Torres-Palma, Elimination of the antibiotic norfloxacin in municipal wastewater, urine and seawater by electrochemical oxidation on IrO_2 anodes, *Sci. Total Environ.*, 2017, **575**, 1228–1238.

72 V. Amstutz, A. Katsaounis, A. Kapalka, C. Comninellis and K. M. Udert, Effects of carbonate on the electrolytic removal of ammonia and urea from urine with thermally prepared IrO_2 electrodes, *J. Appl. Electrochem.*, 2012, **42**, 787–795.

73 C. Wang, L. Yin, Z. Xu, J. Niu and L.-A. Hou, Electrochemical degradation of enrofloxacin by lead dioxide anode: Kinetics, mechanism and toxicity evaluation, *Chem. Eng. J.*, 2017, **326**, 911–920.

74 M. Miyata, I. Ihara, G. Yoshid, K. Toyod and K. Umetsu, Electrochemical oxidation of tetracycline antibiotics using a Ti/IrO_2 anode for wastewater treatment of animal husbandry, *Water Sci. Technol.*, 2011, **63**, 456–461.

75 H. Hai, X. Xing, S. Li, S. Xia and J. Xia, Electrochemical oxidation of sulfamethoxazole in BDD anode system: Degradation kinetics, mechanisms and toxicity evaluation, *Sci. Total Environ.*, 2020, 139909.

76 L. Zhu, B. Santiago-Schübel, H. Xiao, H. Hollert and S. Kueppers, Electrochemical oxidation of fluoroquinolone antibiotics: Mechanism, residual antibacterial activity and toxicity change, *Water Res.*, 2016, **102**, 52–62.

77 E. Bocos, O. Iglesias, M. Pazos and M. Á. Sanromán, Nickel foam a suitable alternative to increase the generation of Fenton's reagents, *Process Saf. Environ. Prot.*, 2016, **101**, 34–44.

78 X. Yu, M. Zhou, Y. Hu, K. G. Serrano and F. Yu, Recent updates on electrochemical degradation of bio-refractory organic pollutants using BDD anode: A mini review, *Environ. Sci. Pollut. Res.*, 2014, **21**, 8417–8431.

79 W. Yang, M. Zhou, N. Oturan, Y. Li and M. A. Oturan, Electrocatalytic destruction of pharmaceutical imatinib by electro-Fenton process with graphene-based cathode, *Electrochim. Acta*, 2019, **305**, 285–294.

80 Y. Wang, S. Liu, R. Li, Y. Huang and C. Chen, Electrocatalytic degradation of sulfisoxazole by using graphene anode, *J. Environ. Sci.*, 2016, **43**, 54–60.

81 R. Kaur, J. P. Kushwaha and N. Singh, Amoxicillin electrocatalytic oxidation using Ti/RuO_2 anode: Mechanism, oxidation products and degradation pathway, *Electrochim. Acta*, 2019, **296**, 856–866.

82 N. Oturan, J. Wu, H. Zhang, V. K. Sharma and M. A. Oturan, Electrocatalytic destruction of the antibiotic tetracycline in aqueous medium by electrochemical advanced oxidation processes: Effect of electrode materials, *Appl. Catal., B*, 2013, **140**, 92–97.

83 K. D. Radosavljević, J. D. Lović, D. Ž. Mijin, S. D. Petrović, M. B. Jadranin, A. R. Mladenović and M. L. A. Ivić, Degradation of azithromycin using Ti/RuO_2 anode as catalyst followed by DPV, HPLC–UV and MS analysis, *Chem. Pap.*, 2017, **71**, 1217–1224.

84 Z. Frontistis, M. Antonopoulou, D. Venieri, I. Konstantinou and D. Mantzavinos, Boron-doped diamond oxidation of amoxicillin pharmaceutical formulation: Statistical evaluation of operating parameters, reaction pathways and antibacterial activity, *J. Environ. Manage.*, 2017, **195**, 100–109.

85 Z. Frontistis, D. Mantzavinos and S. Meriç, Degradation of antibiotic ampicillin on boron-doped diamond anode using the combined electrochemical oxidation-Sodium persulfate process, *J. Environ. Manage.*, 2018, **223**, 878–887.

86 D. A. Coledam, J. M. Aquino, B. F. Silva, A. J. Silva and R. C. Rocha-Filho, Electrochemical mineralization of norfloxacin using distinct boron-doped diamond anodes in a filter-press reactor, with investigations of toxicity and oxidation by-products, *Electrochim. Acta*, 2016, **213**, 856–864.

87 S. O. Ganiyu, N. Oturan, S. Raffy, M. Cretin, R. Esmilaire, E. van Hullebusch, G. Esposito and M. A. Oturan, Sub-stoichiometric titanium oxide (Ti_4O_7) as a suitable ceramic anode for electrooxidation of organic pollutants: a case study of kinetics, mineralization and toxicity assessment of amoxicillin, *Water Res.*, 2016, **106**, 171–182.

88 D. Kong, B. Liang, H. Yun, H. Cheng, J. Ma, M. Cui, A. Wang and N. Ren, Cathodic degradation of antibiotics: Characterization and pathway analysis, *Water Res.*, 2015, **72**, 281–292.

89 D. Kong, B. Liang, H. Yun, J. Ma, Z. Li, A. Wang and N. Ren, Electrochemical degradation of nitrofurans furazolidone by cathode: Characterization, pathway and antibacterial activity analysis, *Chem. Eng. J.*, 2015, **262**, 1244–1251.

90 F. L. Guzmán-Duque, R. E. Palma-Goyes, I. González, G. Peñuela and R. A. Torres-Palma, Relationship between anode material, supporting electrolyte and current density during electrochemical degradation of organic compounds in water, *J. Hazard. Mater.*, 2014, **278**, 221–226.

91 D. Rosestolato, J. Fregoni, S. Ferro and A. De Battisti, Influence of the nature of the electrode material and process variables on the kinetics of the chlorine evolution reaction. The case of IrO_2-based electrocatalysts, *Electrochim. Acta*, 2014, **139**, 180–189.

92 L. Tong, P. Eichhorn, S. Pérez, Y. Wang and D. Barceló, Photodegradation of azithromycin in various aqueous systems under simulated and natural solar radiation: Kinetics and identification of photoproducts, *Chemosphere*, 2011, **83**, 340–348.

93 F. Sopaj, M. A. Rodrigo, N. Oturan, F. I. Podvorica, J. Pinson and M. A. Oturan, Influence of the anode materials on the electrochemical oxidation efficiency. Application to oxidative degradation of the pharmaceutical amoxicillin, *Chem. Eng. J.*, 2015, **262**, 286–294.

94 C. Comninellis, Electrocatalysis in the electrochemical conversion/combustion of organic pollutants for waste water treatment, *Electrochim. Acta*, 1994, **39**, 1857–1862.

95 B. Boye, E. Brillas, B. Marselli, P.-A. Michaud, C. Comninellis, G. Farnia and G. Sandonà, Electrochemical incineration of chloromethylphenoxy herbicides in acid medium by anodic oxidation with boron-doped diamond electrode, *Electrochim. Acta*, 2006, **51**, 2872–2880.

96 E. Brillas, S. Garcia-Segura, M. Skoumal and C. Arias, Electrochemical incineration of diclofenac in neutral aqueous medium by anodic oxidation using Pt and boron-doped diamond anodes, *Chemosphere*, 2010, **79**, 605–612.

97 A. Özcan, Y. Şahin, A. S. Koparal and M. A. Oturan, Propham mineralization in aqueous medium by anodic oxidation using boron-doped diamond anode: Influence of experimental parameters on degradation kinetics and mineralization efficiency, *Water Res.*, 2008, **42**, 2889–2898.

98 J. n. R. Domínguez, T. González, P. Palo and J. Sánchez-Martín, Electrochemical advanced oxidation of carbamazepine on boron-doped diamond anodes. Influence of operating variables, *Ind. Eng. Chem. Res.*, 2010, **49**, 8353–8359.

99 E. Guinea, E. Brillas, F. Centellas, P. Cañizares, M. A. Rodrigo and C. Sáez, Oxidation of enrofloxacin with conductive-diamond electrochemical oxidation, ozonation and Fenton oxidation. A comparison, *Water Res.*, 2009, **43**, 2131–2138.

100 D. M. de Araújo, P. Cañizares, C. A. Martínez-Huitle and M. A. Rodrigo, Electrochemical conversion/combustion of a model organic pollutant on BDD anode: Role of sp^3/sp^2 ratio, *Electrochem. Commun.*, 2014, **47**, 37–40.

101 C. Von Sonntag and U. Von Gunten, *Chemistry of ozone in water and wastewater treatment*, IWA publishing, 2012.

102 K. B. Gregory, D. R. Bond and D. R. Lovley, Graphite electrodes as electron donors for anaerobic respiration, *Environ. Microbiol.*, 2004, **6**, 596–604.

103 P. Guo, H. Song and X. Chen, Electrochemical performance of graphene nanosheets as anode material for lithium-ion batteries, *Electrochem. Commun.*, 2009, **11**, 1320–1324.

104 G. Zhang, F. Yang, M. Gao, X. Fang and L. Liu, Electro-Fenton degradation of azo dye using polypyrrole/anthraquinonedisulphonate composite film modified graphite cathode in acidic aqueous solutions, *Electrochim. Acta*, 2008, **53**, 5155–5161.

105 A. K. Geim, Graphene: Status and prospects, *Science*, 2009, **324**, 1530–1534.

106 Y. Jin, M. Jia, M. Zhang and Q. Wen, Preparation of stable aqueous dispersion of graphene nanosheets and their electrochemical capacitive properties, *Appl. Surf. Sci.*, 2013, **264**, 787–793.

107 R. Kaur, J. P. Kushwaha and N. Singh, Electro-oxidation of ofloxacin antibiotic by dimensionally stable Ti/RuO_2 anode: Evaluation and mechanistic approach, *Chemosphere*, 2018, **193**, 685–694.

108 Y. Wang, C. Shen, M. Zhang, B.-T. Zhang and Y.-G. Yu, The electrochemical degradation of ciprofloxacin using a SnO_2-Sb/Ti anode: influencing factors, reaction pathways and energy demand, *Chem. Eng. J.*, 2016, **296**, 79–89.

109 K. Yang, Y. Liu, J. Liu and J. Qiao, Preparation optimization of multilayer-structured SnO_2–Sb–Ce/Ti electrode for efficient electrocatalytic oxidation of tetracycline in water, *Chin. J. Chem. Eng.*, 2018, **26**, 2622–2627.

110 P. Duan, X. Hu, Z. Ji, X. Yang and Z. Sun, Enhanced oxidation potential of Ti/SnO_2-Cu electrode for electrochemical degradation of low-concentration ceftazidime in aqueous solution: Performance and degradation pathway, *Chemosphere*, 2018, **212**, 594–603.

111 X. Bian, Y. Xia, T. Zhan, L. Wang, W. Zhou, Q. Dai and J. Chen, Electrochemical removal of amoxicillin using a Cu doped PbO_2 electrode: Electrode characterization, operational parameters optimization and degradation mechanism, *Chemosphere*, 2019, **233**, 762–770.

112 Y. Xia and Q. Dai, Electrochemical degradation of antibiotic levofloxacin by PbO_2 electrode: Kinetics, energy demands and reaction pathways, *Chemosphere*, 2018, **205**, 215–222.

113 Y. Wang, C. Zhou, J. Wu and J. Niu, Insights into the electrochemical degradation of sulfamethoxazole and its metabolite by Ti/SnO_2-Sb/Er-PbO_2 anode, *Chin. Chem. Lett.*, 2020, **31**(10), 2673–2677.

114 Y. Zhang, P. He, L. Zhou, F. Dong, D. Yang, H. Lei, L. Du, L. Jia and S. Zhou, Optimized terbium doped Ti/PbO_2 dimensional stable anode as a strong tool for electrocatalytic degradation of imidacloprid waste water, *Ecotoxicol. Environ. Saf.*, 2020, **188**, 109921.

115 X. Wang, Y. Xie, G. Yang, J. Hao, J. Ma and P. Ning, Enhancement of the electrocatalytic oxidation of antibiotic wastewater over the conductive black carbon-PbO_2 electrode prepared using novel green approach, *Front. Environ. Sci. Eng.*, 2020, **14**, 22.

116 X. Guo, J. Wan, X. Yu and Y. Lin, Study on preparation of SnO_2-TiO_2/Nano-graphite composite anode and electro-catalytic degradation of ceftriaxone sodium, *Chemosphere*, 2016, **164**, 421–429.

117 D. Li, X. Guo, H. Song, T. Sun and J. Wan, Preparation of RuO_2-TiO_2/Nano-graphite composite anode for electrochemical degradation of ceftriaxone sodium, *J. Hazard. Mater.*, 2018, **351**, 250–259.

118 H. Liu, J. Qu, T. Zhang, M. Ren, Z. Zhang, F. Cheng and D. He, Y.-n. Zhang, Insights into degradation pathways and toxicity changes during electro-catalytic degradation of tetracycline hydrochloride, *Environ. Pollut.*, 2020, **258**, 113702.

119 B. Tang, J. Du, Q. Feng, J. Zhang, D. Wu, X. Jiang, Y. Dai and J. Zou, Enhanced generation of hydroxyl radicals on well-crystallized molybdenum trioxide/nano-graphite anode with sesame cake-like structure for degradation of bio-refractory antibiotic, *J. Colloid Interface Sci.*, 2018, **517**, 28–39.

120 P. Duan, X. Yang, G. Huang, J. Wei, Z. Sun and X. Hu, La_2O_3-CuO_2/CNTs electrode with excellent electrocatalytic oxidation ability for ceftazidime removal from aqueous solution, *Colloids Surf., A*, 2019, **569**, 119–128.

121 X. Hu, Y. Yu and Z. Sun, Preparation and characterization of cerium-doped multiwalled carbon nanotubes electrode for the electrochemical degradation of low-concentration ceftazidime in aqueous solutions, *Electrochim. Acta*, 2016, **199**, 80–91.

122 P. Duan, S. Gao, J. Lei, X. Li and X. Hu, Electrochemical oxidation of ceftazidime with graphite/CNT-Ce/PbO_2–Ce anode: Parameter optimization, toxicity analysis and degradation pathway, *Environ. Pollut.*, 2020, 114436.

123 P. Duan, S. Gao, X. Li, Z. Sun and X. Hu, Preparation of CeO_2-ZrO_2 and titanium dioxide coated carbon nanotube electrode for electrochemical degradation of ceftazidime from aqueous solution, *J. Electroanal. Chem.*, 2019, **841**, 10–20.

124 F. Deng, S. Qiu, H. Olvera-vargas, Y. Zhu, W. Gao, J. Yang and F. Ma, Electrocatalytic sulfathiazole degradation by a novel nickel-foam cathode coated with nitrogen-doped porous carbon, *Electrochim. Acta*, 2019, **297**, 21–30.

125 Y. Lin, J. Yu, Z. Xing, X. Guo, X. Yu, B. Tang and J. Zou, Enhanced generation of H_2O_2 and radicals on Co_9S_8/partly-graphitized carbon cathode for degradation of bio-refractory organic wastewater, *Electrochim. Acta*, 2016, **213**, 341–350.

126 Y. Sun, P. Li, H. Zheng, C. Zhao, X. Xiao, Y. Xu, W. Sun, H. Wu and M. Ren, Electrochemical treatment of chloramphenicol using Ti-Sn/γ-Al_2O_3 particle electrodes with a three-dimensional reactor, *Chem. Eng. J.*, 2017, **308**, 1233–1242.

127 W. Sun, Y. Sun, K. J. Shah, P.-C. Chiang and H. Zheng, Electrocatalytic oxidation of tetracycline by Bi-Sn-Sb/γ-Al_2O_3 three-dimensional particle electrode, *J. Hazard. Mater.*, 2019, **370**, 24–32.

128 Y. Mu, C. Huang, H. Li, L. Chen, D. Zhang and Z. Yang, Electrochemical degradation of ciprofloxacin with a Sb-doped SnO_2 electrode: Performance, influencing factors and degradation pathways, *RSC Adv.*, 2019, **9**, 29796–29804.

129 Y. Li, J. Niu and W. Wang, Photolysis of enrofloxacin in aqueous systems under simulated sunlight irradiation: Kinetics, mechanism and toxicity of photolysis products, *Chemosphere*, 2011, **85**, 892–897.

130 B. Huang, Y. Zhu, J. Li, G. Zeng and C. Lei, Uncovering the intrinsic relationship of electrocatalysis and molecular electrochemistry for dissociative electron transfer to polychloroethanes at silver cathode, *Electrochim. Acta*, 2017, **231**, 590–600.

131 J. Fan, G. Zhao, H. Zhao, S. Chai and T. Cao, Fabrication and application of mesoporous Sb-doped SnO_2 electrode with high specific surface in electrochemical degradation of ketoprofen, *Electrochim. Acta*, 2013, **94**, 21–29.

132 C. R. Costa, F. Montilla, E. Morallón and P. Olivi, Electrochemical oxidation of synthetic tannery wastewater in chloride-free aqueous media, *J. Hazard. Mater.*, 2010, **180**, 429–435.

133 H.-y. Ding, Y.-j. Feng and J.-f. Liu, Preparation and properties of Ti/SnO_2–Sb_2O_5 electrodes by electrodeposition, *Mater. Lett.*, 2007, **61**, 4920–4923.

134 J. Kong, S. Shi, L. Kong, X. Zhu and J. Ni, Preparation and characterization of PbO_2 electrodes doped with different rare earth oxides, *Electrochim. Acta*, 2007, **53**, 2048–2054.

135 A. Chen, X. Zhu, J. Xi, H. Qin and Z. Ji, Ultra-high oxidation potential of Ti/$CuSnO_2$ anodes fabricated by spray pyrolysis for wastewater treatment, *J. Alloys Compd.*, 2016, **683**, 501–505.

136 A. N. S. Rao and V. T. Venkatarangaiah, Metal oxide-coated anodes in wastewater treatment, *Environ. Sci. Pollut. Res.*, 2014, **21**, 3197–3217.

137 S. D. Bukkitgar, N. P. Shetti, R. M. Kulkarni, S. B. Halbhavi, M. Wasim, M. Mylar, P. S. Durgi and S. S. Chirmure, Electrochemical oxidation of nimesulide in aqueous acid solutions based on TiO_2 nanostructure modified electrode as a sensor, *J. Electroanal. Chem.*, 2016, **778**, 103–109.

138 Y. Song, G. Wei and R. Xiong, Structure and properties of PbO_2–CeO_2 anodes on stainless steel, *Electrochim. Acta*, 2007, **52**, 7022–7027.

139 E. Brillas and C. A. Martínez-Huitle, Decontamination of wastewaters containing synthetic organic dyes by electrochemical methods. An updated review, *Appl. Catal., B*, 2015, **166**, 603–643.

140 F. C. Moreira, R. A. Boaventura, E. Brillas and V. J. Vilar, Electrochemical advanced oxidation processes: A review on their application to synthetic and real wastewaters, *Appl. Catal., B*, 2017, **202**, 217–261.

141 Z. Wei, D. Liu, W. Wei, X. Chen, Q. Han, W. Yao, X. Ma and Y. Zhu, Ultrathin TiO_2 (B) nanosheets as the inductive agent for transfrering H_2O_2 into superoxide radicals, *ACS Appl. Mater. Interfaces*, 2017, **9**, 15533–15540.

142 Y. Yao, G. Teng, Y. Yang, C. Huang, B. Liu and L. Guo, Electrochemical oxidation of acetamiprid using Yb-doped PbO_2 electrodes: Electrode characterization, influencing factors and degradation pathways, *Sep. Purif. Technol.*, 2019, **211**, 456–466.

143 M. s. Elementdata, Properties of elements in periodic table, https://periodictable.com/index.html, (accessed 20 November 2020).

144 A. Thiam, I. Sirés, R. Salazar and E. Brillas, On the performance of electrocatalytic anodes for photoelectro-Fenton treatment of synthetic solutions and real water spiked with the herbicide chloramben, *J. Environ. Manage.*, 2018, **224**, 340–349.

145 Y. Xu, S. Liu, F. Guo and B. Zhang, Evaluation of the oxidation of enrofloxacin by permanganate and the antimicrobial activity of the products, *Chemosphere*, 2016, **144**, 113–121.

146 B. Yang, R. S. Kookana, M. Williams, G.-G. Ying, J. Du, H. Doan and A. Kumar, Oxidation of ciprofloxacin and

enrofloxacin by ferrate (VI): Products identification, and toxicity evaluation, *J. Hazard. Mater.*, 2016, **320**, 296–303.

147 C. Wang, J. Niu, L. Yin, J. Huang and L.-A. Hou, Electrochemical degradation of fluoxetine on nanotube array intercalated anode with enhanced electronic transport and hydroxyl radical production, *Chem. Eng. J.*, 2018, **346**, 662–671.

148 Y. Zhang, P. He, L. Jia, C. Li, H. Liu, S. Wang, S. Zhou and F. Dong, Ti/PbO_2-Sm_2O_3 composite based electrode for highly efficient electrocatalytic degradation of alizarin yellow R, *J. Colloid Interface Sci.*, 2019, **533**, 750–761.

149 B. Zhao, H. Yu, Y. Lu, J. Qu, S. Zhu and M. Huo, Polyethylene glycol assisted synthesis of a praseodymium-doped PbO_2 electrode and its enhanced electrocatalytic oxidation performance, *J. Taiwan Inst. Chem. Eng.*, 2019, **100**, 144–150.

150 X. Song, Q. Jiang, J. Liu, Y. Shao and Y. Feng, Enhanced electricity generation and water pressure tolerance using carbon black-based sintered filtration air-cathodes in microbial fuel cells, *Chem. Eng. J.*, 2019, **369**, 652–659.

151 J. D. Rodgers, W. Jedral and N. J. Bunce, Electrochemical oxidation of chlorinated phenols, *Environ. Sci. Technol.*, 1999, **33**, 1453–1457.

152 A. Anglada, A. Urtiaga and I. Ortiz, Contributions of electrochemical oxidation to waste-water treatment: Fundamentals and review of applications, *J. Chem. Technol. Biotechnol.*, 2009, **84**, 1747–1755.

153 N. Lavanya, E. Fazio, F. Neri, A. Bonavita, S. Leonardi, G. Neri and C. Sekar, Simultaneous electrochemical determination of epinephrine and uric acid in the presence of ascorbic acid using SnO_2/graphene nanocomposite modified glassy carbon electrode, *Sens. Actuators, B*, 2015, **221**, 1412–1422.

154 J. Shen, T. Li, W. Huang, Y. Long, N. Li and M. Ye, One-pot polyelectrolyte assisted hydrothermal synthesis of RuO_2-reduced graphene oxide nanocomposite, *Electrochim. Acta*, 2013, **95**, 155–161.

155 Y. Yang, J. Li, H. Wang, X. Song, T. Wang, B. He, X. Liang and H. H. Ngo, An electrocatalytic membrane reactor with self-cleaning function for industrial wastewater treatment, *Angew. Chem.*, 2011, **123**, 2196–2198.

156 A.-Y. Zhang, L.-L. Long, C. Liu, W.-W. Li and H.-Q. Yu, Electrochemical degradation of refractory pollutants using TiO_2 single crystals exposed by high-energy {001} facets, *Water Res.*, 2014, **66**, 273–282.

157 I. Zanella, S. Guerini, S. Fagan, J. Mendes Filho and A. Souza Filho, Chemical doping-induced gap opening and spin polarization in graphene, *Phys. Rev. B*, 2008, **77**, 073404.

158 S. i. Matsumoto, Recent advances in automobile exhaust catalysts, *Catal. Today*, 2004, **90**, 183–190.

159 C. Haman, X. Dauchy, C. Rosin and J.-F. Munoz, Occurrence, fate and behavior of parabens in aquatic environments: A review, *Water Res.*, 2015, **68**, 1–11.

160 Y. Li, Y. Li, B. Xie, J. Han, S. Zhan and Y. Tian, Efficient mineralization of ciprofloxacin using a 3D $Ce_xZr_{1-x}O_2$/RGO composite cathode, *Environ. Sci.: Nano*, 2017, **4**, 425–436.

161 L. Ma-Hock, V. Strauss, S. Treumann, K. Küttler, W. Wohlleben, T. Hofmann, S. Gröters, K. Wiench, B. van Ravenzwaay and R. Landsiedel, Comparative inhalation toxicity of multi-wall carbon nanotubes, graphene, graphite nanoplatelets and low surface carbon black, *Part. Fibre Toxicol.*, 2013, **10**, 23.

162 G. Zhang, S. Wang, S. Zhao, L. Fu, G. Chen and F. Yang, Oxidative degradation of azo dye by hydrogen peroxide electrogenerated in situ on anthraquinonemonosulphonate/polypyrrole composite cathode with heterogeneous CuO/γ-Al_2O_3 catalyst, *Appl. Catal., B*, 2011, **106**, 370–378.

163 F. Yu, M. Zhou and X. Yu, Cost-effective electro-Fenton using modified graphite felt that dramatically enhanced on H_2O_2 electro-generation without external aeration, *Electrochim. Acta*, 2015, **163**, 182–189.

164 J. Lee, M.-S. Park and K. J. Kim, Highly enhanced electrochemical activity of Ni foam electrodes decorated with nitrogen-doped carbon nanotubes for non-aqueous redox flow batteries, *J. Power Sources*, 2017, **341**, 212–218.

165 J. Qin, Q. Chen, C. Yang and Y. Huang, Research process on property and application of metal porous materials, *J. Alloys Compd.*, 2016, **654**, 39–44.

166 S. Gupta and N.-H. Tai, Carbon materials and their composites for electromagnetic interference shielding effectiveness in X-band, *Carbon*, 2019, **152**, 159–187.

167 S. Song, M. Wu, Y. Liu, Q. Zhu, P. Tsiakaras and Y. Wang, Efficient and stable carbon-coated nickel foam cathodes for the electro-Fenton process, *Electrochim. Acta*, 2015, **176**, 811–818.

168 Y. Fan, Z. Ai and L. Zhang, Design of an electro-Fenton system with a novel sandwich film cathode for wastewater treatment, *J. Hazard. Mater.*, 2010, **176**, 678–684.

169 J. Liang, D. Tang, L. Huang, Y. Chen, W. Ren and J. Sun, High oxygen reduction reaction performance nitrogen-doped biochar cathode: A strategy for comprehensive utilizing nitrogen and carbon in water hyacinth, *Bioresour. Technol.*, 2018, **267**, 524–531.

170 E. Seydi, M. Fatahi, P. Naserzadeh and J. Pourahmad, The effects of para-phenylenediamine (PPD) on the skin fibroblast cells, *Xenobiotica*, 2019, **49**, 1143–1148.

171 N. A. Elessawy, J. El Nady, W. Wazeer and A. Kashyout, Development of high-performance supercapacitor based on a novel controllable green synthesis for 3D nitrogen doped graphene, *Sci. Rep.*, 2019, **9**, 1–10.

172 S. Navalon, A. Dhakshinamoorthy, M. Alvaro and H. Garcia, Heterogeneous Fenton catalysts based on activated carbon and related materials, *ChemSusChem*, 2011, **4**, 1712–1730.

173 C. Zhang, Y. Jiang, Y. Li, Z. Hu, L. Zhou and M. Zhou, Three-dimensional electrochemical process for wastewater treatment: A general review, *Chem. Eng. J.*, 2013, **228**, 455–467.

174 B. Hou, R. Deng, B. Ren and Z. Li, Facile preparation of a novel catalytic particle electrode from sewage sludge and its electrocatalytic performance in three-dimensional heterogeneous electro-Fenton, *Water Sci. Technol.*, 2017, **76**, 2350–2356.

175 T. Liu, J. Luo, X. Meng, L. Yang, B. Liang, M. Liu, C. Liu, A. Wang, X. Liu and Y. Pei, Electrocatalytic dechlorination of halogenated antibiotics via synergistic effect of chlorine-cobalt bond and atomic H, *J. Hazard. Mater.*, 2018, **358**, 294–301.

176 H. Liu, J. Han, J. Yuan, C. Liu, D. Wang, T. Liu, M. Liu, J. Luo, A. Wang and J. C. Crittenden, Deep dehalogenation of florfenicol using crystalline CoP nanosheet arrays on a Ti plate via direct cathodic reduction and atomic H, *Environ. Sci. Technol.*, 2019, **53**, 11932–11940.

177 L. Yang, Z. Chen, D. Cui, X. Luo, B. Liang, L. Yang, T. Liu, A. Wang and S. Luo, Ultrafine palladium nanoparticles supported on 3D self-supported Ni foam for cathodic dechlorination of florfenicol, *Chem. Eng. J.*, 2019, **359**, 894–901.

178 I. Saidi, I. Soutrel, F. Fourcade, A. Amrane, N. Bellakhal and F. Geneste, Electrocatalytic reduction of metronidazole using titanocene/Nafion®-modified graphite felt electrode, *Electrochim. Acta*, 2016, **191**, 821–831.

179 G. W. Bishop, J. A. Karty and D. G. Peters, Catalytic reduction of 1, 1, 1-trichloro-2, 2, 2-trifluoroethane (CFC-113a) by cobalt (I) salen electrogenerated at vitreous carbon cathodes in dimethylformamide, *J. Electrochem. Soc.*, 2007, **154**, F65.

180 N. Jiang, B. You, M. Sheng and Y. Sun, Electrodeposited cobalt-phosphorous-derived films as competent bifunctional catalysts for overall water splitting, *Angew. Chem.*, 2015, **127**, 6349–6352.

181 S. Zhang, L. Wang, C. Liu, J. Luo, J. Crittenden, X. Liu, T. Cai, J. Yuan, Y. Pei and Y. Liu, Photocatalytic wastewater purification with simultaneous hydrogen production using MoS_2 QD-decorated hierarchical assembly of $ZnIn_2S_4$ on reduced graphene oxide photocatalyst, *Water Res.*, 2017, **121**, 11–19.

182 Q. Ji, D. Yu, G. Zhang, H. Lan, H. Liu and J. Qu, Microfluidic flow through polyaniline supported by lamellar-structured graphene for mass-transfer-enhanced electrocatalytic reduction of hexavalent chromium, *Environ. Sci. Technol.*, 2015, **49**, 13534–13541.

183 Z. Xing, Q. Liu, A. M. Asiri and X. Sun, Closely interconnected network of molybdenum phosphide nanoparticles: A highly efficient electrocatalyst for generating hydrogen from water, *Adv. Mater.*, 2014, **26**, 5702–5707.

184 C. Zhang, Y. Huang, Y. Yu, J. Zhang, S. Zhuo and B. Zhang, Sub-1.1 nm ultrathin porous CoP nanosheets with dominant reactive (200) facets: A high mass activity and efficient electrocatalyst for the hydrogen evolution reaction, *Chem. Sci.*, 2017, **8**, 2769–2775.

185 R. E. Smith, T. J. Davies, N. d. B. Baynes and R. J. Nichols, The electrochemical characterisation of graphite felts, *J. Electroanal. Chem.*, 2015, **747**, 29–38.

186 A. J. Seen, Nafion: An excellent support for metal-complex catalysts, *J. Mol. Catal. A: Chem.*, 2001, **177**, 105–112.

187 P. Serp and B. Machado, *Nanostructured carbon materials for catalysis*, Royal Society of Chemistry, 2015.

188 P. Serp and K. Philippot, *Nanomaterials in catalysis*, Wiley Online Library, 2013.

189 B. Liang, H.-Y. Cheng, D.-Y. Kong, S.-H. Gao, F. Sun, D. Cui, F.-Y. Kong, A.-J. Zhou, W.-Z. Liu and N.-Q. Ren, Accelerated reduction of chlorinated nitroaromatic antibiotic chloramphenicol by biocathode, *Environ. Sci. Technol.*, 2013, **47**, 5353–5361.

190 D. H. Apaydin, S. Schlager, E. Portenkirchner and N. S. Sariciftci, Organic, organometallic and bioorganic catalysts for electrochemical reduction of CO_2, *ChemPhysChem*, 2017, **18**, 3094–3116.

191 M. Wang and F. Li, Electrochemical water oxidation and reduction catalyzed by organometallic compounds, *Applied Homogeneous Catalysis with Organometallic Compounds: A Comprehensive Handbook in Four Volumes*, 2017, pp. 1135–1194.

192 B. P. Chaplin, M. Reinhard, W. F. Schneider, C. Schüth, J. R. Shapley, T. J. Strathmann and C. J. Werth, Critical review of Pd-based catalytic treatment of priority contaminants in water, *Environ. Sci. Technol.*, 2012, **46**, 3655–3670.

193 J. Lu, J. Bao, X. Lu, D. Zheng and X. Li, Application of a Pd-TiO_2 nanotube/Ti electrode prepared by atomic layer deposition to reductive dechlorination of trichloroethylene, *Electrochem. Commun.*, 2019, **103**, 72–76.

194 R. Mao, X. Zhao, H. Lan, H. Liu and J. Qu, Graphene-modified Pd/C cathode and Pd/GAC particles for enhanced electrocatalytic removal of bromate in a continuous three-dimensional electrochemical reactor, *Water Res.*, 2015, **77**, 1–12.

195 J. J. Lopez Penalver, C. V. Gomez Pacheco, M. Sanchez Polo and J. Rivera Utrilla, Degradation of tetracyclines in different water matrices by advanced oxidation/reduction processes based on gamma radiation, *J. Chem. Technol. Biotechnol.*, 2013, **88**, 1096–1108.

196 J. Wang, D. Zhi, H. Zhou, X. He and D. Zhang, Evaluating tetracycline degradation pathway and intermediate toxicity during the electrochemical oxidation over a Ti/Ti_4O_7 anode, *Water Res.*, 2018, **137**, 324–334.

197 L. Ji, W. Chen, L. Duan and D. Zhu, Mechanisms for strong adsorption of tetracycline to carbon nanotubes: A comparative study using activated carbon and graphite as adsorbents, *Environ. Sci. Technol.*, 2009, **43**, 2322–2327.

198 X. Li, H. Xu and W. Yan, Fabrication and characterization of PbO_2 electrode modified with polyvinylidene fluoride (PVDF), *Appl. Surf. Sci.*, 2016, **389**, 278–286.

199 S. Rawls, *Antibiotics, β-Lactam*, Elsevier, 2014, pp. 207–209.

200 K. Chizari, A. Deneuve, O. Ersen, I. Florea, Y. Liu, D. Edouard, I. Janowska, D. Begin and C. Pham-Huu, Nitrogen-doped carbon nanotubes as a highly active metal-free catalyst for selective oxidation, *ChemSusChem*, 2012, **5**, 102–108.

201 J. Lei, P. Duan, W. Liu, Z. Sun and X. Hu, Degradation of aqueous cefotaxime in electro-oxidation—electro-Fenton—persulfate system with Ti/CNT/SnO_2–Sb–Er anode and Ni@NCNT cathode, *Chemosphere*, 2020, **250**, 126163.

202 J. Yu, D. Zhao, X. Xu, X. Wang and N. Zhang, Study on RuO_2/SnO_2: novel and active catalysts for CO and CH_4 oxidation, *ChemCatChem*, 2012, **4**, 1122–1132.

203 W. Li, W. Chen, Q. Yan, Q. Guo and W. Wang, *Study on the microstructure and properties of different intermediate coatings to* RuO_2*-*TiO_2*-*SnO_2*/Ti Anodes, Recent Advances in Structural Integrity Analysis-Proceedings of the International Congress (APCF/SIF-2014):(APCFS/SIF 2014)*, 2015.

204 M. G. Papich, *Saunders handbook of veterinary drugs*, Elsevier, 2007.

205 X. Chen, F. Gao and G. Chen, Comparison of Ti/BDD and Ti/SnO_2–Sb_2O_5 electrodes for pollutant oxidation, *J. Appl. Electrochem.*, 2005, **35**, 185–191.

206 J. Grimm, D. Bessarabov, W. Maier, S. Storck and R. Sanderson, Sol-gel film-preparation of novel electrodes for the electrocatalytic oxidation of organic pollutants in water, *Desalination*, 1998, **115**, 295–302.

207 F.-L. Zhu, Y.-S. Meng and X.-Y. Huang, Electro-catalytic degradation properties of Ti/SnO_2–Sb electrodes doped with different rare earths, *Rare Met.*, 2016, **35**, 412–418.

208 J. Wang, X. Xiao, Y. Liu, K. Pan, H. Pang and S. Wei, The application of CeO_2-based materials in electrocatalysis, *J. Mater. Chem. A*, 2019, **7**, 17675–17702.

209 W. Hu, M. Zheng, B. Xu, Y. Wei, W. Zhu, Q. Li and H. Pang, Design of hollow carbon-based materials derived from metal–organic frameworks for electrocatalysis and electrochemical energy storage, *J. Mater. Chem. A*, 2021, **9**, 3880–3917.

210 D. Zhang, T. Liu, K. Yin, C. Liu and Y. Wei, Selective H_2O_2 production on N-doped porous carbon from direct carbonization of metal organic frameworks for electro-Fenton mineralization of antibiotics, *Chem. Eng. J.*, 2020, **383**, 123184.

211 X. Xu, S. Zhang, J. Tang, L. Pan, M. Eguchi, J. Na and Y. Yamauchi, Nitrogen-doped nanostructured carbons: A new material horizon for water desalination by capacitive deionization, *EnergyChem*, 2020, 100043.

212 Y. Zhang, J. Liu, S.-L. Li, Z.-M. Su and Y.-Q. Lan, Polyoxometalate-based materials for sustainable and clean energy conversion and storage, *EnergyChem*, 2019, **1**, 100021.

213 T. Olmez-Hanci, I. Arslan-Alaton and D. Dursun, Investigation of the toxicity of common oxidants used in advanced oxidation processes and their quenching agents, *J. Hazard. Mater.*, 2014, **278**, 330–335.

214 B. I. Escher, N. Bramaz and C. Ort, JEM Spotlight: Monitoring the treatment efficiency of a full scale ozonation on a sewage treatment plant with a mode-of-action based test battery, *J. Environ. Monit.*, 2009, **11**, 1836–1846.

215 R. R. Z. Tarpani and A. Azapagic, Life cycle costs of advanced treatment techniques for wastewater reuse and resource recovery from sewage sludge, *J. Cleaner Prod.*, 2018, **204**, 832–847.

216 M. J. da Costa Fonseca, J. R. P. da Silva, C. P. Borges and F. V. da Fonseca, Ethinylestradiol removal of membrane bioreactor effluent by reverse osmosis and UV/H_2O_2: A technical and economic assessment, *J. Environ. Manage.*, 2021, **282**, 111948.